DOCTORAL THESIS

Therapeutic potential of a Wnt modulator ICG-001 on nasopharyngeal carcinoma

Chan, Lai Sheung

Date of Award:
2017

HONG KONG BAPTIST UNIVERSITY

Doctor of Philosophy

THESIS ACCEPTANCE

DATE: June 28, 2017

STUDENT'S NAME: CHAN Lai Sheung

THESIS TITLE: Therapeutic Potential of a Wnt Modulator ICG-001 on Nasopharyngeal Carcinoma

This is to certify that the above student's thesis has been examined by the following panel members and has received full approval for acceptance in partial fulfillment of the requirements for the degree of Doctor of Philosophy.

Chairman:	Prof. So Shu Kong Professor, Department of Physics, HKBU (Designated by Dean of Faculty of Science)
Internal Members:	Dr. Zhao Zhongying Associate Professor, Department of Biology, HKBU (Designated by Head of Department of Biology)
	Dr. Ng Danny W K Assistant Professor, Department of Biology, HKBU
External Members:	Prof. Qi Robert Zhong Professor Division of Life Science The Hong Kong University of Science and Technology
	Prof. Kong Siu Kai Professor School of Life Sciences The Chinese University of Hong Kong
In-attendance:	Prof. Mak Nai Ki Professor, Department of Biology, HKBU

Issued by Graduate School, HKBU

Therapeutic Potential of a Wnt Modulator ICG-001 on Nasopharyngeal Carcinoma

CHAN Lai Sheung

A thesis submitted in partial fulfillment of the requirements

for the degree of

Doctor of Philosophy

Principal Supervisor:

Prof. MAK Nai Ki (Hong Kong Baptist University)

July 2017

DECLARATION

I hereby declare that this thesis represents my own work which has been done after registration for the degree of PhD at Hong Kong Baptist University, and has not been previously included in a thesis or dissertation submitted to this or any other institution for a degree, diploma or other qualifications.

I have read the University's current research ethics guidelines, and accept responsibility for the conduct of the procedures in accordance with the University's Committee on the Use of Human & Animal Subjects in Teaching and Research (HASC). I have attempted to identify all the risks related to this research that may arise in conducting this research, obtained the relevant ethical and/or safety approval (where applicable), and acknowledged my obligations and the rights of the participants.

Signature: 

Date: July 2017

ABSTRACT

According to the cancer stem cells (CSCs) hypothesis, CSCs are responsible for the treatment failures. CSCs are a subset of cells possessing stemness properties within the heterogeneous tumor mass. Therapeutic intervention on Wnt signaling is of our great interest because an aberrant Wnt signaling is an important driver to maintain the potency of CSCs. In nasopharyngeal carcinoma (NPC), deregulated expression of the Wnt signaling components is frequently observed. ICG-001 is a selective Wnt modulator (CBP antagonist) that specifically interrupts the interaction between β-catenin and CBP, thereby encourages the interaction between β-catenin and p300 and the subsequent differentiation and reduction of the CSCs subset. For this reason, the present study aimed to evaluate the therapeutic potential of ICG-001 in NPC.

Results showed that ICG-001 inhibited both the migration of the NPC cells and the formation of tumor spheres. In the first part of the mechanistic studies (Chapter 3), ICG-001 was found to restore the expression of miR-150 in NPC cells. MiR-150 was further found to directly reduce CD44 expression and inhibit NPC cell migration. In the second part of the mechanistic studies (Chapter 4), ICG-001 was found to reduce the expression of Evi1 in NPC cells. The effect was accompanied with the inhibition of both the NPC cells migration and the tumor spheres formation. Two molecular axes, namely miR-96/Evi1/miR-449a and survivin/Evi1/miR-449a, were found to be involved in the inhibition of the tumor cell migration and spheroids formation. The therapeutic potential of using this CBP antagonist (ICG-001) in NPC, namely the *in vitro* and *in vivo* efficacy of ICG-001 combined with cisplatin, was examined (Chapter 5). Concurrent treatment of ICG-001 and cisplatin exhibited a synergistic inhibition on the *in vitro* growth and the tumor sphere forming capacity of NPC cells as well as the growth of NPC xenografts. Taken together, results presented in this thesis suggested that ICG-001 (PRI-724 is the analog of ICG-001 currently used in clinical trials) has a therapeutic potential in NPC.

ACKNOWLEDGEMENTS

My most sincere gratitude goes to my principal supervisor, Prof. Nai Ki Mak, who granted me an opportunity to join his research group in 2013. I appreciate not only his continuous contributions of guidance, suggestions and encouragement to support my studies, but also his understanding, patience and trust, so that I can manage well both my studies and family life in these four years. I would also like to express my deep appreciation to my co-supervisor, Prof. Ricky N.S. Wong, who keeps giving me the encouragement to do the research since I was a project student in the Bachelor Degree.

I appreciate Prof. Michael Kahn (University of Southern California, U.S.A.) very much for kindly providing us ICG-001 and ICG-001-phosphate. Special thanks to Prof. Kwok Wai Lo (CUHK) for the support in the nude mice experiments. I am especially grateful to Miss Carman Lo (CUHK) for her generous help in all the animal studies conducted for this thesis and the maintenance of NPC xenograft-derived EBV-positive C17 cells. I would also like to express my gratitude to Prof. Rotraud Wieser (Medizinische Universitaet Wien, Wien, Austria) who generously provided us the Evi1 expression plasmid.

Thanks Dr. Hong Lok Lung, for the insightful discussions and suggestions about the research in my later work. I am impressed by his enthusiasm and pragmatic attitude in research work. I am so blessed to meet my incredible comrades, Dr. Luo Chen, Dr. Venus Man, Mr. Shawn Chiang and Miss Cecilia Chow. We shared the dreams, laughers and frustrations all the way together. Thanks also go

to the ex-FYP students, Miss Winger Mak, Miss Heyley Lui, Mr. Jason Chow and Mr. Elvin Ho, for the funs they brought to the T1013. Miss Winger Mak also helped me a lot in the literature search.

“Si Hing” Dr. Patrick Yue, the lovely couple Dr. H.H. Kwok and Mrs Christy Poon, and Miss Eman Lee are my old friends and old research buddies that have accompanied me in research work for a decade. Dr. H.H. Kwok is also the one who generated mutant CD44 3’-UTR luciferase reporter for my thesis. I also want to thank my classmates, Dr. Baki Billah and Miss Tian-yi Ma, for spending an enjoyable time together during the coursework. Also, I missed so much the laughers from the lunch with Dr, Candy Chan, Kin, Ka-chun, Miko, Ashley and Cherry during different periods of my work.

Last but not least, the completion of my thesis should also be credited to my beloved family members, my parent, parent-in-law, my husband Tommy, daughter Lok Lam, son Hou Ming and my brother-in-law. Thanks for their understanding and support for all of my decisions. Especially to my mom, words cannot describe how grateful I am for her. I couldn’t focus on my studies without her dedicated care of my children.

THANK YOU ALL.

TABLE OF CONTENTS

Declaration i

Abstract ii

Acknowledgements iii

Table of Contents v

List of Tables xi

List of Figures xii

List of Abbreviations xvi

Chapter 1 Introduction 1

1.1 Nasopharyngeal carcinoma (NPC) 2

1.1.1 Epidemiology 2

1.1.2 Histological classification 4

1.1.3 Diagnosis and staging 4

1.1.4 Etiology 8

1.1.5 Treatments 9

1.1.6 Wnt signaling in NPC tumorigenesis 10

1.2 Cancer stem cells (CSCs) 12

1.2.1 Hypothesis 12

1.2.2 Definition and properties 14

1.2.3 CSCs in NPC 15

1.2.4 Wnt/β-catenin and therapeutic implication 16

1.3 MicroRNAs (miRNAs) 18

1.3.1 Canonical biogenesis pathway 18

1.3.2 Cellular functions 19

1.4 CBP antagonists: ICG-001 and PRI-724 20

1.4.1 Molecular mechanisms of action 20

1.4.2 Progress of clinical trials using CBP antagonists in cancer therapy 20

1.5 Scopes of the study 22

Chapter 2 Materials and Methods 23

2.1 Materials 24

2.2 Cell culture 24

2.3 Plasmid constructs 25

2.4 Cell growth assay 27

2.5 Transient transfection 27

2.6 Transwell migration assay 28

2.7 Tumor spheroid formation assay 28

2.8 Western blotting 29

2.9 miRNA target prediction 30

2.10 Luciferase reporter assay 31

2.10.1 TCF/LEF reporter assay 31

2.10.2 miRNA target analysis 31

2.11 Quantitative real-time PCR (qRT-PCR) 32

2.11.1 Total RNA extraction 32

2.11.2 mRNA expression analysis 32

2.11.3 miRNA expression analysis 33

2.12 Co-Immunoprecipitation 33

2.13 Nude mice tumorigenicity assay 34

2.13.1 Housing 34

2.13.2 Surgery 34

2.13.3 NPC xeno-2117 xenograft study 34

2.13.4 NPC C17 xenograft study 35

2.14 Drug combination studies 36

2.15 Statistical analysis 37

Chapter 3 CD44 is involved in the anti-migratory effect of ICG-001 on NPC 38

3.1 Introduction 39

3.2 Results 41

3.2.1 Effect of ICG-001 on the growth of NPC cells 41

3.2.2 ICG-001 inhibits canonical Wnt signaling in NPC cells 41

3.2.3 ICG-001 inhibits the migration of NPC cells 42

3.2.4 Knockdown of β-catenin or CBP inhibits the migration of C666-1 cells 42

3.2.5 ICG-001 down-regulates the expression of CD44 42

3.2.6 Knockdown of CD44 inhibits the migration of C666-1 cells but not the growth of tumor spheres 43

3.2.7 Association between ezrin and CD44 in C666-1cells 43

3.2.8 ICG-001 enhances the expression of miR-150 44

3.2.9 CD44 is a novel target of miR-150 44

3.2.10 Overexpression of miR-150 resulted in the reduction of the migration of C666-1 cells but not the growth 45

of tumor spheres

3.2.11 ICG-001 inhibits Dnmt1 expression 45

3.2.12 Silencing Dnmt1 restores the expression of miR-150 46

3.3 Discussion 47

Chapter 4 Evi1 is involved in the growth suppression and migration of NPC cells 77

4.1 Introduction 78

4.2 Results 80

4.2.1 ICG-001 inhibits tumor spheroid formation of C666-1 cells 80

4.2.2 ICG-001 inhibits the growth of established tumor spheres of C666-1 cells 80

4.2.3 Effect of ICG-001 pre-treatment on the growth of C666-1 tumor spheres 81

4.2.4 ICG-001 down-regulates the expression of Evi1 81

4.2.5 Effect of Evi1 on the formation of tumor spheres and the migration of C666-1 cells 81

4.2.6 ICG-001 enhances the expression of miR-96 which targets the Evi1 transcript 82

4.27 Effect of miR-96 on the formation of tumor spheres and the migration of C666-1 cells 83

4.2.8 ICG-001 enhances the expression of miR-449a 83

4.2.9 Overexpression of miR-449a inhibits the formation of tumor sphere and the migration of C666-1 cells 84

4.2.10 Effect of silencing or overexpression of Evi1 on the expression of miR-96 and miR-449a 84
4.2.11 The coordination between miR-96 and miR-449a 84
4.2.12 Knockdown of β-catenin or CBP inhibits tumor spheroid formation 85
4.2.13 Knockdown of β-catenin or CBP enhances the expression of miR-96 and miR-449a 85
4.2.14 Knockdown of p300 reduces the expression of miR96 and miR449a 85
4.2.15 ICG-001 reduces the protein expression of survivin 86
4.2.16 Silencing of survivin represses the expression of Evi1 86
4.2.17 Effect of survivin knockdown on the expression of miR-96 and miR-449a 87
4.3 Discussion 88

Chapter 5 ICG-001 enhances the treatment efficacy of cisplatin on NPC 128

5.1 Introduction 129
5.2 Results 130
5.2.1 Effect of ICG-001/cisplatin concurrent therapy on the growth of NPC cells 130
5.2.2 Effect of ICG-001/cisplatin concurrent therapy on tumor spheroid formation 131
5.2.3 Effect of ICG-001/cisplatin concurrent therapy in nude mice tumorigenicity assay 131

5.3 Discussion 133

Chapter 6 Conclusions and future perspectives 152

6 Conclusions and future perspectives 153

References 157

Curriculum Vitae 172

LIST OF TABLES

Table 1.1	Estimated worldwide cancer incidence (all ages, both sexes) in 2012	4
Table 1.2	The UICC/AJCC staging system for NPC, 7th edition (2010)	6
Table 1.3	Wnt-targeting compounds in development	17
Table 2.1	List of siRNA for transient transfection	27
Table 2.2	List of miRNA oligonucleotides for transient transfection	28
Table 2.3	List of primary antibodies for immunoblotting	30
Table 2.4	List of secondary antibodies for immunoblotting	30
Table 2.5	List of primers used in mRNA expression analysis	32
Table 2.6	List of TaqMan probes used in miRNA expression analysis	33
Table 2.7	Groups of mice used in the combined drug study	36

LIST OF FIGURES

Figure 1.1	Location of NPC	2
Figure 1.2	Worldwide estimated rates of incidence and mortality of NPC in 2012	3
Figure 1.3	Stage distribution of NPC in Hong Kong in 2014	7
Figure 1.4	Hierarchy model and stochastic model	13
Figure 1.5	Structures of ICG-001	21
Figure 2.1	Map of pEFzeo-Evi1 plasmid	26
Figure 3.1	ICG-001 inhibits growth of C666-1 cells in dose-dependent manner	51
Figure 3.2	ICG-001 inhibits canonical Wnt signaling in C666-1 cells	52
Figure 3.3	ICG-001 inhibits the migration of C666-1 cells	53
Figure 3.4	Knock-down of β-catenin inhibits the migration of C666-1 cells.	54
Figure 3.5	Knock-down of CBP inhibits the migration of C666-1 cells	56
Figure 3.6	ICG-001 down-regulates CD44 expression	58
Figure 3.7	Effect of CD44 in the migration of NPC cells	60
Figure 3.8	Co-IP assay indicated that CD44 associated with ezrin in C666-1 cells	63
Figure 3.9	ICG-001 enhances the expression of miR-150 in NPC cells	64
Figure 3.10	miR-150 directly targets CD44 transcript	67

Figure 3.11	Overexpressing miR-150 inhibits the migration of C666-1 cells, but not the spheroid formation	69
Figure 3.12	ICG-001 down-regulates Dnmt1 expression	72
Figure 3.13	Dnmt1 activity regulates the expression level of miR-150	73
Figure 3.14	A schematic diagram of Dnmt1/miR-150/CD44 axis in ICG-001-treated cells.	75
Figure 4.1	Effect of ICG-001 on tumor spheroid formation of C666-1 cells	91
Figure 4.2	Effect of ICG-001 on growth of established tumor spheres of C666-1 cells	93
Figure 4.3	Effect of ICG-001 pre-treatment on the growth of C666-1 tumor spheres	95
Figure 4.4	ICG-001 down-regulates Evi1 expression	97
Figure 4.5	Effect of Evi1 on the formation of tumor spheres and the migration of C666-1 cells	99
Figure 4.6	ICG-001 enhances the expression of miR-96 in NPC cells	103
Figure 4.7	miR-96 directly targets Evi1 transcript	105
Figure 4.8	Effect of miR-96 on the formation of tumor spheres and the migration of C666-1 cells	108
Figure 4.9	ICG-001 enhances the expression of miR-449a in NPC cells	111
Figure 4.10	Effect of miR-449a on the formation of tumor spheres and the migration of C666-1 cells	113

Figure 4.11	Effect of Evi1 on the expression of miR-96 and miR-449a	116
Figure 4.12	miR-96 positively regulate the expressionof miR-449a	117
Figure 4.13	Effect of β-catenin siRNA on the formation of tumor spheres and expression levels of miR-96 and miR-449a	118
Figure 4.14	Effect of CBP siRNA on the formation of tumor spheres and expression levels of miR-96 and miR-449a	120
Figure 4.15	Effect of p300 siRNA on the expression levels of miR-96 and miR-449a	122
Figure 4.16	ICG-001 down-regulates survivin expression	124
Figure 4.17	Effect of survivin siRNA on the expression of Evi1 protein, miR-96 and miR-449a	125
Figure 4.18	A schematic diagram of Evi1/miR-449a axis regulated by survivin or miR-96 in ICG-001-treated cells.	127
Figure 5.1	Synergistic inhibitory effect of ICG-001 and cisplatin on the growth of C666-1 cells	136
Figure 5.2	Synergistic inhibitory effect on the growth of C666-1 cells	137
Figure 5.3	The combined effect of ICG-001 and cisplatin on C666-1 tumor spheroid formation	139
Figure 5.4	Dose response study of cisplatin on X2117 NPC xenografts	141
Figure 5.5	Synergistic anti-tumor effect of ICG-001 and cisplatin on X2117 NPC xenografts	143
Figure 5.6	Dose response study of cisplatin on C17 NPC xenograft	146
Figure 5.7	Synergistic anti-tumor effect of cisplatin and ICG-001 on C17 NPC xenografts	149

Figure 6.1 A schematic diagram of the biological pathways studied in the thesis 155

LIST OF ABBREVIATIONS

2-D	2-dimensional
3’-UTR	3’ untranslated region
3-D	3-dimentional
DAPI	4,6-Diamidino-2-phenylindole
5-FU	5-fluorouracil
APC	Adenomatosis polyposis coli
ALDH1	Aldehyde dehydrogenase isoform 1
AACR	American Association of Cancer Research
AJCC	American Joint Committee on Cancer
ABC	ATP-binding cassette
CBP	cAMP response element-binding (CREB)-binding protein
CSCs	Cancer stem cells
CK2	casein-kinase II
Cisplatin	*Cis*-diamminedichloroplatinum II
CD44	Cluster of differentiation 44
CI	Combination index
CGH	Comparative genomic hybridization
cDNA	Complementary DNA
DGCR8	DiGeorge syndrome critical region 8 (DGCR8
p300	E1A binding protein p300
Evi1	Ecotropic viral integration site 1
EBV	Epstein Barr virus
eIF4F	Eukaryotic initiation factor 4F
XPO5	Exportin-5
FBS	Fetal bovine serum
Fz	Frizzled
GCLS	Gastric carcinoma with lymphoid stroma
GAPDH	Glyceraldehyde-3-phosphate dehydrogenase
GSK3β	Glycogen synthase kinase 3β
HLA	Human leukocyte antigen
IMRT	Intensity-modulated radiotherapy
IARC	International Agency for Research on Cancer
i.p.	Intraperitoneal
JAK/STAT	Janus-activated kinase/signal transducer and activator of Transcription

mRNA	Messenger RNA
miRNA	MicroRNA
miRISCs	MiRNA-induced silencing complexes
DMF	N,N-Dimethylformamide
NPC	Nasopharyngeal carcinoma
NF-kB	Nuclear factor-kB
OCT4	Octamer-binding transcription factor 4
P-gp	P-glycoprotein
PBS	Phosphate-buffered saline
PI3K/PTEN	phosphatidylinositol 3-kinase/phosphatase and tensin homolog
Pre-miRNAs	Precursor miRNAs
Pri-miRNAs	Primary miRNAs
qRT-PCR	Quantitative real-time PCR
Ran-GTP	Ras-related nuclear protein guanosine triphosphate
RFP	Red fluorescent protein
Pol II	RNA polymerase II
SOX2	Sex determining region Y (SRY)-box 2
siRNA	Small interfering RNA
SDS	Sodium dodecyl sulfate
TCF/LEF	T cell factor/lymphoid enhancer factor-1
TBL1XR1	transducin beta like 1 X-linked receptor 1
UICC	Union for International Cancer Control
WIF	Wnt inhibitory factor
WHO	World Health Organization

CHAPTER 1

Introduction

1.1 Nasopharyngeal carcinoma (NPC)

1.1.1 Epidemiology

NPC is a malignant tumor arising from nasopharynx epithelium (Figure 1.1) and exhibits marked geographical and gender preferences. According to the International Agency for Research on Cancer (IARC), 86,691 NPC cases (60,896 in males, 25,795 in females) and 50,831 deaths (35,753 in males, 15,075 in females) were reported worldwide in 2012. Though the incidence rate of NPC only accounted for about 0.62% of total cancers diagnosed in world, 81% (70,108) of the NPC cases (86,691) were reported in Asia. In addition, both worldwide incidence and mortality rates of NPC were around 2.5 times higher in males than in females (Figure 1.2, Table 1.1) (Ferlay *et al.*, 2013). In Hong Kong, there were 834 new cases of NPC in 2014, accounted for 1.5% to female and 4.1% to male of all cancers (Hong Kong Cancer Registry, 2016). On the other hand, 15% - 58% of the NPC patients were diagnosed with recurrent NPC, usually with more aggressive phenotypes than the primary tumor. The average 5-year survival rate after re-treatment was only about 20% (Xu *et al.*, 2013).

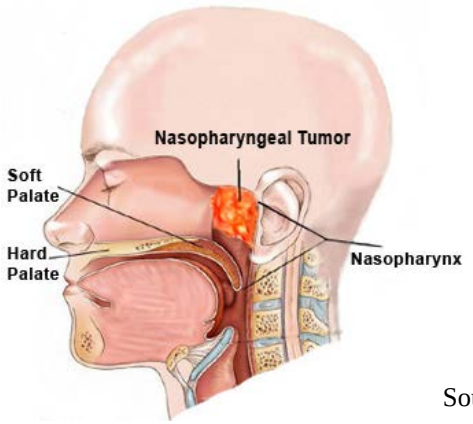

Source: International Medical University Malaysia, 2013

Figure 1.1 | Location of NPC.

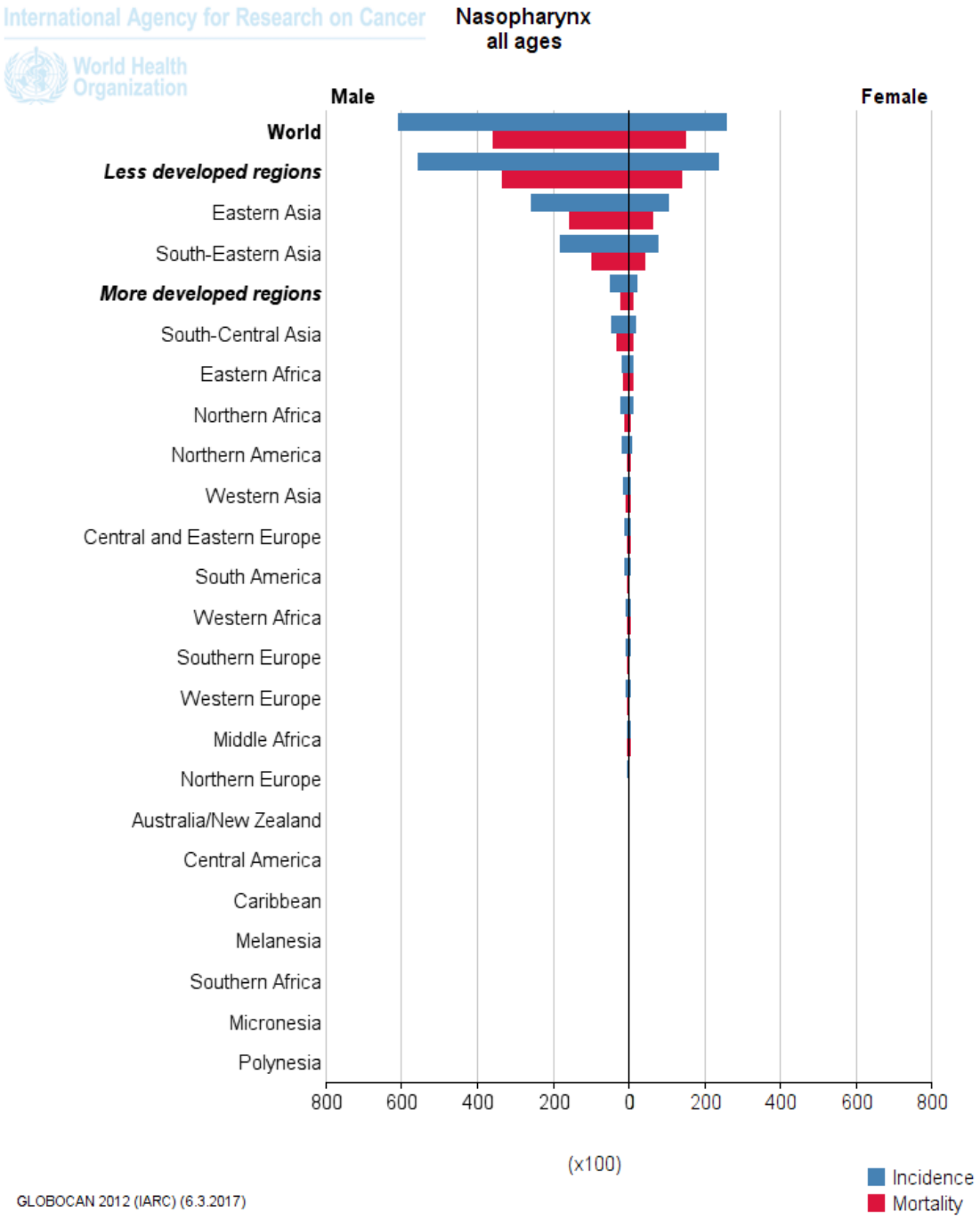

Source: IARC, 2013

Figure 1.2 | Worldwide estimated rates of incidence and mortality of NPC in 2012.

Table 1.1 | Estimated worldwide cancer incidence (all ages, both sexes) in 2012

Cancer	Numbers
All cancers excl. non-melanoma skin cancer	14,067,894
Nasopharynx	86,691

Source: IARC, 2013

1.1.2 Histological classification

The World Health Organization (WHO) has broadly classified NPC into three histological subtypes: (1) keratinizing squamous cell carcinoma, (2) non-keratinizing differentiated carcinoma, and (3) non-keratinizing undifferentiated carcinoma (Wang *et al.,* 2016). Type III NPC is the commonest subtype accounting for more than 95% of all cases in endemic regions, and is characterized to have a strong association with Epstein Barr virus (EBV) and be resistant to radiotherapy and chemotherapy (Union for International Cancer Control, WHO, 2014).

1.1.3 Diagnosis and staging

According to the Union for International Cancer Control (UICC) and American Joint Committee on Cancer (AJCC), NPC is clinically staged using the TNM staging system. T describes the size and location of the tumor; N describes the nearby lymph nodes involvement; and M describes the metastatic spread. By combining the individual aspect of TNM, NPC can be clinically classified into four stages: I, II, III and IV. Details of the staging system of NPC are listed in Table 1.2 (Chan *et al.,* 2012). A definitive diagnosis of NPC requires biopsy

analysis and imaging tests to determine the stage of cancer for each patient, so that the doctors can plan the best treatment. The stage distribution of NPC in Hong Kong in 2014 based on the UICC/AJCC staging guideline is shown in Figure 1.3. Stage III and stage IV are the major cases in NPC (Hong Kong Cancer Registry, 2016).

Early detection of NPC is important, because the 5-year survival rate in NPC in early stage exceeds 80% but less than 10% in Stage IV (Jain *et al.*, 2016). However, over 70% of NPC patients were first diagnosed with Stage III or IV (Hong Kong Cancer Registry, 2016). Early-staged NPC is relatively difficult to be detected since nasopharynx is located at the back of the nose and the early symptoms could be unnoticed. Nasoendoscopy and biopsy can be used in the early NPC screening. However, those methods are not as simple or cost-effective as measuring the circulating EBV DNA in the blood sample. Since nearly all NPC is associated with EBV, elevated level of EBV DNA in the blood may be correlated to NPC. Therefore, EBV DNA is suggested to be a diagnostic marker for early NPC detection (Lee *et al.*, 2015; Chua *et al.*, 2016).

Table 1.2 | The UICC/AJCC staging system for NPC, 7th edition (2010)

Primary tumor (T)			
T1	Tumor confined to the nasopharynx, or extends to oropharynx and/or nasal cavity without parapharyngeal extension		
T2	Tumor with parapharyngeal extension		
T3	Tumor involves bony structures of skull base and/or paranasal sinuses		
T4	Tumor with intracranial extension and/or involvement of cranial nerves, hypopharynx, orbit, or with extension to the infratemporal fossa/masticator space		
Regional lymph nodes (N)			
N1	Unilateral metastasis in cervical lymph node(s), ≤6 cm in greatest dimension, above the supraclavicular fossa, and/or unilateral or bilateral, retropharyngeal lymph nodes, ≤6 cm, in greatest dimension		
N2	Bilateral metastasis in cervical lymph node(s), ≤6 cm in greatest dimension, above the supraclavicular fossa		
N3	Metastasis in a lymph node(s) >6 cm and/or to supraclavicular fossa		
N4	>6 cm in dimension		
N5	Extension to the supraclavicular fossa		
Distant metastasis (M)			
M0	No distant metastasis		
M1	Distant metastasis		
Anatomic stage/prognostic groups			
Stage 0	Tis	N0	M0
Stage I	T1	N0	M0
Stage II	T1	N1	M0
	T2	N0	M0
	T2	N1	M0
Stage III	T1	N2	M0
	T2	N2	M0
	T3	N0	M0
	T3	N1	M0
	T3	N2	M0
Stage IVA	T4	N0	M0
	T4	N1	M0
	T4	N2	M0
Stage IVB	Any T	N3	M0
Stage IVC	Any T	Any N	M1

Source: Chan *et al.*, 2012

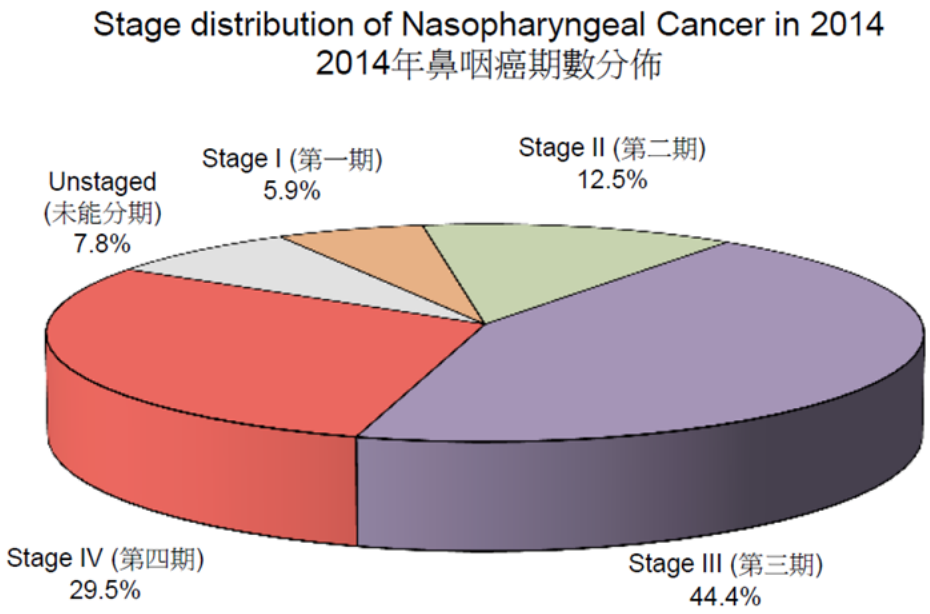

Source: Hong Kong Cancer Registry, Hospital Authority, HKSAR, 2016

Figure 1.3 | Stage distribution of NPC in Hong Kong in 2014.

1.1.4 Etiology

NPC pathogenesis is widely considered to be associated with three etiological factors, namely EBV infection, genetic susceptibility and dietary practices. The etiological factors may interact in an intricate way to trigger NPC pathogenesis, which accumulative genetic and epigenetic changes in premalignant nasopharyngeal epithelium may contribute to a higher vulnerability to EBV infection, or inversely, EBV is suggested to encourage the patho-epigenetics of NPC (Niller *et al.*, 2014; Chua *et al.*, 2016; Dai *et al.*, 2016).

By serology, EBV infection was detected as early as in newborn babies; over 90% of the adult population worldwide was infected with EBV without any symptoms (Cohen *et al.*, 2011; Xiong et al., 2014). Healthy individuals can usually recover from the primary EBV infection because of an effective immune response and with virus harmlessly staying in B cells. But some individuals may unfortunately develop EBV-associated carcinoma such as NPC (Kuppers, 2003; Hatton *et al.*, 2016). Inactivation of p16 and overexpression of cyclin D1 have been proposed to favor the viral genome maintenance in NPC (Lo *et al.*, 2012; Tsang *et al.*, 2012). Epigenetic modifications in host cells by EBV infection have been shown to be long-lasting that persist even the virus being deprived (Birdwell *et al.*, 2014).

Genetic susceptibility is another risk determinant for NPC in endemic regions. *Human leukocyte antigen (HLA)* gene (on chromosome 6p21) is perhaps the most studied susceptibility locus for NPC. More recently, other susceptibility loci for NPC were gradually identified, such as *TNFRSF19* (13q12), *CDKN2A-CDKN2B* (9p21) and particularly *MECOM* (3q26) (MDS1 and Evi1 Complex Locus) (Bei *et al.*, 2010; Chua *et al.*, 2016).

Dietary and social practices also affect the risk of NPC pathogenesis. NPC patients commonly claim to have a history of salted fish consumption (Guo *et al.*, 2009). Long-term exposure to the N-nitrosamine from the salted fish is believed to induce NPC development. Other habits such as smoking and alcohol drinking are the potential risk factors for NPC as well (Chua *et al.*, 2016).

1.1.5 Treatments

Radiotherapy is the mainstay modality in NPC treatments. Among all the current radiation technologies, intensity-modulated radiotherapy (IMRT) is the most preferred approach that the radiation beams are shaped to closely fit the gross tumor and minimize harming the adjacent normal tissues. Radiotherapy alone is generally suggested to NPC patients with stage I (Lee *et al.*, 2015).

Chemotherapy refers to a method giving patients anti-cancer drugs intravenously or orally. *Cis*-diamminedichloroplatinum II (Cisplatin) and 5-fluorouracil (5-FU) are the most frequently-used chemotherapy drugs. Chemo-radiotherapy, a combined strategy of chemotherapy and radiotherapy, has been reported to have better treatment outcomes than either therapy alone from at least nice clinical trials. Patients with Stages II to IVB are usually suggested to receive chemo-radiotherapy (Lee *et al.*, 2015).

An endoscopic surgery provides an alternative treatment option to local recurrent NPC or the cancer spread to the lymph nodes in the neck that do not respond to the radiotherapy. Recurrent NPC patients who underwent surgery have appeared a better survival rate than the re-radiation therapy group (Hao and Tsang, 2010).

A therapeutic plateau in the refinement of radiotherapy and chemotherapy has been reached. Numerous studies underway are trying to find a breakthrough in NPC therapy, including the development of molecular-targeted agents and immunotherapy. Antibodies against EGFR (e.g. cetuximab) and VEGF (e.g. bevacizumab) and some tyrosine kinase inhibitors against multiple receptors (e.g. sunitinib) are in the phases of clinical testing for NPC (Chua *et al.*, 2016; Tan *et al.*, 2016). However, concurrent therapy of cetuximab and radiotherapy has only been shown to achieve a similar efficacy with the standard chemoradiotherapy (Su *et al.*, 2015). Also, inhibition of the receptors like VEGF has been shown to increase the risk of bleeding in NPC patients (Hui *et al.*, 2011; Soria and Deutsch, 2011). Development of vaccines targeting to EBV may be another way out in NPC treatments (Chua *et al.*, 2016; Tan *et al.*, 2016). However, EBV infection has been shown to result in a long-lasting epigenetic modification even though the EBV was gone later in the cells (Birdwell *et al.*, 2014). Therefore, there is a need to refine the existing treatment strategies and develop novel therapeutics for NPC patients.

1.1.6 Wnt signaling in NPC tumorigenesis

Etiological factors particularly EBV infection seem necessary but not sufficient enough for NPC tumorigenesis. The elemental factor regulating NPC carcinogenesis is the aberrant changes of the molecular signaling pathways in the cells. Wnt signaling is one of the most critical pathways in NPC development (Chou *et al.*, 2008).

Wnt signaling has been divided into canonical (β-catenin-dependent) and non-canonical (β-catenin-independent) pathways. The canonical pathway is the most studied Wnt signaling and particularly important in NPC. In the Wnt/β-catenin pathway, binding of Wnt proteins to the frizzled (Fz) family receptors leads to the inhibition of axin/Glycogen synthase kinase-3β (GSK3β)/Adenomatosis polyposis coli (APC) protein complex and results in stabilizing cytoplasmic β-catenin. The stabilized β-catenin subsequently translocates into the nucleus and interacts with T cell factor/lymphoid enhancer factor-1 (TCF/LEF) that in turn triggers specific gene transcriptions (Tulalamba and Janvilisri, 2012).

Dysregulation of Wnt signaling is associated with NPC tumorigenesis. 93% of NPC tumors overexpressed with Wnt protein (Zeng *et al.*, 2007) while 73% of the tumors had Wnt inhibitory factor (WIF, an endogenous Wnt antagonist) underexpressed (Shi *et al.*, 2006). WIF was found to be frequently methylated, in agreement with the low expression level detected in NPC tumors (Li *et al.*, 2011a). Overexpression of Wnt protein, upregulation of Fz receptor and phosphorylation of GSK3β all favor the accumulation of β-catenin in nucleus that encourages the tumor growth. Beside, β-catenin can activate proliferative signaling molecules such as cyclin D1 and c-Myc, and also be able to form complex with E-cadherin to maintain cell adhesion (Chou *et al.*, 2008; Tulalamba and Janvilisri, 2012). Therefore, Wnt signaling is considered as a strong candidate for therapeutic intervention.

1.2 Cancer stem cells (CSCs)

1.2.1 Hypothesis

The concept of CSCs is an old idea, dating back to the very first report at 19th century suggesting that cancer might be caused by the malfunction of the embryonic stem cells (Cohnheim, 1880; Wu *et al.*, 2016). To our best knowledge, this subset of cancer cells had been sparsely studied until 1994 when the first experimental proof of CSCs existence was reported (Lapidot *et al.*, 1994). Existence of CSCs in solid tumor had not been identified until 2003 (Al-Hajj *et al.*, 2003). The concept of CSCs reemerged, and CSCs have been an intense cancer research focus since then. To date, CSCs have been identified in various types of cancer and its existence confers the cancer cells to become intra-tumor heterogeneous which different cancer cells show morphological and phenotypic diversity.

Three models have been proposed to explain the intra-tumor heterogeneity, namely the hierarchy models, stochastic model, and a unified model integrating both (Dick, 2009; Cabrera *et al.*, 2015).

- Hierarchy model is also known as the CSCs model, asserting that a small subset of cells are able to form tumors. These cells are termed CSCs and capable of self-renewing and differentiating into non-tumorigenic progeny. This model suggests that CSCs are the only source to drive the cancer progression (Figure 1.4, Dick, 2009).

- Stochastic model follows the clonal evolution theory introduced by Peter Nowell (1976). This model proposed that the cancer cells are biologically equivalent, however, each cell has equal potential to undergo random changes over time by intrinsic (e.g. genetic and epigenetic alterations) or extrinsic influences (e.g. environment factors) (Figure 1.4, Dick, 2009).

- A unified model bridging hierarchy and stochastic models was recently proposed. This model is based on the concept of CSC plasticity and bidirectional conversion. Available evidence indicated that a certain group of cancer cells could be switched between tumorigenic and non-tumorigenic status in response to appropriate stimuli (Cabrera *et al.*, 2015).

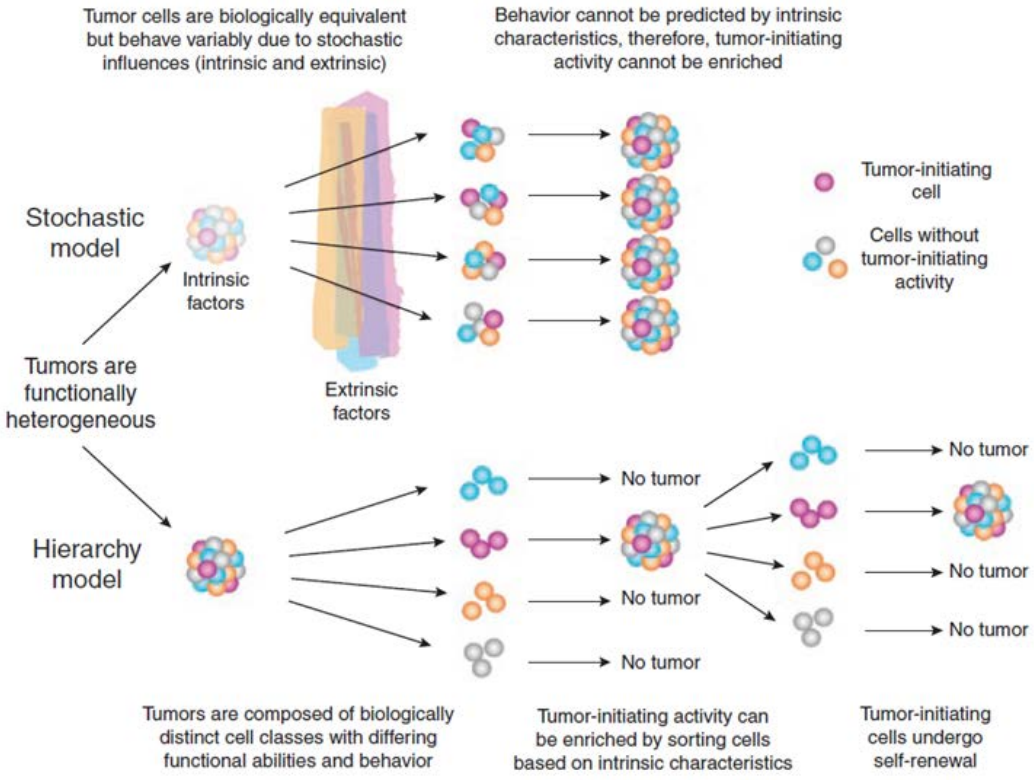

Source: Dick JE, 2009

Figure 1.4 | Hierarchy model and stochastic model.

1.2.2 Definition and properties

The consensus definition of CSCs was first reached at the 2006 American Association of Cancer Research (AACR) Workshop on Cancer Stem Cell, describing that CSCs as a small subset of cancer cells within the tumor mass and should be tumorigenic, self-renewal, differentiable and continuously proliferative (Clarke *et al.*, 2006).

CSCs have several defined properties, including self-renewal, tumorigenic, differentiable, resistant to cancer treatment and metastatic (Liu *et al.*, 2012; Atena *et al.*, 2014; Chen *et al.*, 2016).

- Self-renewal

  Self-renewal ability determines the potency of the cell population. It can be examined *in vivo* by serial transplantation of tumor cells in immunodeficient mice, as agreed in the 2006 AACR Workshop on Cancer Stem Cells (Clarke *et al.*, 2006). Or it can be examined *in vitro* by tumor sphere formation assay. It is believed that CSCs can be enriched in the tumor sphere formation assay which the anchorage-independent, serum-free and low cell density conditions only favor the growth of CSCs. Like the normal stem cells, Wnt/β-catenin, Notch and Hedgehog signaling pathways are believed to control the self-renewal ability of CSCs as well.

- Tumorigenicity and differentiation

  Tumorigenicity of tumor cells can be studied *in vivo* by transplantation assay in immunodeficient mice by observing the tumor growth or studied *in vitro* using soft agar colony formation assay. Cell differentiation can be studied by

tracing specific differentiation markers.

- Treatment resistance

  CSCs have been shown to have a high tolerance to radiotherapy and chemotherapy. This phenomenon can be explained by the efficient DNA repairing system, increased expression of drug efflux proteins such as ATP-binding cassette (ABC) transporters and up-regulation of anti-apoptotic proteins found in the CSCs. Some CSCs are maintained in a quiescent stage, so that they may show no response to the treatments targeting the proliferating cells (Chen *et al.*, 2016).

- Metastatic potential

  Metastasis is a major cause of mortality in most cancers. It is a complicated process involving invasion, migration and cytoskeleton reorganization. Cluster of differentiation 44 (CD44) is a CSCs marker in some cancers, and the $CD44^{high}$ subpopulations always expressed a greater level of genes related to migration and exhibited invasive and migratory phenotypes (Liu *et al*., 2012).

1.2.3 CSCs in NPC

Characterization of CSCs in NPC has been performed in several studies. Previous pilot study showed that CD44 and sex determining region Y (SRY)-box 2 (SOX2) were over-expressed in a majority of CSCs-enriched tumor spheres derived from EBV-positive C666-1 NPC cells. These $CD44^{high}SOX2^{high}$ cells only existed in a small population in patient-derived xenografts and primary tumors. The $CD44^{high}$ CSCs were demonstrated to be enriched in embryonic stem cell markers (SOX2, octamer-binding transcription factor 4 (OCT4) and NANOG) and be

resistant to 5-FU treatment and exhibit self-renewal ability (Lun *et al.*, 2012). Later, Aldehyde dehydrogenase isoform 1 (ALDH1) was used as another marker in the C666-1 tumor spheres, and ALDH1^{high} cells was demonstrated to possess CSCs properties (Lun *et al.*, 2012; Yu *et al.*, 2013). NPC cells expressing embryonic stem markers or ALDH1 demonstrated a strong association with disease aggressiveness and poor patient survival (Luo *et al.*, 2012a; Luo *et al.*, 2013). With only a few reports on CSCs in NPC, characterization of CSCs in NPC is still largely unexplored.

1.2.4 Wnt/β-catenin and therapeutic implication

Chemo/radio-therapy resistance and cancer relapses are the major challenges in current NPC treatments, which are believed to be caused by the existence of CSCs. A list of dysfunctional signaling pathways was suggested for CSCs, including Wnt, Notch, Hedgehog, phosphatidylinositol 3-kinase/phosphatase and tensin homolog (PI3K/PTEN), Janus-activated kinase/signal transducer and activator of transcription (JAK/STAT) and nuclear factor-kB (NF-kB). Since the Wnt pathway is strongly associated with NPC tumorigenesis, therapeutic targeting of Wnt is of great interest in NPC research. Table 1.3 listed some of the major Wnt-targeting compounds put in the clinical studies. Despite recent advancement of CSC-targeted drugs, lots of doubt and ambiguity are still unresolved. Since the CSCs markers reported nowadays are the makers for normal stem cells as well, accumulating reports questioned on whether the CSC-targeted agents eradicate CSCs concurrently damaging the normal stem cells (Grotenhuis *et al.*, 2012). Therefore, better understanding of the biological mechanisms of CSCs is required in the future development of CSCs-targeted agents.

Table 1.3 | Wnt-targeting compounds in development

Phase I/II Trials	
OMP-18R5 (OncoMed Pharmaceuticals/ Bayer)	This monoclonal antibody targets the Frizzled receptors to block association with Wnt ligands. It was recently shown to potently block the capabilities of pancreatic tumor-initiating cells in a serial dilution assay. In xenograft models of breast, lung, pancreatic, and colon cancer, OMP-18R5 demonstrated significant inhibition of tumor growth, and it synergized with standard-of-care treatment in these models (paclitaxel in breast cancer, for example). (NCT01345201)
OMP-54F28 (OncoMed Pharmaceuticals/ Bayer)	This agent is a fusion protein of the Frizzled8 ligand-binding domain with the Fc region of a human immunoglobulin. It binds and sequesters soluble Wnt ligand, impairing its recognition by receptors on tissues. (NCT01608867)
PRI-724 (Prism Pharma Co, Ltd/Eisai)	This is a small-molecule inhibitor of the interaction between β-catenin and CBP. Disrupting the interaction prevents activated transcription by aberrant Wnt signaling at many levels. It is being studied in both solid tumors and myeloid malignancies. (NCT01606579, NCT01302405)
LGK974 (Novartis Pharmaceuticals)	This small molecule inhibits acyltransferase porcupine. Preclinical work demonstrated this enzyme's action is crucial in the secretion of Wnt ligands out of the cell; therefore, inhibiting porcupine can be a small molecule-based method for inhibiting Wnt ligand-mediated activation. (NCT01351103)
Preclinical Studies	
XAV939 (Novartis Pharmaceuticals)	This small-molecule poly (ADP ribose) polymerase (PARP) inhibitor has demonstrated efficacy in cellular models of cancer survival. In Wnt signaling, PARPs like the tankyrases promote the ribosylation and subsequent degradation of axin, a key scaffolding protein of the destruction complex. By inhibiting tankyrase, the axin protein is stabilized and can promote the degradation of β-catenin.
JW55 (Tocris Bioscience)	This selective tankyrase1/2 inhibitor has been shown to inhibit the growth of colon cancer cells in both cell and animal models.

Source: Hitt E, 2013

http://www.onclive.com/publications/oncology-live/2012/december-2012/wnt-signaling-inhibition-will-decades-of-effort-be-fruitful-at-last?p=2

1.3 MicroRNAs (miRNAs)

1.3.1 Canonical biogenesis pathway

A majority of animal miRNAs are generated from canonical biogenesis pathway. They are largely encoded within intergenic regions or within intronic regions of the host genes. First, miRNA genes are transcribed into primary miRNAs (pri-miRNAs) primarily by RNA polymerase II (Pol II) in nucleus. Microprocessor then cleaves the pri-miRNA at the base of the stem-loop to generate ~ 60 - 70 nucleotide hairpin-shaped precursor miRNAs (pre-miRNAs). The Microprocessor is composed of DROSHA (nuclear RNase III) and DiGeorge syndrome critical region 8 (DGCR8, double-stranded RNA binding protein). An individual pri-miRNA may produce one or more miRNAs. The pre-miRNAs are then exported from the nucleus to cytoplasm through nuclear pore by Exportin-5 (XPO5) at the presence of co-factor ras-related nuclear protein guanosine triphosphate (Ran-GTP). Once in the cytoplasm, pre-miRNA will be dissociated from XPO5 by GTP hydrolysis and subsequently processed into ~22 nucleotide miRNA/miRNA* duplex by Dicer (cytoplasmic RNase III). After the duplex loaded into the miRNA-induced silencing complexes (miRISCs), one strand of which supposedly more thermodynamically stable is preferentially selected as mature miRNA (guide strand), while the other strand (miRNA* or passenger strand) is degraded (Xie and Steitz, 2014; Lin and Gregory, 2015).

1.3.2 Cellular functions

Mature miRNAs are single-stranded, non-coding small RNA with ~22 nucleotides. Animal miRNAs assembled with the miRISCs recognize the target messenger RNA (mRNA) by imperfect base pairing to the 3’ untranslated region (3’-UTR) of the target mRNA, which initiate the post-transcriptional regulation. To date, there are two models for the miRNA–mediated gene silencing: mRNA degradation and translational repression. The first model suggests that mRNAs undergo deadenylation, decapping and 5’-to-3’ exonucleotic dacay, which attributes dominant effects in miRNA-mediated regulation. The precise molecular mechanisms for latter model remain unclear, probably involves the interference on the assembly of the eukaryotic initiation factor 4F (eIF4F) complex. Available evidences even suggest that mRNA degradation and translational repression are not mutually exclusive in the miRNA-mediated gene silencing (Jonas and Izaurralde, 2015).

1.4 CBP antagonists: ICG-001 and PRI-724

1.4.1Molecular mechanisms of action

Despite a high degree of homology, cAMP response element-binding (CREB)-binding protein (CBP) and E1A binding protein p300 (p300) have distinct functions in canonical Wnt/β-catenin pathway. Usage of β-catenin/CBP results in the transcription of genes associated with stemness so that the cell potency will be maintained, whereas usage of β-catenin/p300 can initiate cell differentiation. Small molecule ICG-001 (Figure 1.5) is a selective Wnt modulator. It was demonstrated to specifically bind to CBP, but not p300, and subsequently interrupt β-catenin/CBP-mediated transcription. It is of note that ICG-001 showed no significant activity against receptors, ion channels and enzymes. ICG-001 also appeared to block only a very small region of CBP without disrupting the interactions of CBP with other molecules. Therefore, ICG-001 is highly appreciated for its specificity to β-catenin/CBP interruption (Emami *et al.*, 2004; Kahn, 2011). Blockage of a small subset of CBP interactions may favor the β-catenin/p300-mediated transcription that drives the CSCs undergo differentiation. Reducing the CSCs potency may bring a higher treatment efficacy to the patients

1.4.2 Progress of clinical trials using CBP antagonists in cancer therapy

Wnt dysregulation is a central regulatory pathway in cancer cells. Development of Wnt-targeted agents sheds light on cancer therapy. ICG-001 is currently used in the stage of preclinical studies, including but not limited to the areas of breast, colon and ovarian cancers, leukemia, hepatocellular and nasopharyngeal

carcinoma. Virtually all the observations from *in vitro* and *in vivo* studies were satisfactory and encouraging (Chan *et al.*, 2015; Nagaraj *et al.*, 2015; Szwed *et al.*, 2015; Bordonaro and Lazarova, 2016; Lin *et al.*, 2016; Won *et al.*, 2016).

PRI-724 is a derivative of ICG-001 and claimed to be 20-fold more potent than ICG-001. PRI-724 is currently put into clinically studies. A very recent Phase Ib study in pancreatic cancer (ClinicalTrials.gov identifier NCT01764477) showed that combined use of PRI-724 and gemcitabine is safe and exhibited modest clinical activity (Ko *et al.*, 2016). In addition, a Phase Ia study in advanced solid tumor (ClinicalTrials.gov identifier NCT01302405) showed that this compound had a very acceptable toxicity profile up to 905 mg/m^2 for 7 days (El-Khoueiry *et al.*, 2013). To date, three clinical trials of PRI-724 are ongoing: (1) a Phase II trial of PRI-724 combined with several approved drugs in metastatic colorectal cancer (ClinicalTrials.gov identifier NCT02413853, *last verified in September 2015*), (2) a Phase I/II trial in advanced myeloid malignancies (ClinicalTrials.gov identifier NCT01606579, *last verified in April 2016*), (3) a Phase I trial for Hepatitis C Virus-infected Cirrhosis (ClinicalTrials.gov identifier NCT02195440, *last verified in August 2016*).

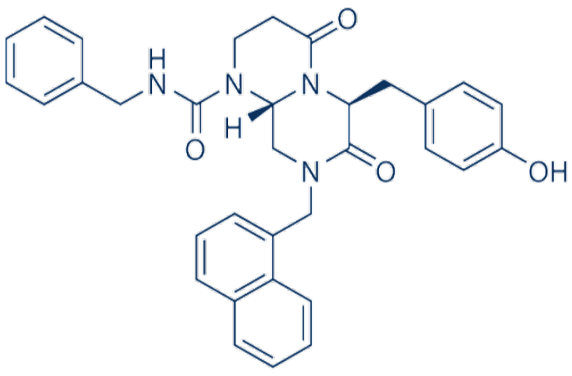

Figure 1.5 | Structures of ICG-001.

1.5 Scopes of the study

The root cause of poor treatment efficacy for locally advanced and metastatic NPC could be explained by the existence of CSCs that appear to be self-renewable and resistant to both radiotherapy and chemotherapy. Wnt signaling is one of the pathways regulating CSCs growth and pluripotency (Takebe *et al.,* 2011). In most of the NPC tumors, an increased expression of Wnt-related proteins and a decreased expression of Wnt inhibitors were reported (Shi *et al.*, 2006; Zeng *et al.*, 2007). It should be noted that Wnt signaling plays a fundamental role in cell proliferation, regeneration and differentiation in a variety of cell types, so using the Wnt antagonist such as ICG-001, instead of Wnt inhibitor, is preferable in NPC treatment from our points of view. Given that NPC development and the aberrant Wnt pathway associates with EBV infection, therefore, the present study evaluated the therapeutic potential of ICG-001 in NPC using the EBV-positive *in vitro* and *in vivo* models. There are three major parts in this thesis:

(1) To study the role of miR-150/CD44 axis in ICG-001-treated NPC cells,

(2) To study the role of Evi1 in ICG-001-treated NPC cells

(3) To evaluate the combined use of ICG-001 and cisplatin in NPC treatment

CHAPTER 2

Materials and Methods

2.1 Materials

ICG-001 and ICG-001-phosphate were kindly provided by Prof. Michael Kahn. A stock solution of ICG-001 at 20 mM was prepared in DMSO for the *in vitro* experiments. ICG-001-phosphate was dissolved in phosphate-buffered saline **(**PBS) to make up to about 250 mg/ml solution for the *in vivo* experiments. Cisplatin was purchased from Sigma (USA), and the stock solution was prepared in DMSO for the *in vitro* experiments and in N,N-Dimethylformamide (DMF) for the *in vivo* experiments.

2.2 Cell culture

The EBV-positive C666-1 NPC cell line was maintained in RPMI-1640 medium (Gibco, USA) supplemented with 10% fetal bovine serum (FBS) (Gibco) and 1% Pen Strep (Gibco) (50 units/ml penicillin and 50 µg/ml streptomycin). The NPC xenograft-derived EBV-positive C17 NPC cells (Prof. KW Lo, CUHK) were cultured in RPMI-1640 medium supplemented with 7.5% FBS, 1% GlutaMAX (Gibco), 100 µg/ml Promocin (InvivoGen, USA) and 7 µM of the Rho kinases I and II inhibitor Y-27632 (Cayman Chemical, USA). The EBV-negative HONE-1 NPC cell line was maintained in DMEM medium (Gibco) supplemented with 5% FBS, 5% newborn calf serum and 1% Pen Strep (50 units/ml penicillin and 50 µg/ml streptomycin). C666-1 and HONE-1 cell lines were authenticated by and obtained from the Hong Kong NPC AoE Cell Line Repository. All the cells were cultured at 37°C in a 5% CO_2 humidified incubator.

2.3 Plasmid constructs

M50 Super 8x TOPFlash (TopFlash, a luciferase reporter plasmid containing TCF/LEF binding sites) (plasmid #12456) and M51 Super 8x FOPFlash (FopFlash, the mutant form of TopFlash) (plasmid #12457) were purchased from Addgene (USA). A pRL *Renilla* Luciferase control reporter vector (pRL-TK) was purchased from Promega (USA). A wild-type 3'-UTR reporter clone for CD44 (wt-CD44 3'UTR) was purchased from OriGene Technologies (USA) and a CD44 3'-UTR mutant construct (mut-CD44 3'UTR) with mutated miR-150 seed region was generated using QuickChange Lightning Multi Site-Directed Mutagenesis Kit (Agilent Technologies, USA) with primer 5'-AGATAAATAGCTTCACCCTTTG GGTGTGGGGGGGAAGCATCTGAAAAATTTCTAGAGGGG-3'. A 3'-UTR reporter clone for Evi1 (Evi1 3'UTR) was also purchased from OriGene Technologies. An expression plasmid encoding Evi1 gene (pEFzeo-Evi1) was kindly provided by Prof Rotraud Wieser (Medizinische Universitaet Wien, Wien, Austria) (Figure 2.1). A pEFzeo control vector (pEFzeo) was generated by deleting the Evi1 DNA insert from pEFzeo-Evi1 construct.

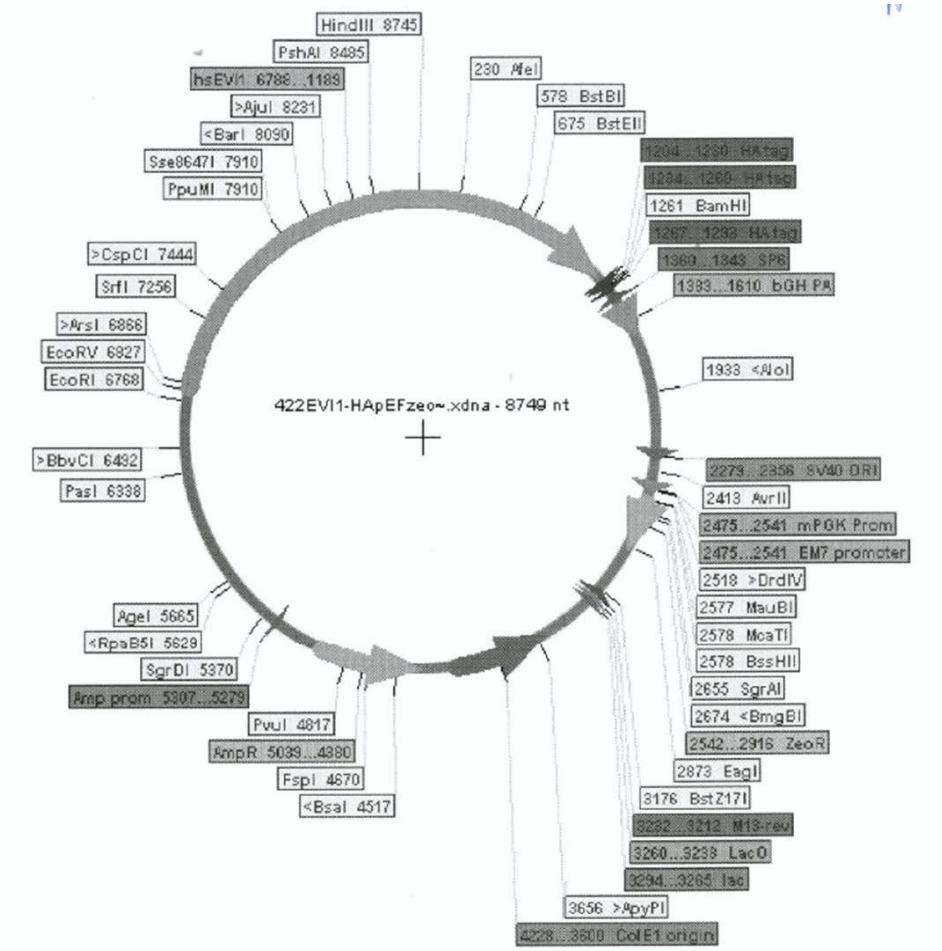

Figure 2.1 | Map of pEFzeo-Evi1 plasmid.

2.4 Cell growth assay

C666-1 cells ($3x10^5$ cells) were seeded onto 35 mm culture dishes and grown for 3 days. Then culture medium was replenished and different drug treatments were performed (Day-0). Total cell numbers of viable cells were counted on Day-3 and –7 using trypan blue staining method.

2.5 Cell transfection

The 35mm culture plates were pre-coated with 6 µg/ml fibronectin at 4°C overnight. The next day, C666-1 cells were seeded onto the fibronectin pre-coated plates, After overnight seeding, cells were transfected with small interfering RNA (siRNA), miRNA oligonucleotides or plasmid DNA complexed with Lipofectamine 2000 (Invitrogen, USA) for 48 or 72 hours. Transfected cells were harvested and subjected to further experiments. The siRNA and miRNA oligonucleotides used in this study were listed in Table 2.1 and 2.2, respectively. The plasmid constructs used were mentioned in Section 2.3.

Table 2.1 | List of siRNA for transient transfection

siRNA	**Supplier and catalogue number**
siCBP	Dharmacon (L-003477-00-0005)
siCD44	Ambion (P/N: 4390824; ID: s2681)
siEvi1	Dharmacon (L-006530-02-0005)
siP300	Dharmacon (L-003486-00-0005)
siSurvivin	Dharmacon (L-003459-00-0005)
siβ-catenin	Ambion (P/N: AM16708; ID: 146154)
siControl	Dharmacon (D-001810-01-20), or Ambion (AM4611)

Table 2.2 | List of miRNA oligonucleotides for transient transfection

miRNA precursors / inhibitors	**Supplier and catalogue number**
miR-150 precursor (Pre-miR-150)	Ambion (P/N: AM17100; ID:PM10070)
miR-96 precursor (Pre-miR-96)	Ambion (P/N: AM17100; ID: PM10422)
miR-449a precursor (Pre-miR-449a)	Ambion (P/N: AM17100; ID: PM11127)
miR-96 inhibitor (Anti-miR-96)	Ambion (P/N:AM17000; ID: AM10422)
miRNA precursor negative control (Pre-control)	Ambion (AM17110)
miRNA inhibitor negative control (Anti-control)	Ambion (AM17010)

2.6 Transwell migration assay

ICG-001-treated or transfected C666-1 cells were seeded in 6.5 mm transwell inserts with 8.0 μm pore polycarbonate membrane (Corning, USA) for 24 hours. RPMI-1640 medium supplemented with 10% fetal bovine serum (FBS) and 1% Pen Strep (50 units/ml penicillin and 50 μg/ml streptomycin) was used in both upper and lower chambers. Cells remaining on the inserts were removed. The migrated cells at the bottom of the membrane were fixed in 4% paraformaldehyde, permeabilized in 0.2% Triton-X and stained with 4,6-Diamidino-2-phenylindole (DAPI) for 15 minutes (Sigma). The cells migrating across the membrane were then visualized under a fluorescent microscope.

2.7 Tumor sphere formation assay

C666-1 cells (2,000 cells/well) in DMEM/F12 medium (Gibco) supplemented with 20 ng/ml EGF (Sigma), 20 ng/ml FGF (Cell Signaling Technology, USA) and 20 ng/ml IGF (Cell Signaling Technology) were seeded in the 24-well

ultra-low attachment culture plates (Corning). The cultures were fed with growth factors every 2-3 days. After incubation, all the tumor spheres were captured under microscope. The number and size of the tumor spheres were measured by ImageJ software.

2.8 Western blotting analysis

ICG-001-treated or the transfected NPC cells were lysed in lysis buffer (250 mM Tris (pH 8), 1% NP-40 and 150 mM NaCl) containing 1% phosphatase inhibitors cocktail (Calbiochem, USA) and 0.25% protease inhibitors cocktail (Sigma). The lysate was centrifuged at 14,000 rpm for 10 minutes at 4°C. Supernatant was collected and the protein concentration was determined by DC Protein Assay Kit (Bio-Rad, USA). Protein denaturation was performed by boiling for 10 minutes in SDS (sodium dodecyl sulfate) sample buffer. Equal amounts of protein samples were then resolved in SDS-polyacrylamide gels and transferred to PVDF membranes (Millipore, USA). Following blocking with 5% non-fat dry milk, the membranes were incubated with primary antibodies and corresponding HRP-conjugated secondary antibodies. The antibodies used for immunoblotting were listed in Table 2.3 and Table 2.4. Protein bands were detected through a chemiluminescent system (LabFrontier, Korea) and visualized on X-ray film. β-actin was used as the internal control. Band intensities were analyzed by using ImageJ software.

Table 2.3 | List of primary antibodies for immunoblotting

Primary antibody	Band size (kDa)	Supplier and catalogue number
CBP	265	Santa Cruz (sc-583)
CD44	80	Cell Signaling Technology (3570)
Dnmt1	200	Cell Signaling Technology (5032)
Evi1	145	Cell Signaling Technology (2593)
Ezrin	81	Cell Signaling Technology (3145)
p300	300	Santa Cruz (sc-584)
Survivin	16	Cell Signaling Technology (2808)
β-catenin	92	Santa Cruz (sc-7963)
β-actin	42	Sigma (A2228)

Table 2.4 | List of secondary antibodies for immunoblotting

Secondary antibody	Supplier and catalogue number
Goat anti-Rabbit IgG (H+L) Secondary Antibody, HRP	Invitrogen (656120)
Goat anti-Mouse IgG (H+L) Secondary Antibody, HRP	Invitrogen (626520)

2.9 miRNA target prediction

Potential targets of miR-150 were predicted using the computational program TargetScan, Release 6.2: June 2012. The targets of miR-96 were predicted by TargetScan, Release 7.1: June 2016.

2.10 Luciferase reporter gene assay

2.10.1 TCF/LEF reporter assay

To study the activity of Wnt signaling, C666-1 cells were transfected with 2 μg TopFlash, a Wnt/β-catenin reporter plasmid, in the presence of Lipofectamine 2000 for 24 hours. An internal control vector, pRL-TK (10 ng), was co-transfected into the cells to normalize the transfection. Cells were then treated with or without ICG-001 for a further 24 hours. FopFlash plasmid was used as a negative control. Firefly luciferase activity of both TopFlash and FopFlash, and Renilla luciferase activity of pRL-TK were measured using a dual luciferase assay kit (Promega) with a microplate luminometer (Tecan, Switzeralnd).

2.10.2 miRNA target analysis

To study the interaction between miR-150 and the 3'-UTR of CD44 mRNA, either wild-type or mutant CD44 3'-UTR luciferase reporter (50 ng) along with miR-150 mimic (Pre-miR-150) or miRNA mimic control (Pre-control) (200 nM) were transfected into C666-1 cells using Lipofectamine 2000 (Invitrogen) for 48 hours. To study the interaction between miR-96 and the 3'-UTR of Evi1 mRNA, Evi1 3'-UTR luciferase reporter (10 ng) along with the miR-96 mimic (Pre-miR-96) or miRNA mimic control (Pre-control) (100 nM) were transfected into C666-1 cells using Lipofectamine 2000 (Invitrogen) for 72 hours. Prior to cell lysis with passive reporter lysis buffer provided by Luciferase Assay System (Promega), the signal of red fluorescent protein (RFP) transcribed by the vector was captured under a fluorescent microscope. Then, the luciferase activities were measured using Luciferase Assay System with a microplate luminometer and normalized to the signals of RFP.

2.11 Quantitative real-time PCR (qRT-PCR)

2.11.1 Total RNA extraction

NPC cells were lysed and homogenized with TRIzol Reagent (Ambion). Phase separation was followed by adding chloroform and centrifugation. RNA in the aqueous phase was then recovered by precipitation with isopropanol. The RNA pellet was washed with 75% ethanol and finally re-dissolved in nuclease-free water. The RNA quantity was determined using the NanoDrop ND-1000 Spectrophotometer (NanoDrop Technologies, USA).

2.11.2 mRNA expression analysis

To quantify mRNA level, total RNA was reverse transcribed to complementary DNA (cDNA) using M-MLV reverse transcriptase (Invitrogen), and then quantified by real-time PCR using Power SYBR Green Master Mix (Applied Biosystems, USA) in StepOnePlus Real-time PCR System (Applied Biosystems). Glyceraldehyde-3-phosphate dehydrogenase (GAPDH) was used as internal control. The relative expression of target transcripts was calculated by $2^{-\Delta\Delta Ct}$ method. The primers used in the study were listed in Table 2.5.

Table 2.5 | List of primers used in mRNA expression analysis

Gene	Forward	Reverse
CD44	TCAGAGGAGTAGGAGAGAGGAAAC	GAAAAGTCAAAGTAACAATAACAGTGG
Evi1	GTACTTGAGCCAGCTTCCAACA	CTTCTTGACTAAAGCCCTTGGA
GAPDH	GAAGGTGAAGGTCGGAGTC	GAAGATGGTGATGGGATTTC

2.11.3 miRNA expression analysis

To detect the expression level of miRNA, total RNA was harvested as mentioned above, then TaqMan MicroRNA Reverse Transcription Kit (Applied Biosystems) was used in reverse transcription. Real-time PCR was subsequently performed in StepOnePlus Real-time PCR System using TaqMan 2X Universal PCR Master Mix (No AmpErase UNG) (Applied Biosystems). Specific primer probes for the miRNAs were from TaqMan MicroRNA Assays (Applied Biosystems, Catalogue number: 4427975) (Table 2.6). Small nuclear RNA RNU6B (U6) was used as internal control. The relative expression of target transcripts was calculated by $2^{-\Delta\Delta Ct}$ method.

Table 2.6 | List of TaqMan probes used in miRNA expression analysis.

Assay name	Assay ID
miR-96	000186
miR-150	000473
miR-449a	001030
U6	001093

2.12 Co-immunoprecipitation (Co-IP) assay

Cells subjected to co-immunoprecipitation experiment were lysed in lysis buffer (50 mM Tris (pH 8), 1% NP-40 and 150 mM NaCl) containing 1% phosphatase inhibitors cocktail (Calbiochem) and 0.25% protease inhibitors cocktail (Sigma). Immunoprecipitation was performed on the cell lysate with anti-CD44 antibody (Cell Signaling Technology) or nonspecific IgG (Cell Signaling Technology) linked to protein G-sepharose (Sigma). The precipitates were washed with lysis buffer and eluted in SDS sample buffer at 95ºC for 10 min. Samples were then analyzed by immunoblotting as described above

2.13 Nude mice tumorigenicity assay

2.13.1 Housing

Female athymic nude mice BALB/c **(**nu/nu**)** were supplied by and housed in the Department of Anatomical and Cellular Pathology and State Key Laboratory in Oncology in South China, The Chinese University of Hong Kong. The mice were housed in sterile rodent micro-isolator systems and given free access to sterile water and food. Animal license was obtained from the Hong Kong Department of Health and all the procedures were approved by the Animal Experimentation Ethics Committee (AEEC) at The Chinese University of Hong Kong. All the animal studies were conducted during the period of March-October, 2014.

2.13.2 Surgery

In order to deliver ICG-001-phosphate steadily and continuously into the mice, Alzet micro-osmotic pumps (Model 1004, DURECT Corporation, USA) were used in the co-treatment *in vivo* experiments. Initially, ICG-001-phosphate was dissolved in PBS to about 250 mg/ml. Osmotic pumps were then filled with PBS or the dissolved ICG-001-phosphate, and primed in the saline as manufacturer's instruction. After 24 hours, the pumps were subcutaneously implanted into the left flank of the anesthetized mice. The wounds were closed by an AutoClip Applier, and Metacam (Boehringer Ingelheim Vetmedica GmbH, Germany) was intraperitoneal (i.p.) injected into the mice for pain relief.

2.13.3 NPC xeno-2117 xenograft study

Equal portions of NPC patient-derived xenograft xeno-2117 (X2117) were passaged and subcutaneously grafted into right flank of the nude mice at 4-6 weeks of age. When the tumors became palpable, the mice were randomized for

various treatments. Dose response of cisplatin on X2117 was tested first. Cisplatin dissolved in saline containing 4% DMF was weekly i.p. injected at 2, 4 or 6 mg/kg into the mice. The vehicle control group of mice was administrated with saline containing 4% DMF. A sub-optimal dose (3 mg/kg/week) of cisplatin was determined from the dose response experiment, and an ICG-001/cisplatin combined therapy was then performed on the mice. Mice were randomized into four groups as described in Table 2.7 in the co-treatment study. Saline with or without cisplatin (3 mg/kg) was i.p. administrated weekly into the mice. ICG-001-phosphate dissolved in PBS was steadily delivered from the osmotic pumps into the mice at an estimated rate of 50 mg/kg/day. The tumor volume in mm^3 (length x width x height) was measured using a Vernier caliper twice a week, and the mice body weight was measured at the same time. The mice were sacrificed at the end of the experiments and the tumors were dissected out.

2.13.4 NPC C17 xenograft study

Equal portions of NPC patient-derived xenograft C17 were passaged and subcutaneously grafted into right flank of the nude mice at 4-6 weeks of age. When the tumors became palpable, the mice were randomized for various treatments. Dose response of cisplatin on C17 xenografts was tested first. Cisplatin dissolved in saline containing 4% DMF was i.p. injected at 2, 3 or 4 mg/kg into the mice every 4 days. The vehicle control group of mice was administrated with saline containing 4% DMF. A sub-optimal dose (1 mg/kg/4 days) of cisplatin was determined from the dose response experiment, and an ICG-001/cisplatin combined therapy was then performed on the mice. Mice were randomized into four groups as described in Table 2.7 in the co-treatment study. Saline with or without cisplatin (1 mg/kg) was i.p. administrated every 4 days into

the mice. ICG-001-phosphate dissolved in PBS was steadily delivered from the osmotic pumps into the mice at an estimated rate of 50 mg/kg/day. The tumor volume in mm^3 (length x width x height) was measured using a Vernier caliper twice a week, and the mice body weight was measured at the same time. The mice were sacrificed at the end of the experiments and the tumors were dissected out.

Table 2.7 | Groups of mice used in the combined drug study

Group	Osmotic pump	i.p. injection
1	PBS	Saline with 4% DMF
2	PBS	Cisplatin in saline with 4% DMF
3	ICG-001-phosphate in PBS	Saline with 4% DMF
4	ICG-001-phosphate in PBS	Cisplatin in saline with 4% DMF

2.14 Drug combination studies

The *in vitro* combination effect of ICG-001 and cisplatin was calculated using CompuSyn software based on the Chou and Talalay combination index (CI) theorem (Chou and Talalay, 1984; Chou, 2010). Plots of the dose-effect curve and normalized isobologram were constructed by the software considering 50% inhibitory concentration of the drugs. CI <1, =1, and >1 indicate synergy, additivity and antagonism, respectively.

The *in vivo* combination effect of ICG-001 and cisplatin was calculated according to the Zheng-Jun Jin method as previously described (Jin, 1980; Li *et al.*, 2013; Liu *et al.*, 2015; Zheng *et al.*, 2015). The method provides a q value from the equation, $q = E_{a+b}/(E_a+E_b-E_a\times E_b)$, where E_a, E_b and E_{a+b} indicate the inhibitory

rates of cisplatin, ICG-001 and the combination of the two drugs, respectively. $q < 0.85$, $0.85 < q < 1.15$, and $q > 1.15$ indicate antagonism, additivity and synergy, respectively.

2.15 Statistics

Data were presented as mean ± standard deviation (SD) of at least three independent experiments. Statistical comparisons between two groups were determined by the Student *t*-test. Statistical significance was set as $p < 0.05$.

CHAPTER 3

CD44 is involved in the anti-migratory effect of ICG-001 on NPC

3.1 Introduction

CD44 is a transmembrane glycoprotein belonging to cell adhesion molecule. In canonical Wnt pathway, formation of β-catenin and TCF/LEF family protein complex together with CBP is required for the transcription of a subset of target genes including CD44 (Wielenga *et al.*, 1999). Recently, CD44 was demonstrated to be able to regulate the Wnt activity (Schmitt *et al.*, 2014). CD44 is therefore a direct Wnt target gene as well as a Wnt regulator.

A large body of evidence associates the Wnt signaling activation with cancer progression, and the tumor cells exhibiting deregulated Wnt activity are functionally linked up to the development of CSCs (Kim and Kahn, 2014). Being one of the biomarkers for characterization of CSCs, CD44 had been reported to be overexpressed in the CSCs-enriched spheroid culture derived from EBV-positive C666-1 cells as well (Lun *et al.*, 2012). The potential use of ICG-001, a specific Wnt modulator, in NPC was first reported by Chan and co-workers (Chan *et al.*, 2015), mentioning that ICG-001 could inhibit the growth of $SOX2^{high}/CD44^{high}$ tumor spheres derived from C666-1 cells. However, the role of CD44 has never been fully elucidated in ICG-001-treated NPC cells. In view of this, CD44 was selected as our focus in this part of study.

MiRNAs participate in both physiological and pathological processes. MiRNAs can regulate gene expression at post-transcriptional level by pairing with the 3′-UTR of mRNA. Many miRNAs had been reported to target CD44 in different tumor types, but the miRNAs involved in the regulation of NPC had never been studied. We hypothesize that ICG-001 could reduce CD44 and hence the

tumorigenic properties of NPC through miRNA regulation in this part of study. The present study reported that a novel miRNA (miR-150) targeting CD44 was upregulated in ICG-001-treated NPC.

3.2 Results

3.2.1 Effect of ICG-001 on the growth of NPC cells

Effect of ICG-001 on the growth of C666-1 cells was first determined in this study. Using trypan blue exclusion staining method, the number of viable cells was counted in response to different concentrations of ICG-001 treatment. Figure 3.1 clearly showed a dose-dependent inhibitory effect of ICG-001 on the growth of C666-1 cells at day-3 and -7 after treatments. This observation supported the earlier finding by Chan and co-workers (2015).

3.2.2 ICG-001 inhibits canonical Wnt signaling in NPC cells

ICG-001 is as a CBP antagonist capable to prevent the interaction between CBP and β-catenin, resulting in suppression of TCF/β-catenin transcription (Takahashi-Yanaga and Kahn, 2010). Therefore, the effect of ICG-001 on the TCF activity on C666-1 cells was determined in this study. After the cells transfected with either TopFlash or FopFlash plasmid for 24 hours, the cells were then further incubated with ICG-001 for another 24 hours. According to Figure 3.2, ICG-001 at 5 and 10 μM could significantly inhibit the TCF reporter activity in cells transfected with TopFlash plasmid, whereas the effect was not significant in the cells transfected with the negative control plasmid (FopFlash). Together with our previous observation on the downregulated expression of Wnt target genes by ICG-001 in C666-1 cells (Chan *et al.*, 2015), we confirmed that ICG-001 inhibited the canonical Wnt signaling in NPC cells by interfering TCF/β-catenin transcription at a CBP-dependent fashion.

3.2.3 ICG-001 inhibits the migration of NPC cells

We have previously demonstrated that ICG-001 could inhibit the growth of CSC-enriched NPC spheroid cells (Chan *et al.*, 2015). In the present study, we further found that ICG-001 could inhibit the migration of NPC cells by about 50% in the transwell migration assay (Figure 3.3).

3.2.4 Knockdown of β-catenin or CBP inhibits the migration of C666-1 cells

Since ICG-001 is capable to interfere with the β-catenin/CBP downstream signaling, it is logical that siRNA silencing of the β-catenin or CBP expression would also inhibit the migration of NPC cells. Results clearly showed that transfection of specific siRNA could successfully reduce the protein expression of either β-catenin or CBP (Figure 3.4A and 3.5A). Reduction of either β-catenin or CBP could result in the reduced migration of the NPC cells, as shown in Figure 3.4B and 3.5B. These observations suggested that β-catenin and CBP were involved in the regulation of migration of C666-1 cells.

3.2.5 ICG-001 down-regulates the expression of CD44

The expression of CD44 has previously been shown to be controlled by Wnt/β-cat signaling (Wielenga *et al.*, 1999). In the present study, we found that ICG-001 could not only reduce the level of CD44 mRNA in C666-1 cells (Figure 3.6A), but also the protein expression of CD44 in both C666-1 and C17 cells (Figure 3.6B, 3.6C), indicating that ICG-001 may modulate Wnt signaling through the regulation of CD44 expression in NPC cells.

3.2.6 Knockdown of CD44 inhibits the migration of C666-1 cells but not the growth of tumor spheres

Since ICG-001 could inhibit the migration and CD44 expression in C666-1 cells, then it would be interesting to know whether CD44 is involved in the cell migration. First, CD44 siRNA was shown to effectively reduce the protein expression of CD44 (Figure 3.7A). Suppression of CD44 was then accompanied with a ~40% reduction in the migrated cell population (Figure 3.7B). On the other hand, tumor spheroid formation assay provides us a 3-dimensional (3-D) culture model to assess the effect of CD44 on the growth of CSCs. Interestingly, the capability of CD44 siRNA-transfected cells to form tumor spheres was similar to the control siRNA transfected cells (Figure 3.7C), indicating that CD44 is not involved in the growth of C666-1 spheroid cells. These data indicated that ICG-001-inhibited cell migration involved CD44 regulation.

3.2.7 Association between ezrin and CD44 in C666-1cells

Ezrin is a key molecule linking the plasma membrane components and cytoskeleton and its association with CD44 is particularly important in mediating the cell migration process (Bretscher *et al.*, 1997; Donatello *et al.*, 2012). To confirm the interaction of CD44 with ezrin in C666-1 cells, co-immunoprecipitation assay was performed. Briefly, whole cell lysate of C666-1 cells was extracted and immuno-precipitated with anti-CD44 antibody, and then the presence of ezrin in the precipitate was checked by Western blot method. Results in Figure 3.8 show that ezrin could be detected in the CD44 precipitate. This observation further confirmed that CD44 associates with the migration regulatory component ezrin and regulates migration of C666-1 cells.

3.2.8 ICG-001 enhances the expression of miR-150

Next, the possible mechanism involving in the downregulation of CD44 in ICG-001-treated NPC cells was examined. Recent miRNA expression study showed that the expression level of miR-150 is reduced in NPC tissues (Wang *et al.*, 2015). Further bioinformatics analysis of the 3'-UTR of CD44 using TargetScan algorithm (Release 6.2: June 2012) revealed that CD44 is a potential target of miR-150 (Figure 3.10A), thereby we hypothesized that miR-150 might take part in regulating the expression of CD44 in ICG-001-treated cells. In the miRNA expression analysis, we measured the levels of miR-150 in C666-1 cells under the monolayer culture and spheroid growing conditions. Results in Figure 3.9A, 3.9B and 3.9C showed that ICG-001 could restore miR-150 expression under these culture conditions. The restored expression of miR-150 was also observed in another EBV-positive C17 (Figure 3.9D) and EBV-negative HONE-1 NPC cells (Figure 3.9E).

3.2.9 CD44 is a novel target of miR-150

A 3'-UTR reporter assay was then used to verify the targeting of the 3'UTR of CD44 mRNA by miR-150. C666-1 cells were transfected with a wild type or mutant CD44 3'-UTR reporter together with pre-miR150 (miR-150 mimic) or miRNA mimic control. Results in Figure 3.10B showed that miR-150 could significantly (p = 0.009) reduce the wild type 3'-UTR reporter activity and its effect on the mutant 3'-UTR was not significant (p = 0.158). To further validate the association between miR-150 and CD44, we checked the protein level of CD44 in miR-150 overexpressing cells using Western blot. In order to elevate the endogenous level of miR-150, we transfected the cells with synthetic miR-150 mimic molecules (Figure 3.10C). Afterwards, the expression of CD44 was found

to be reduced (Figure 3.10D). These observations clearly indicated that CD44 is a novel target of miR-150 in NPC cells.

3.2.10 Overexpression of miR-150 resulted in the reduction of the migration of C666-1 cells but not the growth of tumor spheres

As mentioned in Section 3.2.6, siRNA knockdown of CD44 only inhibits the migration, but not the growth of NPC tumor spheres. These two biological assays, namely tumor cell migration assay and spheroid formation assay, were then used to further evaluate the functional implication of miR-150/CD44 axis in NPC cells. Results in Figure 3.11A showed that the migratory activity of pre-miR-150 transfected C666-1 cells was significantly lower than the control transfected cells. However, exogenous miR-150 has no significant effect on the formation of tumor spheres (Figure 3.11B). Taken together, the miR-150/CD44 axis is involved in the regulation of NPC cell migration.

3.2.11 ICG-001 inhibits Dnmt1 expression

Recent studies indicate that Dnmt1-mediated DNA hypermethylation plays an important role in the inhibition of the transcription of miR-150 in anaplastic large-cell lymphoma (Hoareau-Aveilla *et al.*, 2015), so we sought to determine the role of Dnmt1 in ICG-001-mediated restoration of miR-150 in NPC cells. To address this issue, the effect of ICG-001 on the expression of Dnmt1 was first studied using Western blotting. Result in Figure 3.12 showed that the protein levels of Dnmt1 dropped after the cells treated with ICG-001.

3.2.12 Silencing Dnmt1 restores the expression of miR-150

Effect of Dnmt1 on the expression of miR-150 was subsequently demonstrated in the loss-of-function study. Successful knockdown of Dnmt1 protein expression by siRNA was shown in Figure 3.13A. Results for the restoration of expression of miR-150 in siDnmt1 cells were shown in Figure 3.13B. Results from these studies suggest that Dnmt1 is involved in ICG-001-induced restoration of miR-150.

3.3 Discussion

First of all, we observed a clear association between ICG-001-mediated inhibition of *in vitro* migration of NPC cells and the downregulated CD44 expression. ICG-001 is a CBP antagonist and functions in blocking the interaction between β-catenin and CBP and thereby inhibits the downstream transcription of a subset of Wnt target genes (Takahashi-Yanaga and Kahn, 2010). The reduced expression of CD44 by ICG-001 could be explained by the fact that CD44 is a well-known Wnt downstream target gene (Wielenga *et al.,* 1999; Schmitt *et al.,* 2014). CD44 is highly correlated with the transition between epithelial and mesenchymal states of cells. Tumor cells with reduced CD44 expression always acquire more epithelial phenotypes with fewer tendencies to migrate (Xu *et al*., 2015). Our study exactly demonstrated the role of CD44 in the migration of NPC cells, and additionally, the migration of NPC cells was mediated by Wnt signaling as well. Taken into account that ICG-001 could restore the expression of E-cadherin (an epithelial marker) and suppress vimentin (a mesenchymal marker) (Chan *et al.,* 2015), ICG-001 look likes effective to inhibit the migration of NPC cells via CD44.

Interestingly, we also observed a significant increase in the expression of miR-150 in the ICG-001-treated NPC cells. Previous studies showed that miR-150 is one of the miRNAs downregulated in NPC (Li *et al.,* 2011b; Wang *et al.,* 2015). Further bioinformatics analysis using TargetScan indicated that CD44 is a predicted target of miR-150. Using the CD44 3’UTR luciferase reporter assay, we confirmed in this study that CD44 is a novel target of miR-150. This observation suggested that the restored expression of miR-150 might be at least in part contributing to the

reduced protein expression of CD44 in ICG-001-treated NPC cells.

The biological functions of miR-150 in tumorigenesis are worthy of further discussion. The expression of miR-150 is significantly reduced in various tumors. These included colon cancer (Bao *et al.*, 2014), Chronic myeloid leukemia (Machova *et al.*, 2011), Acute lymphocytic leukemia (Morris *et. al,* 2013), mantle cell lymphoma (Zhao *et al.*, 2010), Burkitt lymphoma (Wang *et al.*, 2014), gastric cancer (Assumpcao *et al.*, 2015), esophageal squamous cell carcinoma (Yokobori *et al.*, 2013), and NK/T-cell lymphoma (Watanabe *et al.*, 2011). In Burkitt lymphoma, re-expression of miR-150 was found not only to inhibit tumor cell proliferation, but also induce the differentiation of the tumor cells by targeting c-Myb (Chen *et al.*, 2013). The involvement of the miR-150/Myb axis and regulation of tumor cell differentiation was also demonstrated in myeloid leukemia (Morris *et al.*, 2013). In NK/T-cell lymphoma, re-expression of miR-150 resulted in inhibition of tumor cell proliferation and induction of apoptosis through the downregulated expression of DKC1 and AKT2 (Watanabe *et al.*, 2011). In esophageal squamous cell carcinoma, the tumor suppressive activity of miR-150 is attributed to its targeting on the EMT inducer ZEB1 (Yokobori *et al.*, 2013). In addition, our results showed that over-expression of miR-150 could make the NPC cells reluctant to migrate. All these observations suggested that miR-150 is a tumor suppressor in several types of tumors and the effect is cellular context dependent.

Apart from the novel function of miR-150, namely the targeting of CD44 and inhibiting the migration of NPC cells, the pivotal role of CD44 in NPC cells was also further supported by the immuno-precipitation/immunoblotting assay that

CD44 co-precipitated with ezrin, an important cytoplasmic component known to be involved in the linkage with the migration controlling machinery in the cytoplasm. The result is reminiscent of the previous observation by Endo and co-workers that overexpression of the EBV viral protein LMP-1 in nasopharyngeal cells would activate ezrin and the subsequent linking of ezrin with CD44 (Endo *et al.*, 2009). Furthermore, immune-histochemical analysis of 200 NPC tissues revealed that the increased expression of ezrin was correlated with a higher rate of lymph node metastasis (Wang *et al.*, 2011). Similar observation was also recently made in EBV-associated gastric carcinoma with lymphoid stroma (GCLS). The higher level of ezrin in GCLS was found to be associated with lymph node metastasis (Tobo *et al.*, 2013). The importance of CD44 and ezrin has also recently been demonstrated in breast cancer. Donatello and co-workers recently showed that CD44 and ezrin are localized at different membrane location in non-migrating cells. Under the condition of stimulation of migration, CD44 binds to ezrin and regulates the migration of the breast tumor cells (Donatello *et al.*, 2012). Taken together, LMP-1/ezrin/CD44 appears to play an important role in promotion of the migration of NPC cells and ICG-001 may have an anti-migratory function through the restoration of the tumor suppressive miR-150 in NPC cells.

Another interesting observation is the involvement of Dnmt1 in the restoration of miR-150 expression. Previous study indicated that Dnmt1 could be transcriptionally regulated by Wnt signaling (Campbell and Szyf, 2013). In NPC, the mutation rate of NPC tumors is relatively low when compared with other types of tumors (Lin *et al.*, 2014; Dai *et al.*, 2016; Zheng *et al.*, 2016), and significant mutation of the major signaling components such as β-catenin or APC in the Wnt signaling pathway was not observed in the NPC tumors. However, the

reduced protein expression of many Wnt signaling negative regulators by epigenetic DNA hypermethylation appear to be the mechanism contributing to the dysregulation of the Wnt signaling (Li *et al.*, 2011a). The contribution of EBV viral protein-induced epigenetic alteration in NPC is also worthy of discussion. The viral proteins such as LMP1 and LMP2 have been implicated to affect the level of cellular DNA methyltransferase (Niller *et al.*, 2014; Perri *et al.*, 2015). The importance of EBV-induced overexpression of Dnmt1 has also been demonstrated in EBV-associated gastric carcinoma (Yau *et al.*, 2014). All the evidence indicates that both the host cell factors and the viral factors may contribute to the dysregulation of Wnt signaling in NPC cells. ICG-001 is a CBP antagonist targeting the distal end of the Wnt signaling pathway (Teo and Kahn, 2010). In the present study, ICG-001 was found to interrupt the β-catenin/CBP Wnt signaling-mediated tumor cell migration via the Dnmt1/miR-150/CD44 axis in NPC cells (Figure 3.14). This study also reported a novel function of miR-150 in NPC cells. Taken together with our previous observations (Chan *et al.*, 2015), therapeutic intervention of the Wnt signaling pathway with this CBP antagonist is a strategy for the inhibition of the growth and dissemination of the NPC tumor cells.

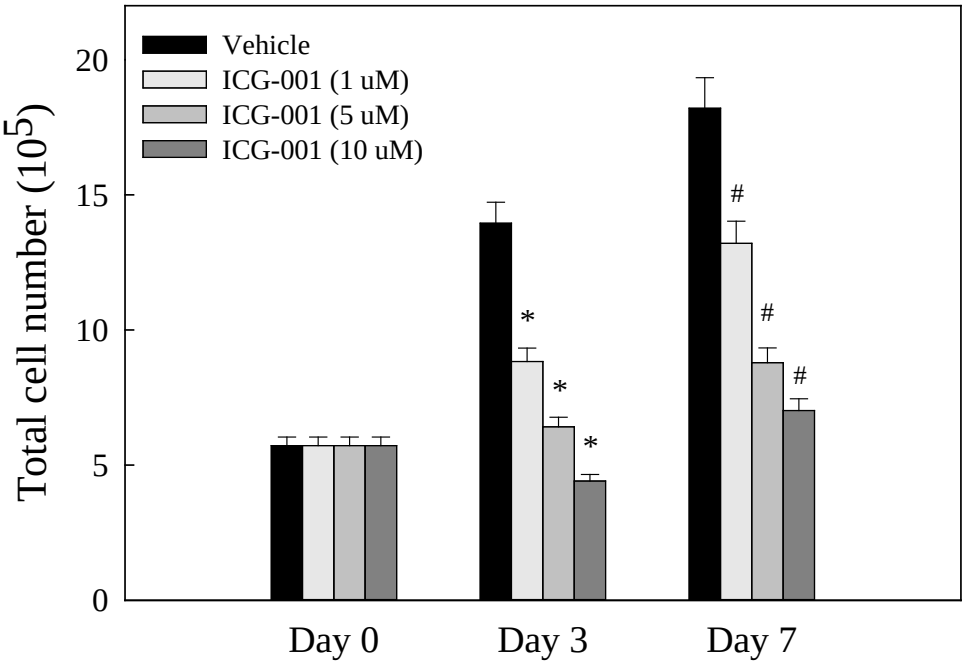

Figure 3.1 | ICG-001 inhibits growth of C666-1 cells in dose-dependent manner. C666-1 cells were treated with ICG-001 (1, 5, 10 μM) for 3 or 7 days. Numbers of viable cells were counted by trypan blue staining method. Cells treated with DMSO are vehicle control groups. Representative result was presented from at least three separate experiments. *$p < 0.05$ and #$p < 0.05$ compared to corresponding vehicle controls.

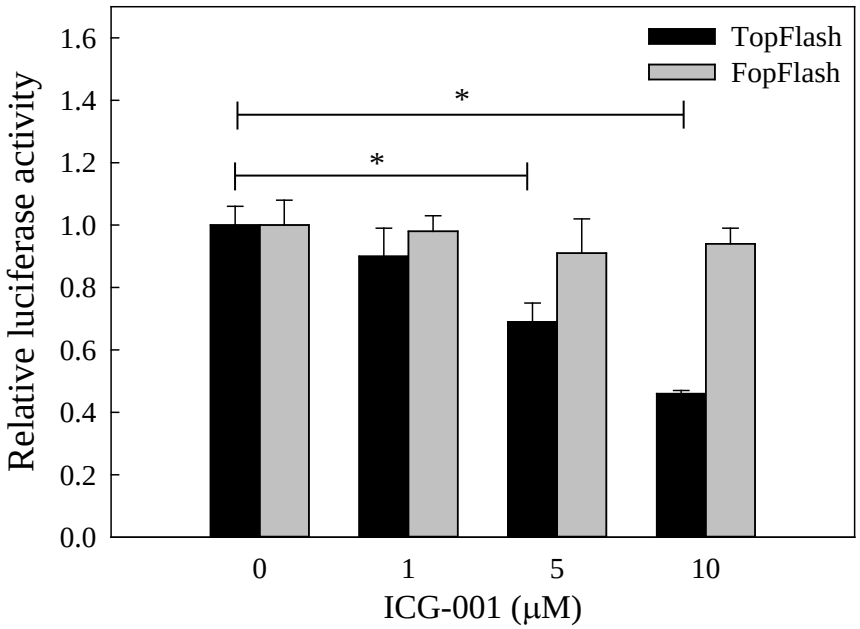

Figure 3.2 | ICG-001 inhibits canonical Wnt signaling in C666-1 cells. Cells were transfected with TopFlash or FopFlash reporter plasmids together with pRL-TK vector, followed by incubation with various concentrations of ICG-001 as indicated. Luciferase activity was normalized by the ratio of firefly and Renilla luciferase signals. Two separate experiments were carried out. *$p < 0.05$ compared to corresponding vehicle controls.

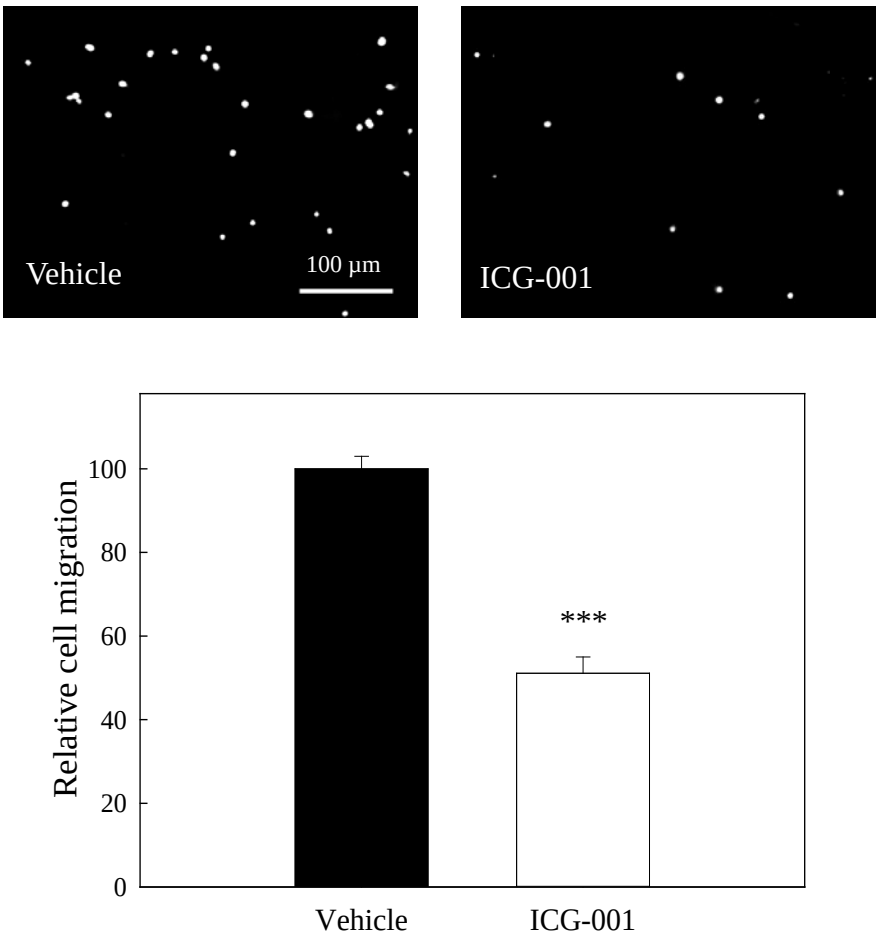

Figure 3.3 | ICG-001 inhibits the migration of C666-1 cells. Cells treated with ICG-001 (10 μM) or DMSO (vehicle control) for 7 days were collected and seeded onto the upper chamber of the transwell inserts. After 24 hour-incubation, the migrated cells were stained and the images were captured by a fluorescent microscope, and representative images were presented in the upper panel. Scale bar = 100 μm. The number of migrated cells were counted and presented in percentage compared to vehicle control group in the lower panel. Four separate experiments were carried out. ***$p < 0.001$ compared to vehicle control.

(A)

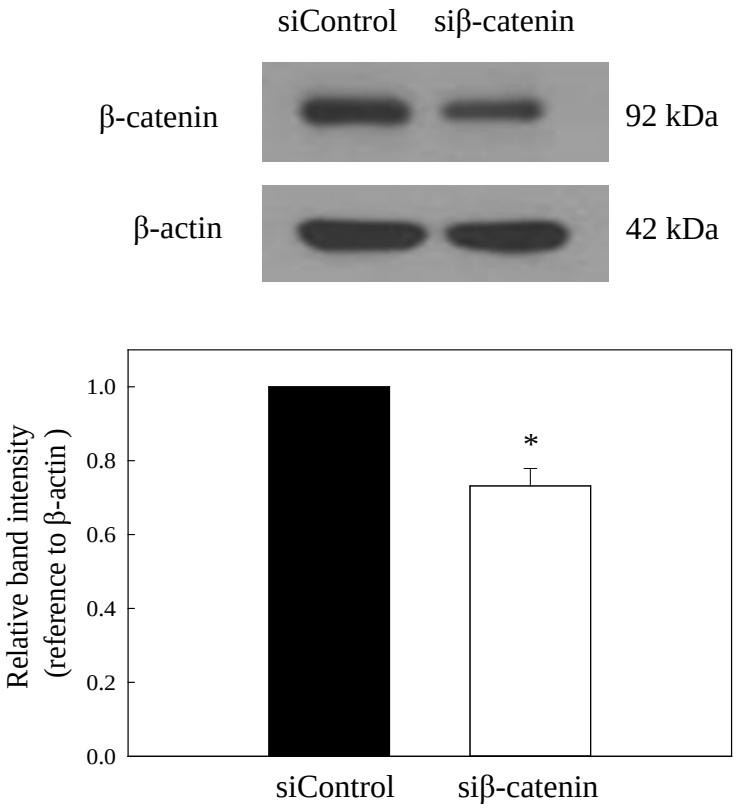
siControl
siβ-catenin
β-catenin
92 kDa
β-actin
42 kDa
Relative band intensity
(reference to β-actin)
1.0
0.8
0.6
0.4
0.2
0.0
*
siControl
siβ-catenin

(B)

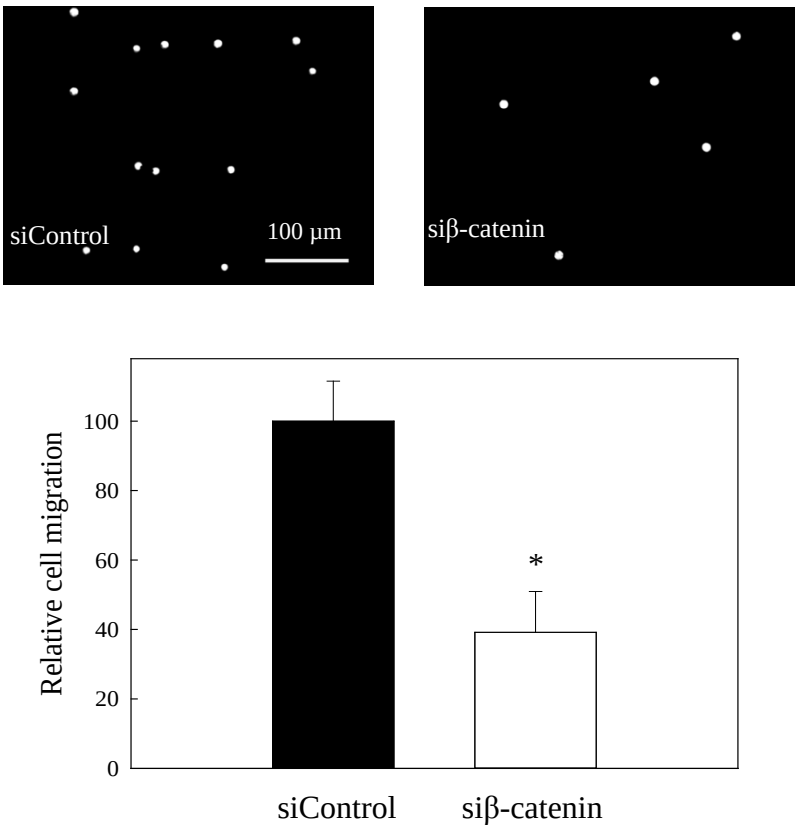
siControl
100 μm
siβ-catenin
Relative cell migration
100
80
60
40
20
0
*
siControl
siβ-catenin

Figure 3.4 | Knock-down of β-catenin inhibits the migration of C666-1 cells. Cells were transfected with siRNA targeting β-catenin (siβ-catenin) or non-targeting control RNA (siControl) at 50 nM. (A) Transfection efficiency of β-catenin siRNA in C666-1 cells was confirmed by Western blotting analysis with β-actin as a control. (B) The transfected cells were seeded onto the upper chamber of the transwell inserts. The migrated cells were stained after 24 hours and the images were captured by a fluorescent microscope, and representative images were presented in the upper panel. Scale bar = 100 μm. The number of migrated cells were counted and presented in percentage compared to the vehicle control group in lower panel. Three separate experiments were carried out. $*p < 0.05$ compared to siRNA control.

(A)

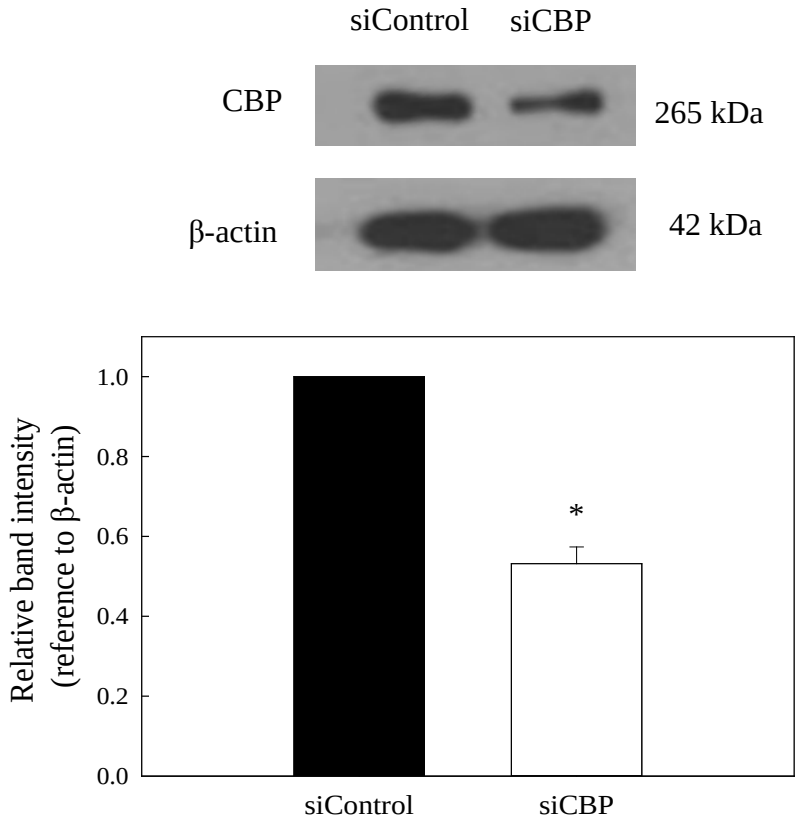
siControl
siCBP
CBP
265 kDa
β-actin
42 kDa
Relative band intensity
(reference to β-actin)
1.0
0.8
0.6
0.4
0.2
0.0
*
siControl
siCBP

(B)

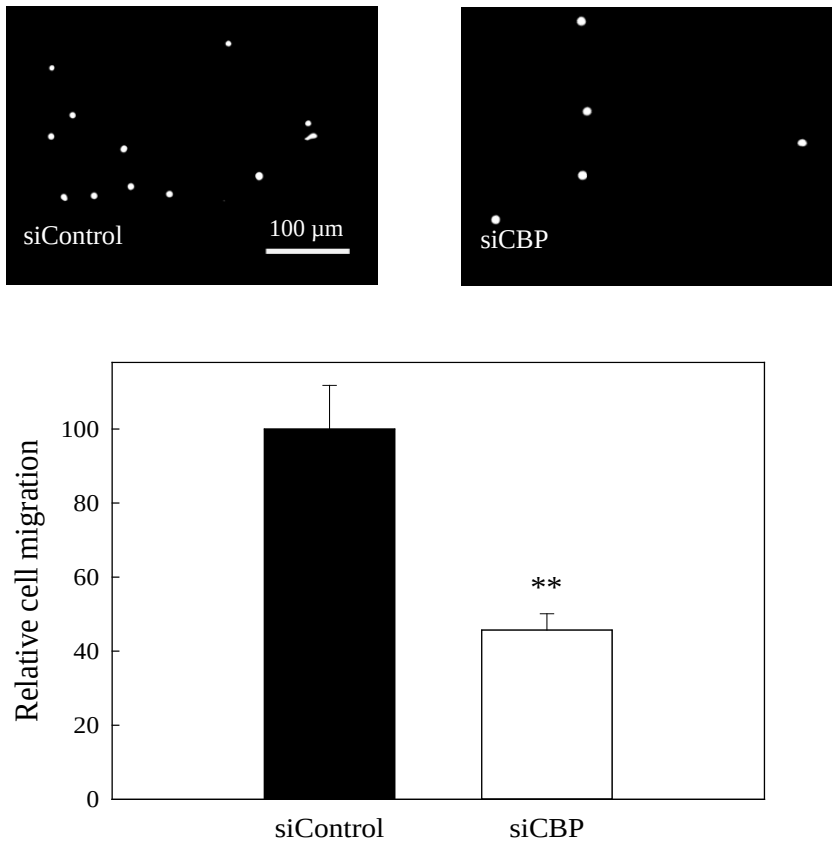
siControl
100 μm
siCBP
Relative cell migration
100
80
60
40
20
0
**
siControl
siCBP

Figure 3.5 | Knock-down of CBP inhibits the migration of C666-1 cells. Cells were transfected with siRNA targeting CBP (siCBP) or non-targeting control RNA (siControl) at 50 nM. (A) Transfection efficiency of CBP siRNA in C666-1 cells was confirmed by Western blotting analysis with β-actin as a control. (B) The transfected cells were seeded onto the upper chamber of the transwell inserts. The migrated cells were stained after 24 hours and the images were captured by a fluorescent microscope, and representative images were presented in upper panel. Scale bar = 100 μm. The number of migrated cells were counted and presented in percentage compared to the vehicle control group in lower panel. At least three separate experiments were carried out. *$p < 0.05$; **$p < 0.01$ compared to siRNA control.

(A)

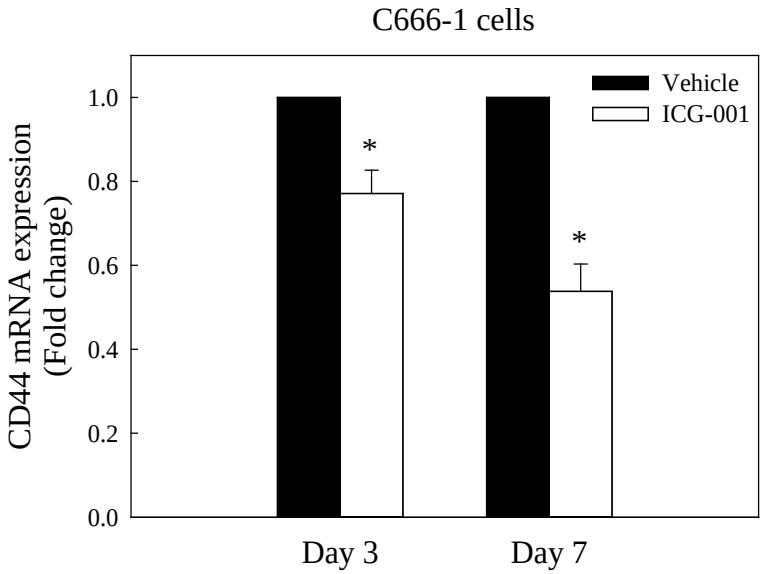
C666-1 cells
CD44 mRNA expression
(Fold change)
1.0
0.8
0.6
0.4
0.2
0.0
Vehicle
ICG-001
*
*
Day 3
Day 7

(B)

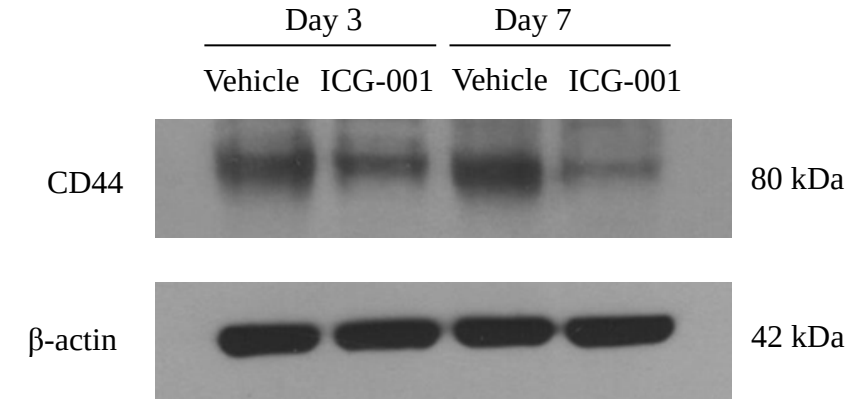
Day 3
Day 7
Vehicle
ICG-001
Vehicle
ICG-001
CD44
80 kDa
β-actin
42 kDa

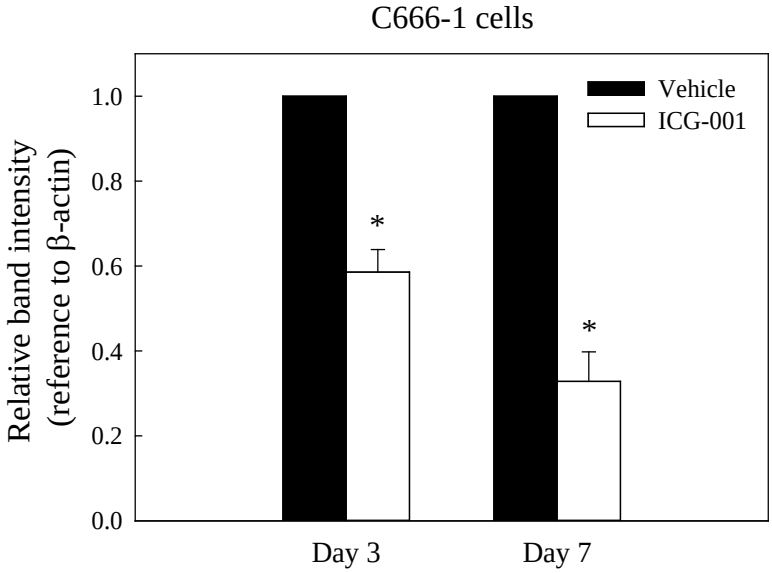
C666-1 cells
Relative band intensity
(reference to β-actin)
1.0
0.8
0.6
0.4
0.2
0.0
Vehicle
ICG-001
*
*
Day 3
Day 7

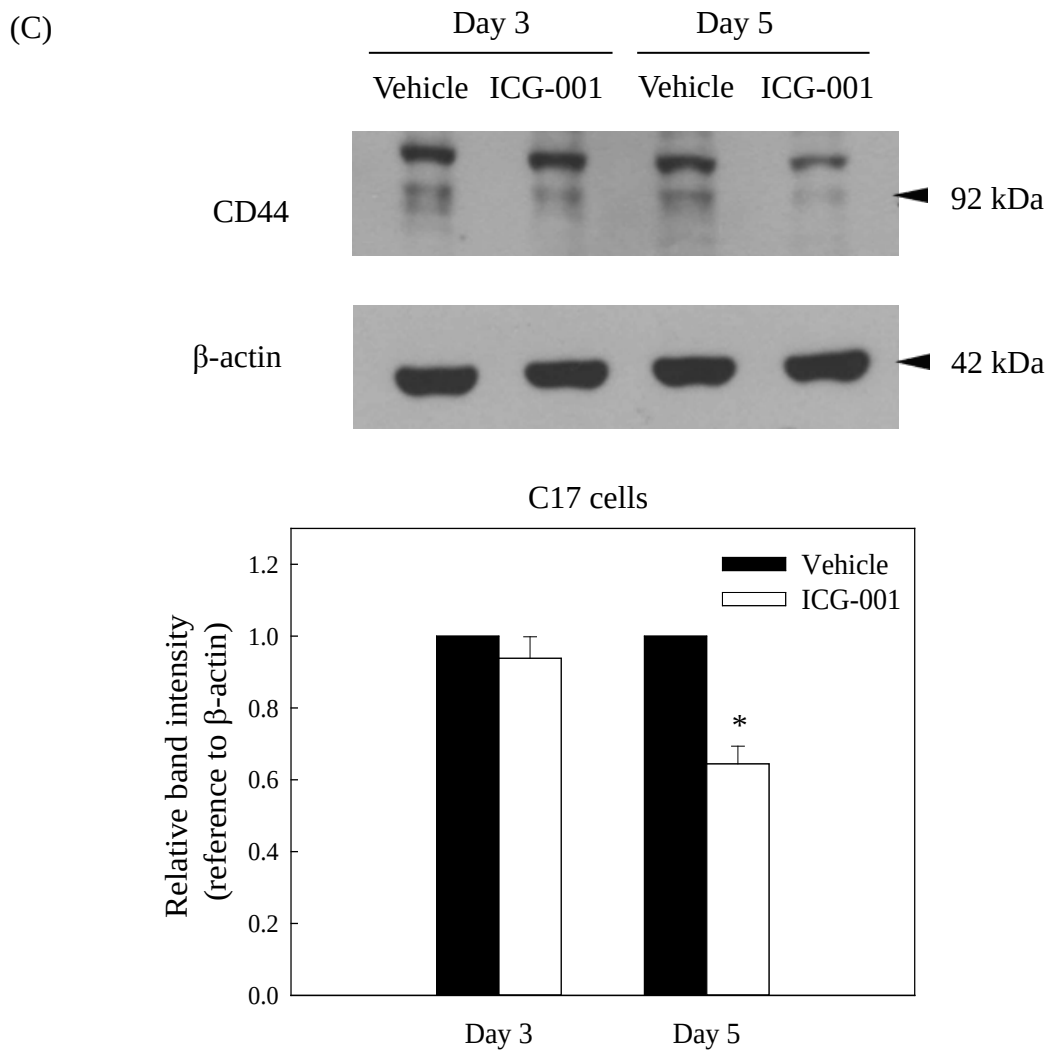

Figure 3.6 | ICG-001 down-regulates CD44 expression. NPC cells were treated with ICG-001 (10 μM) or DMSO (vehicle control) for days indicated. (A) Total RNA of C666-cells was harvested and the relative expression level CD44 mRNA was measured using qRT-PCR. The expressions of CD44 protein in (B) C666-1 cells and (C) C17 cells were determined by Western-blotting analysis. Signal intensities were determined by quantitative densitometry and the results were expressed as fold change of CD44 normalized to β-actin. Values are presented as means ± SD of at least three independent experiments. *$p < 0.05$ compared with vehicle control.

(A)

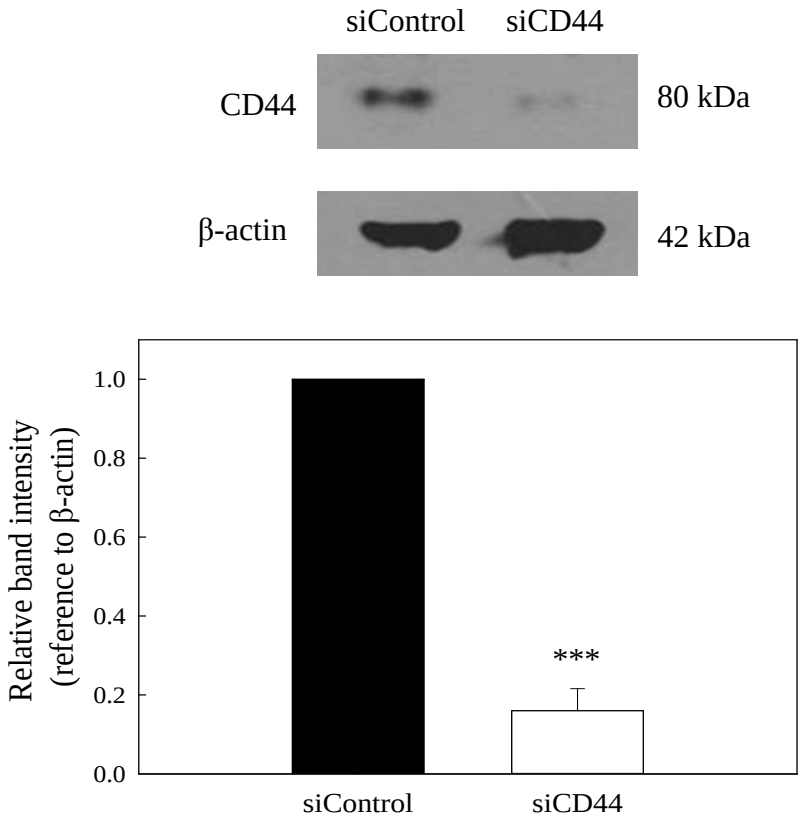
siControl
siCD44
CD44
80 kDa
β-actin
42 kDa
Relative band intensity
(reference to β-actin)
1.0
0.8
0.6
0.4
0.2
0.0
***
siControl
siCD44

(B)

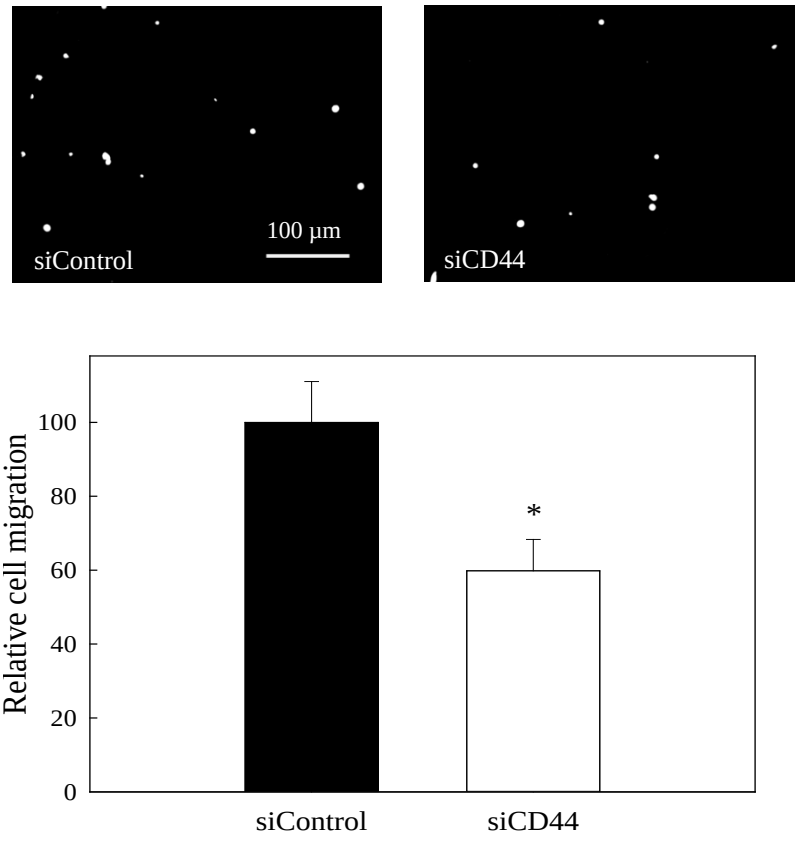
siControl
100 μm
siCD44
Relative cell migration
100
80
60
40
20
0
*
siControl
siCD44

(C)

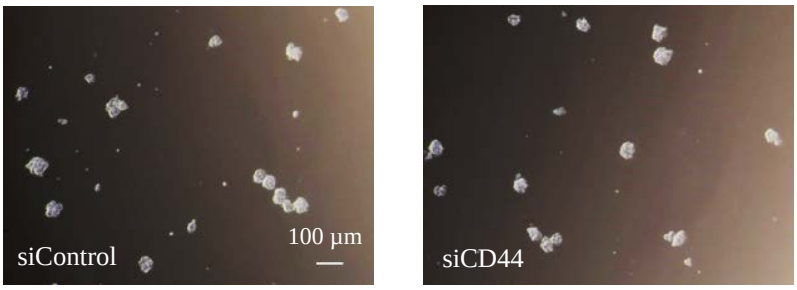
siControl
100 μm
siCD44

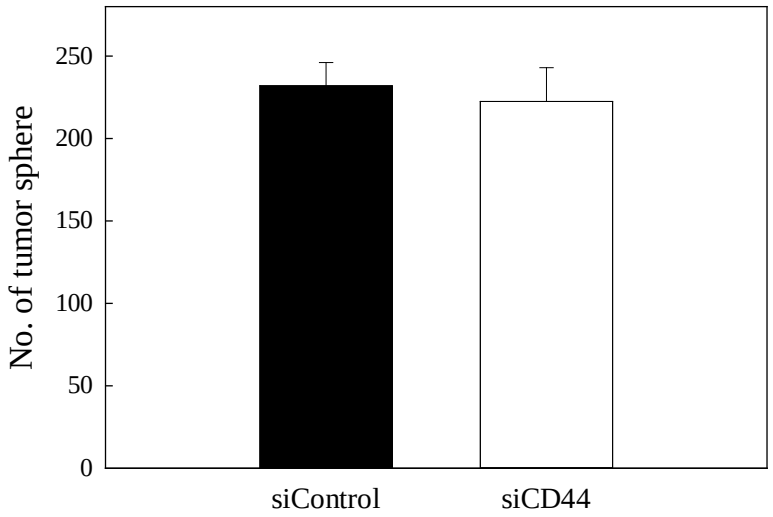
No. of tumor sphere
250
200
150
100
50
0
siControl
siCD44

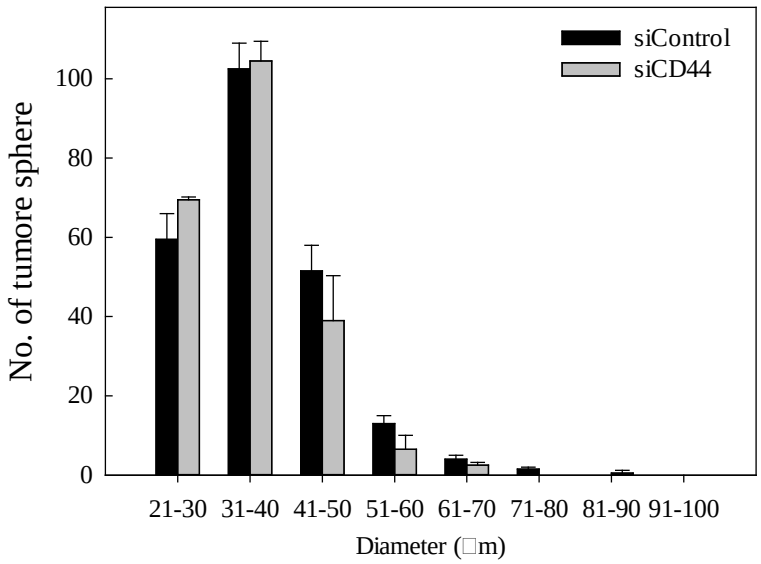
No. of tumore sphere
100
80
60
40
20
0
siControl
siCD44
21-30
31-40
41-50
51-60
61-70
71-80
81-90
91-100
Diameter (□m)

Figure 3.7 | Effect of CD44 in the migration of NPC cells. (A) Transfection efficiency of CD44 siRNA (50 nM) in C666-1 cells was confirmed by Western blotting analysis with β-actin as a control. (B) Cells transfected with CD44 siRNA showed lower migratory ability, as demonstrated by transwell migration assay. Representative images were presented in the upper panel and the number of migrated cells were counted and presented in percentage compared to mimic control group in lower panel. (C) Tumor sphere formation assay: CD44 siRNA showed no effect on the number or size of tumor spheres formed from C666-1 cells. The total number of tumor spheres (upper panel), representative bright field images (middle panel) and their size profile (lower panel) were presented. At least three separate experiments were carried out. $*p < 0.05$; $***p < 0.001$ compared to siRNA control.

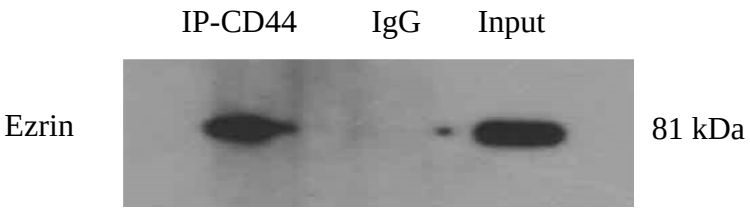

Figure 3.8 | Co-IP assay indicated that CD44 associated with ezrin in C666-1 cells. Ezrin from cell lysate was immunoprecipitated with anti-CD44 antibody and detected using anti-ezrin antibody in Western blotting analysis. Representative image from three individual experiments was presented.

(A)

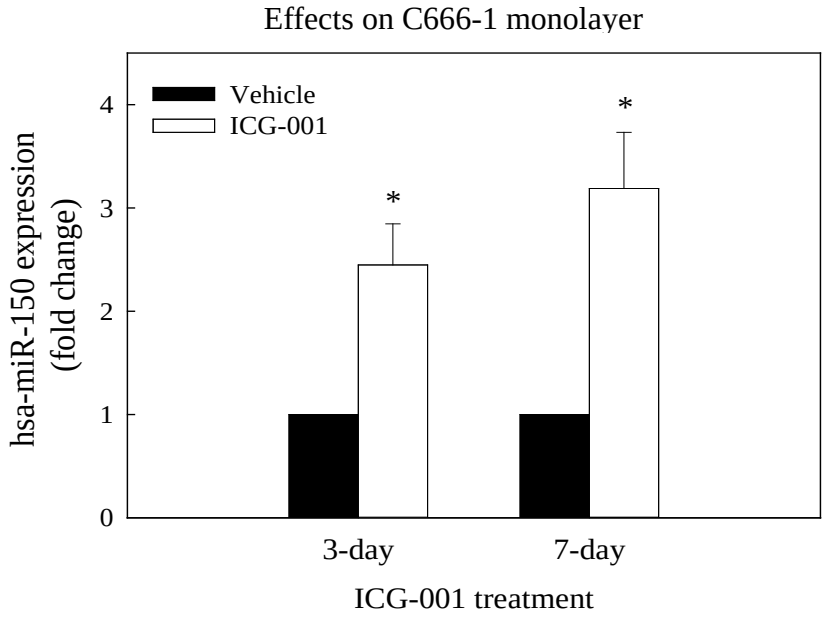
Effects on C666-1 monolayer
Vehicle
ICG-001
hsa-miR-150 expression
(fold change)
0
1
2
3
4
*
*
3-day
7-day
ICG-001 treatment

(B)

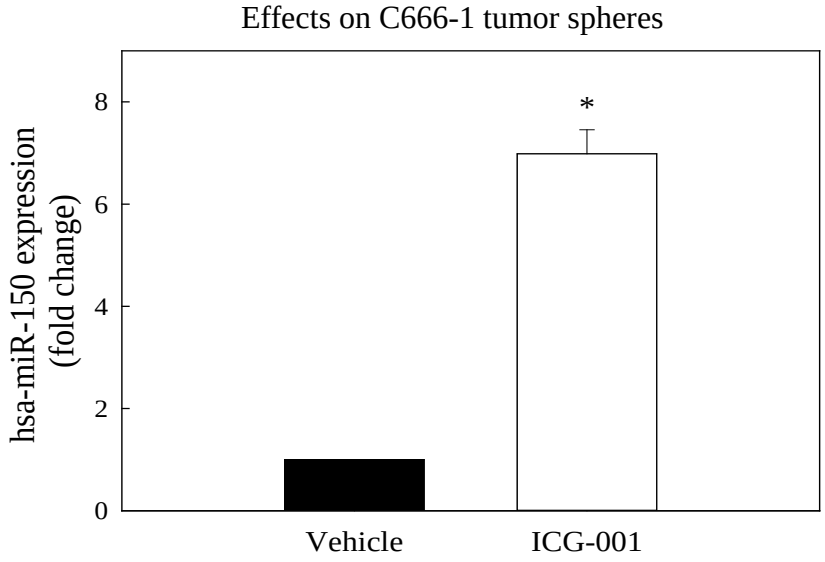
Effects on C666-1 tumor spheres
hsa-miR-150 expression
(fold change)
0
2
4
6
8
*
Vehicle
ICG-001

(C)

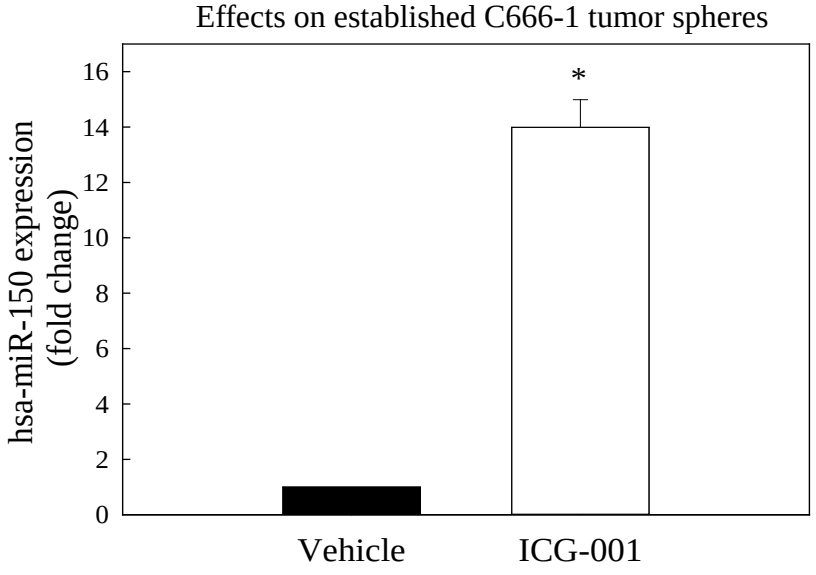
Effects on established C666-1 tumor spheres
hsa-miR-150 expression
(fold change)
0
2
4
6
8
10
12
14
16
*
Vehicle
ICG-001

(D)

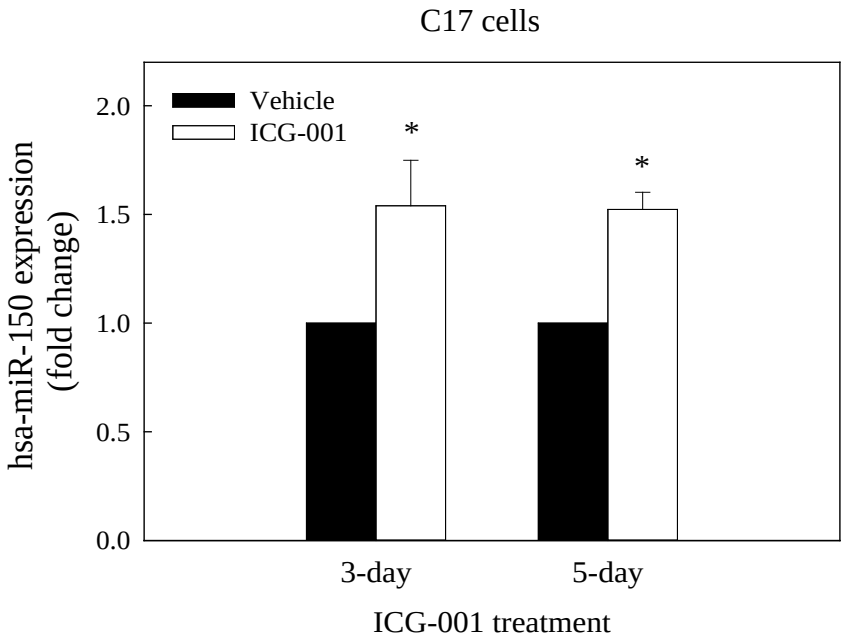
C17 cells
Vehicle
ICG-001
hsa-miR-150 expression
(fold change)
2.0
1.5
1.0
0.5
0.0
*
*
3-day
5-day
ICG-001 treatment

(E)

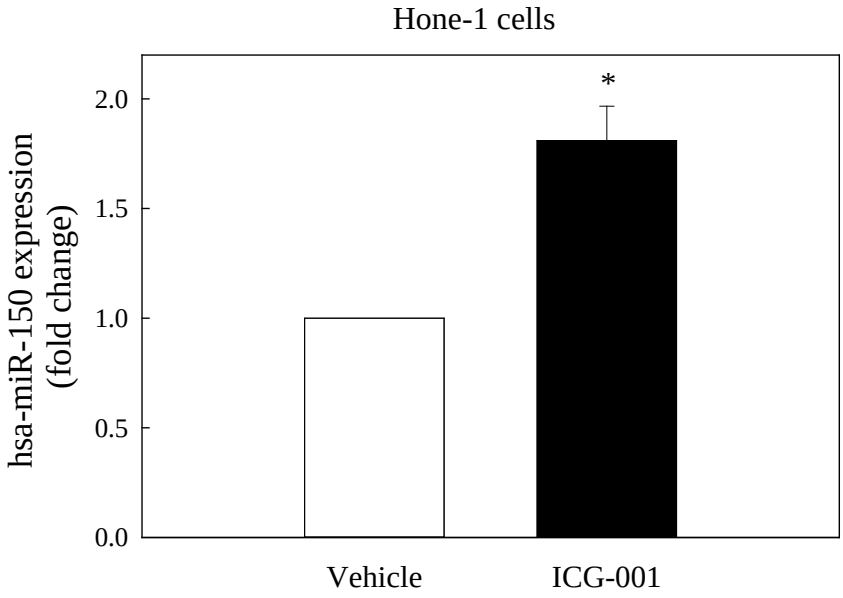
Hone-1 cells
hsa-miR-150 expression
(fold change)
2.0
1.5
1.0
0.5
0.0
*
Vehicle
ICG-001

Figure 3.9 | ICG-001 enhances the expression of miR-150 in NPC cells. (A) C666-1 cells (monolayer culture) were treated with ICG-001 (10 μM) or DMSO (vehicle) for 3 or 7 days. (B) Tumor sphere cultures: C666-1 cells were allowed to grow in ultra-low attachment culture plate along with the treatment of ICG-001 (10 μM) or DMSO for 7 days. (C) Effects on the established tumor spheres: C666-1 cells were allowed to grow for 7 days to form tumor spheres. Then, ICG-001 (10 μM) or DMSO was added to the culture and the cells were further incubated for another 7 days. (D) Another EBV-positive C17 cells were treated with ICG-001 (10 μM) or DMSO (vehicle) for 3 or 5 days. (E) An EBV-negative HONE-1 cells were treated with ICG-001 (10 μM) or DMSO (vehicle) for 5 days. The expression level of miR-150 in various samples was subsequently measured using qRT-PCR. At least three individual experiments were performed, and each experiment was in duplicate. *$p < 0.05$ compared to vehicle.

(A)

CD44 3'UTR ...UUUUUCAGAUGCUUCUGGGAGAC... 3'

hsa-miR-150 GUGACCAUGUUCCCAACCCUC 5'

CD44 3'UTR mutant ...UUUUUCAGAUGCUUCCCCCCCAC 3'

(B)

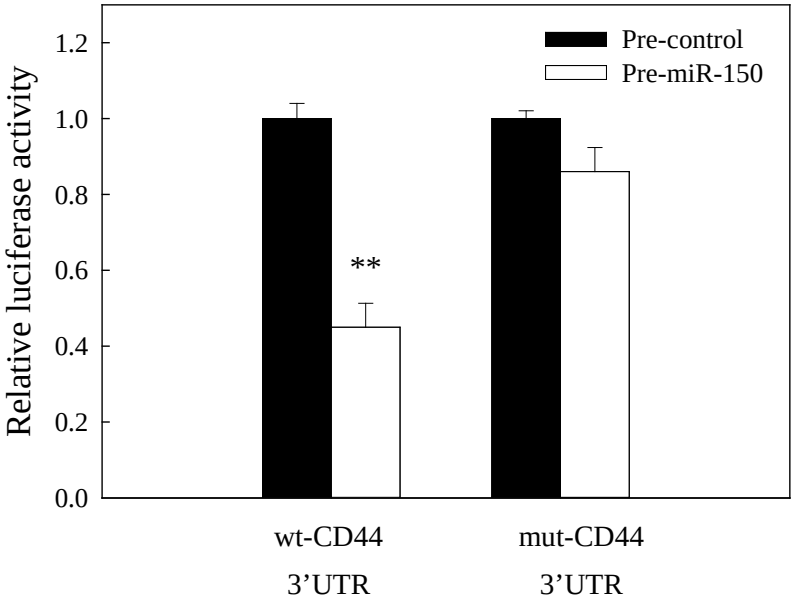

(C)

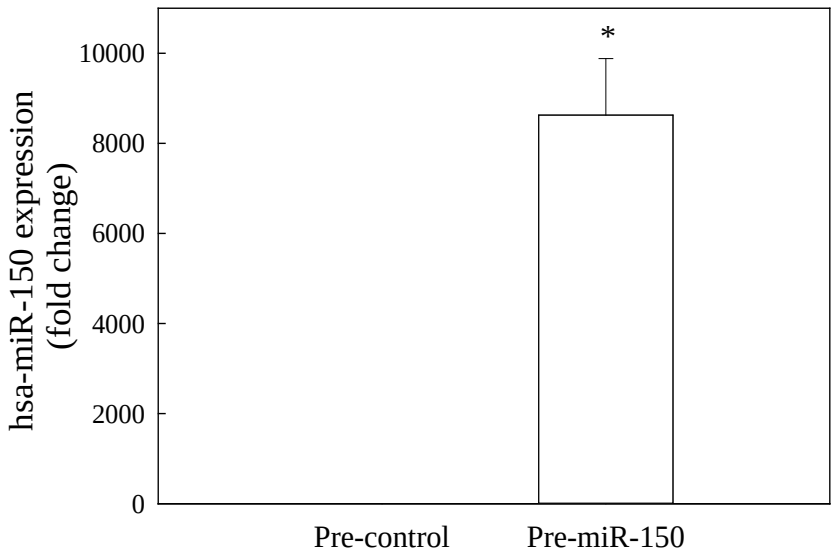

(D)

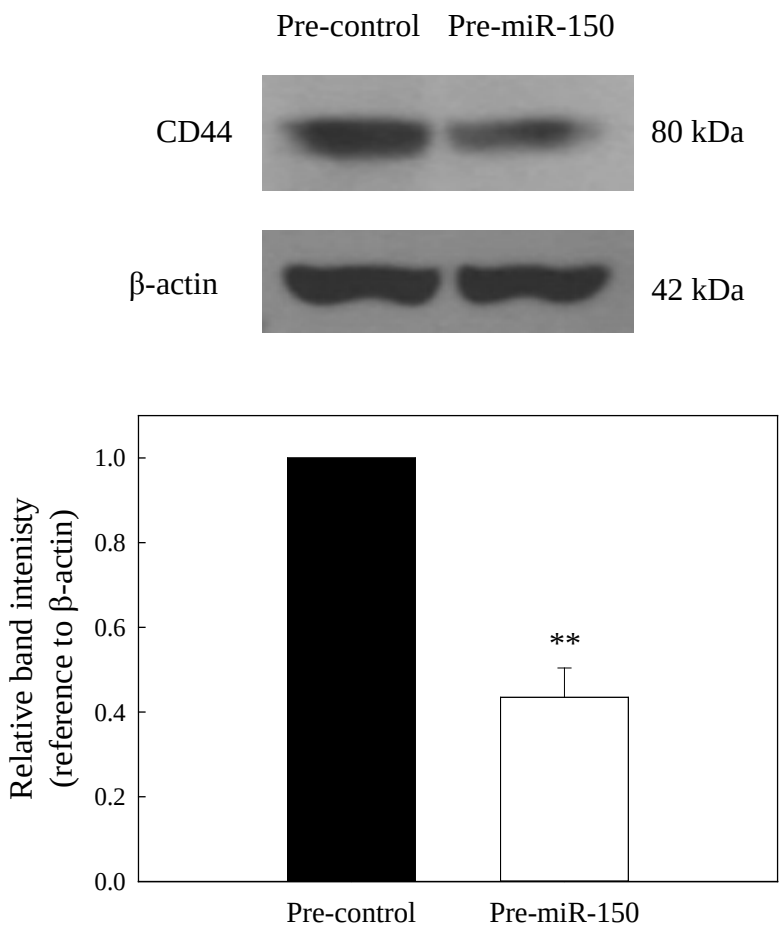

Figure 3.10 | miR-150 directly targets CD44 transcript. (A) Putative binding site of miR-150 on CD44 mRNA 3'-UTR was predicted using TargetScan (Release 6.2: June 2012). (B) C666-1 cells were co-transfected with miR-150 precursor (or miRNA precursor control) (200 nM) and wild-type CD44 3'-UTR reporter vector (wt-CD44 3'UTR) (or mutant CD44 3'-UTR reporter vector, mut-CD44 3'UTR) (50 ng). Luciferase activity was normalized by the RFP signal. (A) The transfection efficiency of miR-150 precursor (pre-miR-150, 50 nM) in C666-1 cells was confirmed by real-time PCR. (B) miR-150 inhibits the protein expression of CD44. Values were presented as the means ± SD of at least three independent experiments. *$p < 0.05$; **$p < 0.01$.

(A)

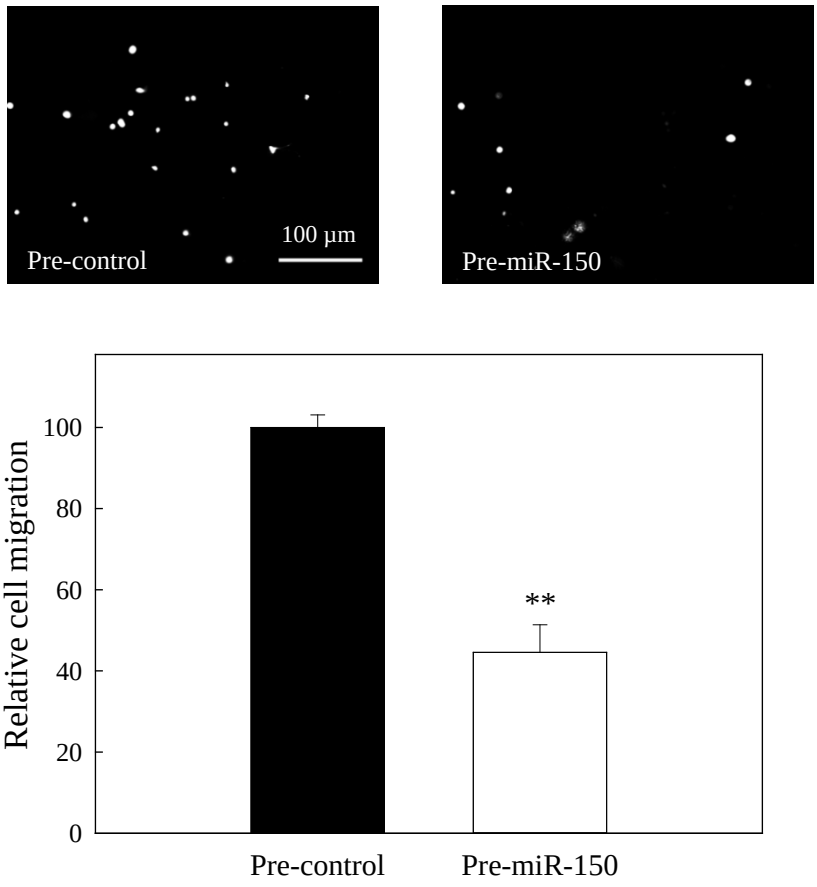
100 μm
Pre-control
Pre-miR-150
Relative cell migration
100
80
60
40
20
0
**
Pre-control
Pre-miR-150

(B)

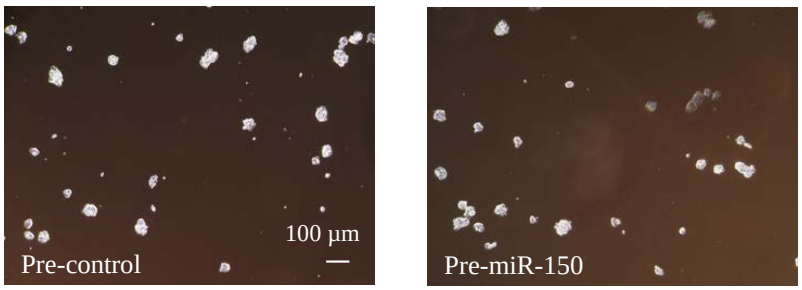
100 μm
Pre-control
Pre-miR-150

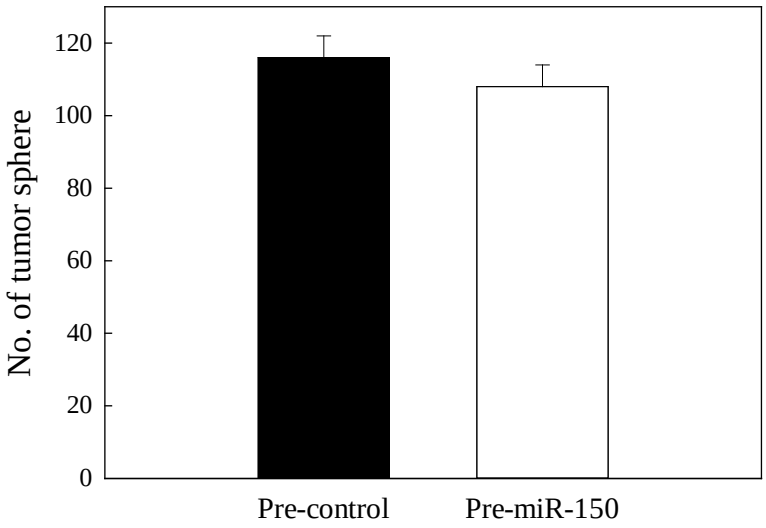
No. of tumor sphere
120
100
80
60
40
20
0
Pre-control
Pre-miR-150

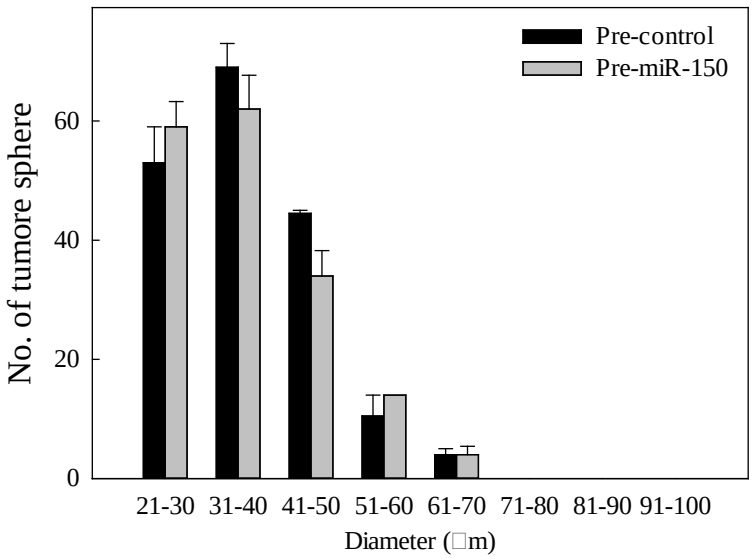
Pre-control
Pre-miR-150
No. of tumore sphere
60
40
20
0
21-30
31-40
41-50
51-60
61-70
71-80
81-90
91-100
Diameter (□m)

Figure 3.11 | Overexpressing miR-150 inhibits the migration of C666-1 cells, but not the spheroid formation. (A) Cells transfected with 50 nM miR-150 precursor showed lower migratory ability, compared to mimic control group. The migrated cells were stained and the images were captured by a fluorescent microscope, and the representative images were presented in the upper panel.. Migrated cells were counted and presented in percentage compared to mimic control group in lower panel. (B) Overexpressing miR-150 did not affect the tumor sphere forming ability of C666-1 cells. The transfected cells were subjected to spheroid formation assay. Images of all tumor spheres were captured under microscope and measured by ImageJ software. The total number of tumor spheres (upper panel), representative bright field images (middle panel) and their size profile (lower panel) were presented. At least three separate experiments were carried out. $^{**}p < 0.01$ compared to mimic control.

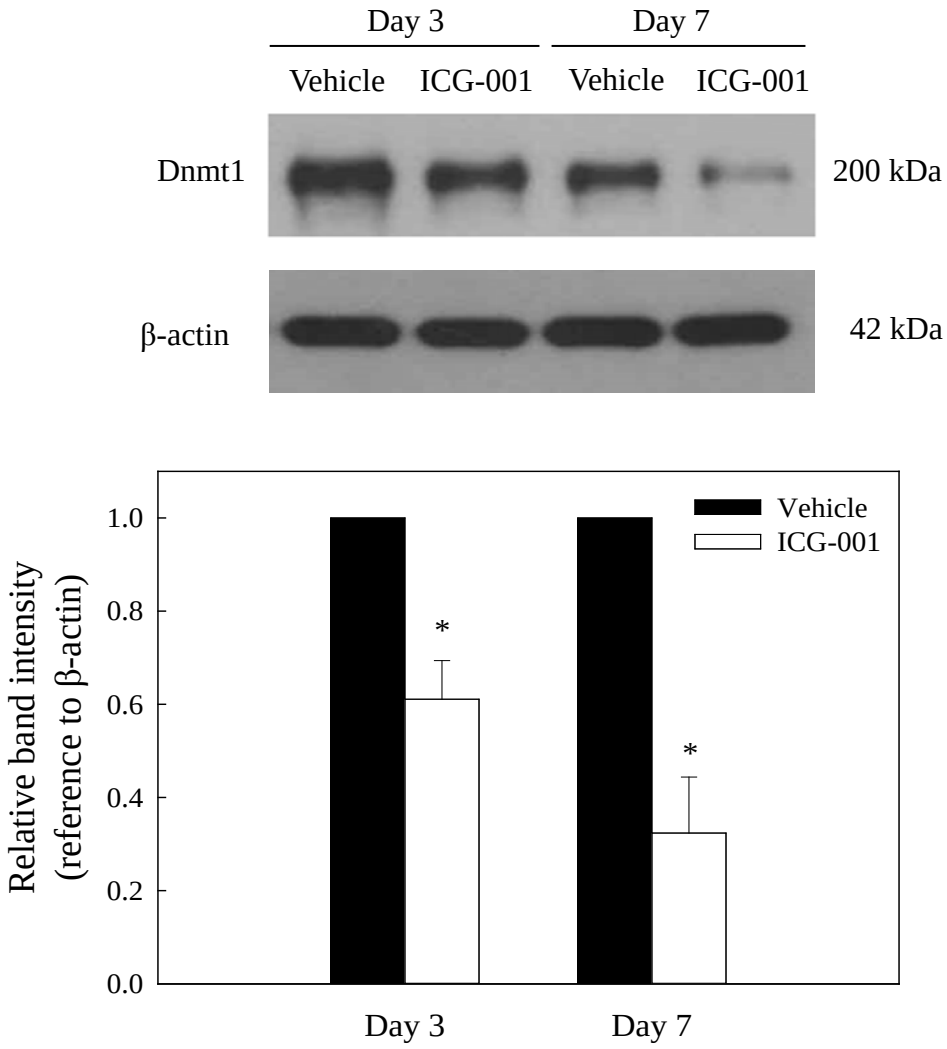

Figure 3.12 | ICG-001 down-regulates Dnmt1 expression. C666-1 cells were treated with ICG-001 (10 μM) or DMSO (vehicle control). The expression of Dnmt1 protein at 3- and 7-day treatment was determined by Western-blotting analysis (upper panel). Signal intensities were determined by quantitative densitometry and expressed as fold change of Dnmt1 normalized to β-actin (lower panel). Values are presented as means ± SD of three independent experiments. *$p < 0.05$ compared with vehicle control

(A)

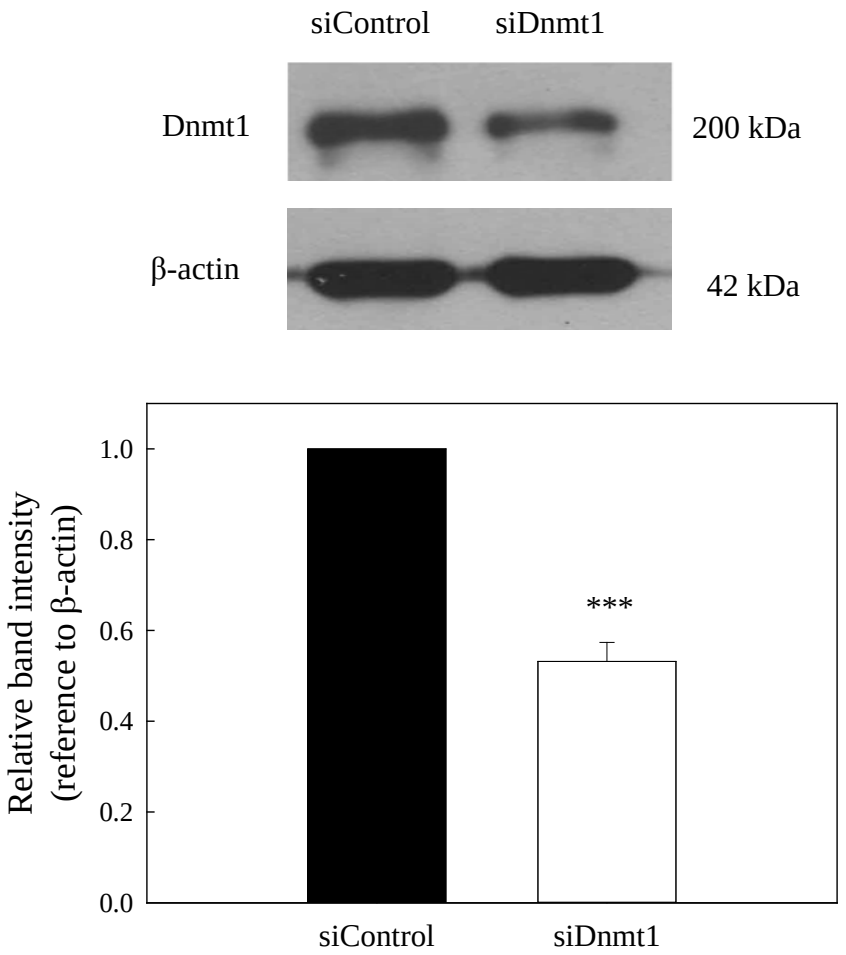
siControl
siDnmt1
Dnmt1
200 kDa
β-actin
42 kDa
Relative band intensity
(reference to β-actin)
1.0
0.8
0.6
0.4
0.2
0.0
***
siControl
siDnmt1

(B)

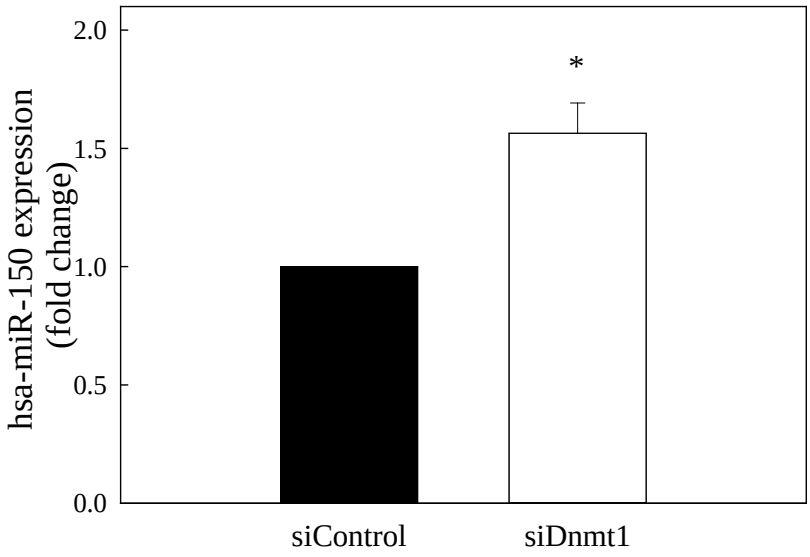
hsa-miR-150 expression
(fold change)
2.0
1.5
1.0
0.5
0.0
*
siControl
siDnmt1

Figure 3.13 | Dnmt1 activity regulates the expression level of miR-150. (A) Transfection efficiency of Dnmt1 siRNA (50 nM) in C666-1 cells was confirmed by Western blotting analysis with β-actin as a control. (B) Cells transfected with Dnmt1 siRNA had lower expression level of miR-150, as determined by qRT-PCR analysis. Three separate experiments were carried out. *$p < 0.05$; ***$p < 0.001$ compared to siRNA negative control.

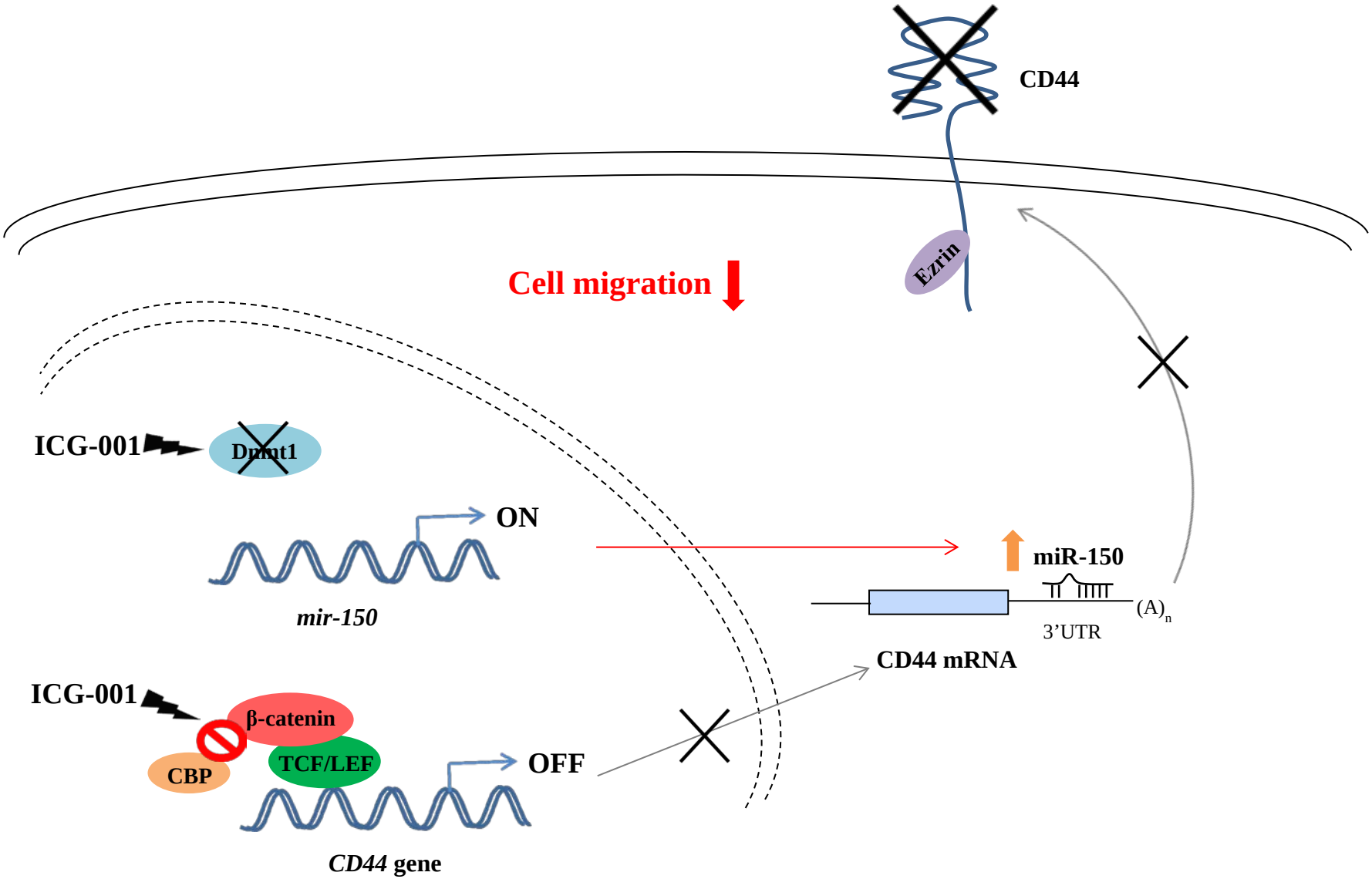
CD44
Ezrin
Cell migration
ICG-001
Dnmt1
ON
mir-150
miR-150
(A)n
3'UTR
CD44 mRNA
ICG-001
β-catenin
CBP
TCF/LEF
OFF
CD44 gene

Figure 3.14 | A schematic diagram of Dnmt1/miR-150/CD44 axis in ICG-001-treated cells. It is proposed that ICG-001 interrupts the β-catenin/CBP Wnt signaling and down-regulates Dnmt1 expression, leading to restore the expression of miR-150 and reduce CD44 expression. Reduced CD44-ezrin interaction is expected to hinder cell migration in ICG-001 treated NPC.

CHAPTER 4

Evi1 is involved in the growth suppression and migration of NPC cells

4.1 Introduction

Ecotropic viral integration site 1 (EVI1) is a nuclear zinc finger protein and is indispensable for self-renewal, maintenance, and proliferation of hematopoietic stem cells. In human, *MECOM* gene is located on chromosome 3q26.2 where Evi1 is encoded. However, Evi1 becomes oncogenic when the gene encountering any defect or inappropriate up-regulation. Evi1 has been mostly studied in myeloid malignancies since it was discovered in 1988. Growing evidence also showed an amplification and/or overexpression of Evi1 in other epithelial cancers such as ovarian, colorectal and liver cancers, people has started to highlight its relevance in cancer biology (Nanjundan *et al.*, 2007; Deng *et al.*, 2013; Yasui *et al.*, 2015).

In NPC, Evi1 was found to be amplified in several comparative genomic hybridization (CGH) analyses. Hui and her collaborator (2005) analyzed 26 NPC samples and found that a high-level amplification was commonly detected in some regions including 3q26.2 where *MECOM* located. This is reminiscent of another CGH analysis carried out by Guo *et al.* (2002), identifying an amplification at 3q26 as well. Later on, chromosome 3q26.2-q26.32 was suggested to be one of the genomic markers for prognosis of advanced NPC because of its consistently high incidence of gain in expression (Sheu *et al.*, 2009).

On the other hand, two independent genome-wide association study (GWAS) of NPC in southern Chinses individuals revealed that the region where *Evi1* located is one of the genetic susceptibility loci for NPC (Bei *et al.*, 2010; Tang *et al.*,

2012). Also, the SNP on *Evi1* gene was claimed to confer a protective effect for NPC risk by Lung's group (Ko *et al.*, 2014).

Although these findings reinforced the correlation between Evi1 and tumorigenesis of NPC, there is lack of molecular and functional studies on Evi1 regulation in NPC. In this part of study, therefore, we tried to 1) characterize the role of Evi1 in NPC cells, and (2) examine Evi1 in ICG-001-inhibited growth of tumor spheres and migration of NPC cells.

4.2 Results

4.2.1 ICG-001 inhibits tumor spheroid formation of C666-1 cells

Growing evidence suggests that the cases refractory to conventional radiotherapy and chemotherapy are attributed to the presence of CSCs within the tumor. Alternative cancer treatment targeting CSCs, thereby, is a promising strategy in the treatment of cancer patients. For this reason, effect of ICG-001 on growth of CSCs-enriched cultures was evaluated using tumor spheroid formation assay. As shown in Figure 4.1, when C666-1 cells were grown under the 3-D culturing condition with ICG-001 added at the very beginning of the assay, both number and diameter of the tumor spheres were found to be significantly inhibited dose-dependently.

4.2.2 ICG-001 inhibits the growth of established tumor spheres of C666-1 cells

Since ICG-001 had a remarkable inhibitory effect on the tumor sphere forming capacity, the inhibitory effect on the further growth of the established tumor spheres was subsequently evaluated. C666-1 cells were allowed to form tumor spheres for 7 days in a 3-D cell culture, and the established spheres were then treated with ICG-001 for another 7 days. Comparing to the control group, ICG-001 was found to dose-dependently (1 – 20 μM) to inhibit the growth of spheres (Figure 4.2).

4.2.3 Effect of ICG-001 pre-treatment on the growth of C666-1 tumor spheres

C666-1 cells were firstly treated with ICG-001 in the 2-dimensional (2-D) culture system. The treated cells were then harvested, washed and plated for the tumor sphere formation assay. Results in Figure 4.3 showed that cells pre-treated with ICG-001 failed to form tumor spheres, indicating that ICG-001-treated NPC cells lost the capacity to form tumor spheres.

4.2.4 ICG-001 down-regulates the expression of Evi1

Evi1 is generally considered as a proto-oncogene in various cancers. In the present study, the effects of ICG-001 treatment on the expression of Evi1 were examined. As shown in Figure 4.4A and 4.4B, both the transcripts and proteins of Evi1 in C666-1 cells were effectively reduced by ICG-001. Likewise, reduction in Evi1 protein by ICG-001 was also found in another EBV-positive NPC cell line (C17 cells) in Figure 4.4C. These results indicated that the expression of Evi1 in NPC cells could be inhibited by ICG-001.

4.2.5 Effect of Evi1 on the formation of tumor spheres and the migration of C666-1 cells

As previously shown in Section 3.2.3 and 4.2.1-3, ICG-001 could inhibit both the migration and tumor sphere forming capacities in NPC cells. Functional studies of Evi1 were subsequently performed using loss- and gain-of-function approaches to further examine the role of Evi1 in the migration and tumor sphere formation. A successful knock-down or overexpression of Evi1 protein were achieved by transfecting the cells with siRNA or an expression plasmid, respectively, and the corresponding images of protein bands and quantification analysis were presented

in Figure 4.5A. Number of tumor spheres and migrated cells were reduced when the expression of Evi1 in the cells was silenced by siRNA. In the gain-of-function study, the number of tumor spheres was increased when Evi1 was overexpressed in the cells. Interestingly, Evi1 seemed to have no significant effect on the size of tumor spheres formed (Figure 4.5B and 4.5C).

4.2.6 ICG-001 enhances the expression of miR-96 which targets the Evi1 transcript

There was a report showing that Evi1 protein level could be reduced when the pancreatic cancer cells were transfected with a synthetic miR-96 precursor (Tanaka *et al.*, 2014), so we speculated that the inhibition of Evi1expression in ICG-001-treated cells might also be regulated by miR-96. Using qRT-PCR analysis, we found that ICG-001 could stimulate the expression of miR-96 in all the C666-1, C17 and Hone-1 NPC cells (Figure4.6). Although Evi1 had previously been shown to be affected by miR-96, the target validation analysis had never been reported. So the association between miR-96 and Evi1 was further performed. Using TargetScan software (Release 7.1: June 2016), putative binding sites of miR-96 was predicted within the 3'UTR of Evi1 transcript (Figure 4.7A). After introducing the cells with miR-96 precursor, luciferase activity of the reporter plasmid containing sequence of 3'UTR of Evi1 was reduced, meaning that miR-96 could bind to the 3'UTR of Evi1 and suppress its transcription (Figure 4.7B). In the presence of miR-96 precursor, the cellular level of miR-96 was greatly elevated, and the reduction in the expression of both Evi1 transcript and protein were found in NPC cells. This phenomenon was in accordance with pancreatic cancer cells reported by Tanaka *et al.* (2014). By contrast, when miR-96 inhibitor was added, less miR-96 was detected, and then an increase in the

level of Evi1 transcript and protein could be seen in the cells (Figure 4.7C, 4.7D and 4.7E). Collectively, ICG-001 inhibited Evi1 expression at least partially through the stimulation of the expression of miR-96.

4.2.7 Effect of miR-96 on the formation of tumor spheres and the migration of C666-1 cells

Functional analysis of miR-96 on the tumor sphere formation and cell migration was carried out. Introduction of miR-96 precursors resulted in the reduction in the number and size of tumor spheres and also the migratory ability of the cells. Conversely, inhibiting endogenous miR-96 facilitated the tumor sphere forming and migratory capacities of C666-1 cells (Figure 4.8). A connection between miR-96 and the biological activities of C666-1 cells was then established in this part of the study.

4.2.8 ICG-001 enhances the expression of miR-449a

Previous study showed that there was a specific Evi1 binding site in the promoter region of *miR-449a* gene (De Weer *et al.*, 2011). Also, miR-449a was found to be down-regulated in two separate profile analysis on NPC tissues (Chen *et al.*, 2009; Luo *et al.*, 2012b). Given that Evi1 expression was affected by ICG-001 treatment in NPC cells, we first examined the expression level of miR-449a in ICG-001-treated NPC cells. According to Figure 4.9, expression of miR-449a was consistently up-regulated in C666-1, C17 and Hone-1 cells after receiving ICG-001 treatment. These results indicated that miR-449a might be another candidate miRNA being regulated by ICG-001 in NPC cells.

4.2.9 Overexpression of miR-449a inhibits the formation of tumor sphere and the migration of C666-1 cells

Further functional analysis of miR-449a on the tumor sphere formation and cell migration was carried out. Introduction of miR-449a resulted in the reduction of the size and number of tumor spheres, as well as the number of migrated cells (Figure 4.10).

4.2.10 Effect of silencing or overexpression of Evi1 on the expression of miR-96 and miR-449a

Results from the above studies indicated that miR-96 could affect the expression of Evi1 in NPC cells. In addition, Evi1 has been reported as a transcription factor of *miR-449a* gene (De Weer *et al.*, 2011). Therefore, the function of Evi1 on the expression of mature miR-96 and miR-449a was analyzed in this part of the study. Results showed that the cells transfected with Evi1 siRNA expressed more miR-96 and miR-449a. In contrast, the cells expressing more Evi1 possessed a lower level of these two miRNAs (Figure 4.11). These results indicated that miR-96 might inhibit Evi1 expression and vice versa. The observation is in accordance with Tanaka's study (2014) that Evi1 could affect the expression of miR-449a.

4.2.11 The coordination between miR-96 and miR-449a

According to Figure 4.12A, overexpression of miR-96 in C666-1 cells enhanced the expression of miR-449a, and inhibition on miR-96 reduced the expression of miR-449a. However, from Figure 4.12B, overexpression of miR-449a only slightly increased the expression of miR-96, but the difference is not statistically significant (p = 0.159). This finding suggested that miR-96 could regulate

miR-449a, but not vice versa. Up to here, we speculate miR-96/Evi1/miR-449a may be a potential molecular axis in ICG-001-inhibited tumorigenesis in NPC.

4.2.12 Knockdown of β-catenin or CBP inhibits tumor spheroid formation

Since ICG-001 is a CBP antagonist to inhibit the β-catenin/CBP-mediated transcription, and both β-catenin and CBP were demonstrated to involve in the migration of C666-1 cells in Chapter 3, we speculate that both β-catenin and CBP might involve in the tumor sphere formation. Results showed that silencing either β-catenin (Figure 4.13 A and B) or CBP (Figure 4.14A and B) actually impeded C666-1 cells to form tumor spheres. These observations suggested that the tumor spheroid formation of NPC cells is Wnt-dependent.

4.2.13 Knockdown of β-catenin or CBP enhances the expression of miR-96 and miR-449a

Next, we sought to know whether β-catenin or CBP could regulate the expression of miR-96 and miR-449a. As shown in Figure4.13C and Figure 4.14C, both expression levels of miR-96 and miR-449a were increased when either β-catenin or CBP was silenced in the cells.

4.2.14 Knockdown of p300 reduces the expression of miR96 and miR449a

In the canonical Wnt signaling, cell growth / differentiation is controlled by the interaction between β-catenin and the co-activator CBP (for cell proliferation), or the interaction between β-catenin and another structurally similar co-activator p300 (for the cell differentiation and inhibit cell proliferation) (Manegold *et al.*, 2011). Since that suppression of the growth of tumor spheres and restoration of miR-96 and 449a are β-catenin- and CBP-dependent, as described above, then the

effect of p300 knockdown on the expression of these two miRNAs was further examined. As shown in Figure4.15, the levels of miR-96 and miR-449a could be reduced when p300 was silenced in NPC cells. These observations suggested that the β-catenin-mediated cell growth/cell differentiation pathways are involved in the expressions of miR-96 and 449.

4.2.15 ICG-001 reduces the protein expression of survivin

Survivin is a well-known direct β-catenin responsive gene (Ring *et al.*, 2014) and survivin is also one of the best identified genes overexpressed in NPC (Tulalamba and Janvilisri, 2012). The first report mentioning ICG-001inhibiting survivin expression was published by Emami *et al.* (2004) using colon cancer as a model. In the present study, the expression of survivin in C666-1 NPC cells was also confirmed to be inhibited by ICG-001 treatment (Figure 4.16).

4.2.16 Silencing of survivin represses the expression of Evi1

Since the expression of Evi1 could be inhibited by ICG-001, and Evi1 was recently reported as a downstream target of survivin in hematopoietic stem cells (Fukuda *et al.*, 2015), then the correlation between the expression of survivin and Evi1 was further examined using knockdown experiment. Results in Figure 4.17A showed that the expression of Evi1 was reduced by around 30% in NPC cells after transfection with siRNA targeting survivin, indicating that the expression of Evi1 could be partly regulated by survivin. This part of study established the role of survivin in the regulation of Evi1 in NPC cells.

4.2.17 Effect of survivin knockdown on the expression of miR-96 and miR-449a

In Section 4.2.11, the miR-96/Evi1/miR-449a axis has been implicated in ICG-001-inhibited NPC tumorigenesis. In this part of study, the relationship between survivin and miR-96/Evi1/miR-449a was further examined. Results in Figure 4.17B showed that silencing of survivin resulted in the restoration of miR449a expression. However, a significant effect of knockdown of survivin on the up-regulated expression of miR-96 was not observed ($p = 0.280$). Results from these experiments indicated that survivin may be another upstream regulator of Evi1/miR-449a in ICG-001-mediated inhibition of tumor sphere formation in NPC.

4.3 Discussion

A potent inhibitory effect of ICG-001 on the cell migration and tumor sphere growth was clearly observed in NPC cells in this study. Subsequent characterization of the functional roles of Evi1 on the migratory and tumor sphere forming capacities helped us further explain the potent inhibitory effect of ICG-001in NPC cells. There are only a few reports to study the role of Evi1 in cell migration and also in the control of the growth of tumor spheres. Nanjundan *et al.*, (2007) was the first group to study the direct relationship between Evi1 and cell migration. They found that ovarian cancer cells overexpressed with Evi1 had a stronger migration activity using transwell migration assay. Later on, the pancreatic cancer cells with Evi1 knockdown were also found to exhibit a retarded migration tendency in the wound healing assay (Tanaka *et al.*, 2014). Recently, Evi1 was implicated to the cell migration and the tumor sphere formation in prostate cancer cells (Queisser *et al.*, 2016). In this part of study, we showed that knockdown of Evi1 in NPC cells inhibited the cell motility and tumor sphere forming capacity, but the overexpression could further enhance these processes in NPC cells. Since ICG-001 could reduce the expression of Evi1, we speculate that Evi1 is another regulator involved in ICG-001-mediated inhibition of NPC cells.

Previously, Evi1 was found to interact with some proteins belonging to the Wnt pathway, such as casein-kinase II (CK2) and transducin beta like 1 X-linked receptor 1 (TBL1XR1), according to a SILAC-based quantitative proteomic analysis (Bard-Chapeau *et al.*, 2013). More interestingly, silencing of β-catenin could downregulate Evi1 expression, and LEF/β-catenin complex could transcriptionally regulate Evi1 promoter (Manachai *et al.*, 2017). Since ICG-001

could reduce β-catenin expression, this may explain the inhibition of expression of Evi1 in ICG-001-teated cells. On the other hand, ICG-001 could also reduce the expression of survivin in NPC cells. Being a β-catenin/CBP-regulated gene, survivin was demonstrated to be capable of suppressing Evi1 expression in this study, which is concordant with the observation reported by Fukuda *et al.* (2015). Considering the processes of cell motility and the tumor sphere formation are Wnt-dependent, the findings here shed light on the potential use of ICG-001 in NPC through modulating the Wnt signaling pathway.

Next, we characterized the tumor-suppressive functions of miR-96 and miR-449a in ICG-001-treated NPC cells. We found that ICG-001 could increase the expression of both miR-96 and miR-449a and their increased expression might in turn reduce the cell motility and tumor sphere forming capacity of NPC cells. By analyzing the NPC biopsies staging from I to IV, miR-449a was consistently downregulated in different clinical stages (Luo *et al.*, 2012b). Rescuing the expression of miR-449a by ICG-001 may interfere with the progression of NPC. A key characteristic of miR-96 is its context-dependent phenotype in carcinogenesis (Ma *et al.*, 2016). MiR-96 was found to be oncogenic in breast, colon and prostate cancer (Hong *et al.*, 2016; Rapti *et al.*, 2016; Xu *et al.*, 2016b), but may become tumor suppressive in pancreatic cancer, renal and particularly in nasopharyngeal carcinoma (Feng *et al.*, 2014; Huang *et al.*, 2014; Yu *et al.*, 2015; Cheung *et al.*, 2016). In view of this, ICG-001 may be used to exert its anti-tumor effect by upregulating the expression of tumor-suppressive miRNAs.

In the miRNA target analysis performed in this study, miR-96 was found to regulate Evi1 expression at post-transcriptional level. We also observed that

miR-96 and Evi1 were negatively regulated by each other. From the qRT-PCR results, we proposed that miR-449a was a downstream effector of miR-96. It is worthy to note that Evi1 was previously suggested to link with miR-96 in a reciprocal feedback loop (Tanaka *et al.*, 2014) and reported to directly repress the transcription of *miR-449a* gene (De Weer *et al.*, 2011), we speculate that miR-96/Evi1/miR449a may be form a molecular axis in ICG-001-mediated inhibition of NPC cells. While silencing of survivin was able to regulate Evi1/miR-449a, but had no significant effect on the expression level of miR-96, survivin may be another upstream regulator of Evi1/miR-449a axis..

Taken together, data in this chapter suggested that ICG-001 could inhibit cell migration and tumor sphere growth of NPC cells via survivin and miR-96 that both funneled down to regulate Evi1 and miR-449a (Figure 4.18).

(A)

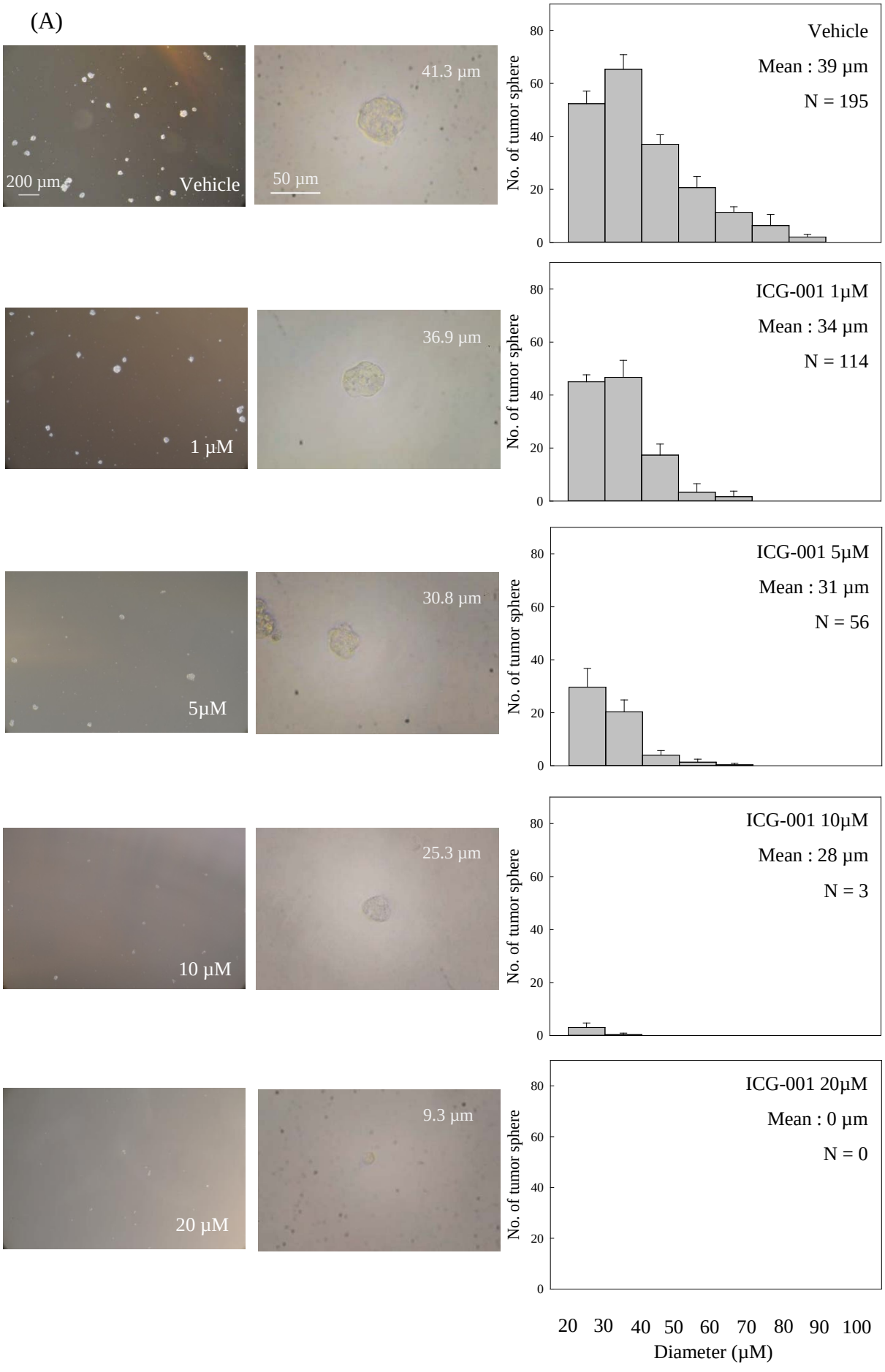
200 μm
Vehicle
41.3 μm
50 μm
Vehicle
Mean : 39 μm
N = 195
1 μM
36.9 μm
ICG-001 1μM
Mean : 34 μm
N = 114
5μM
30.8 μm
ICG-001 5μM
Mean : 31 μm
N = 56
10 μM
25.3 μm
ICG-001 10μM
Mean : 28 μm
N = 3
20 μM
9.3 μm
ICG-001 20μM
Mean : 0 μm
N = 0
No. of tumor sphere
0
20
40
60
80
20 30 40 50 60 70 80 90 100
Diameter (μM)

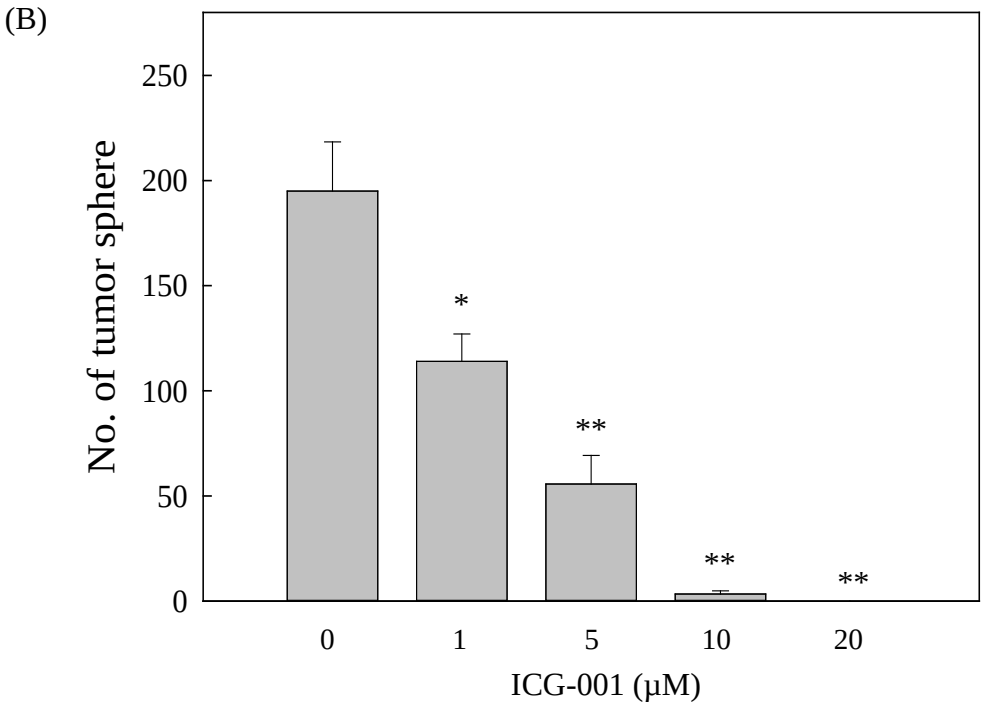

Figure 4.1 | Effect of ICG-001 on tumor spheroid formation of C666-1 cells. C666-1 cells (2,000 cells/well) were grown in DMEM/F12 (1:1) medium supplemented with EGF, FGF and IGF in 24-well ultra-low attachment culture plates. The mixtures were treated with ICG-001 at 1, 5, 10 or 20 μM for 7 days. Cells treated with 0.05% DMSO were used as vehicle control group. Images of tumor spheres from the whole culture were captured under microscope. (A) Representative bright field images with low magnification (left panel), high magnification (middle panel) and the size profiles of the tumor spheres. (B) The total number of tumor spheres. Three individual experiments were carried out, and each experiment was performed in triplicate. *$p < 0.05$; **$p < 0.01$.

(A)

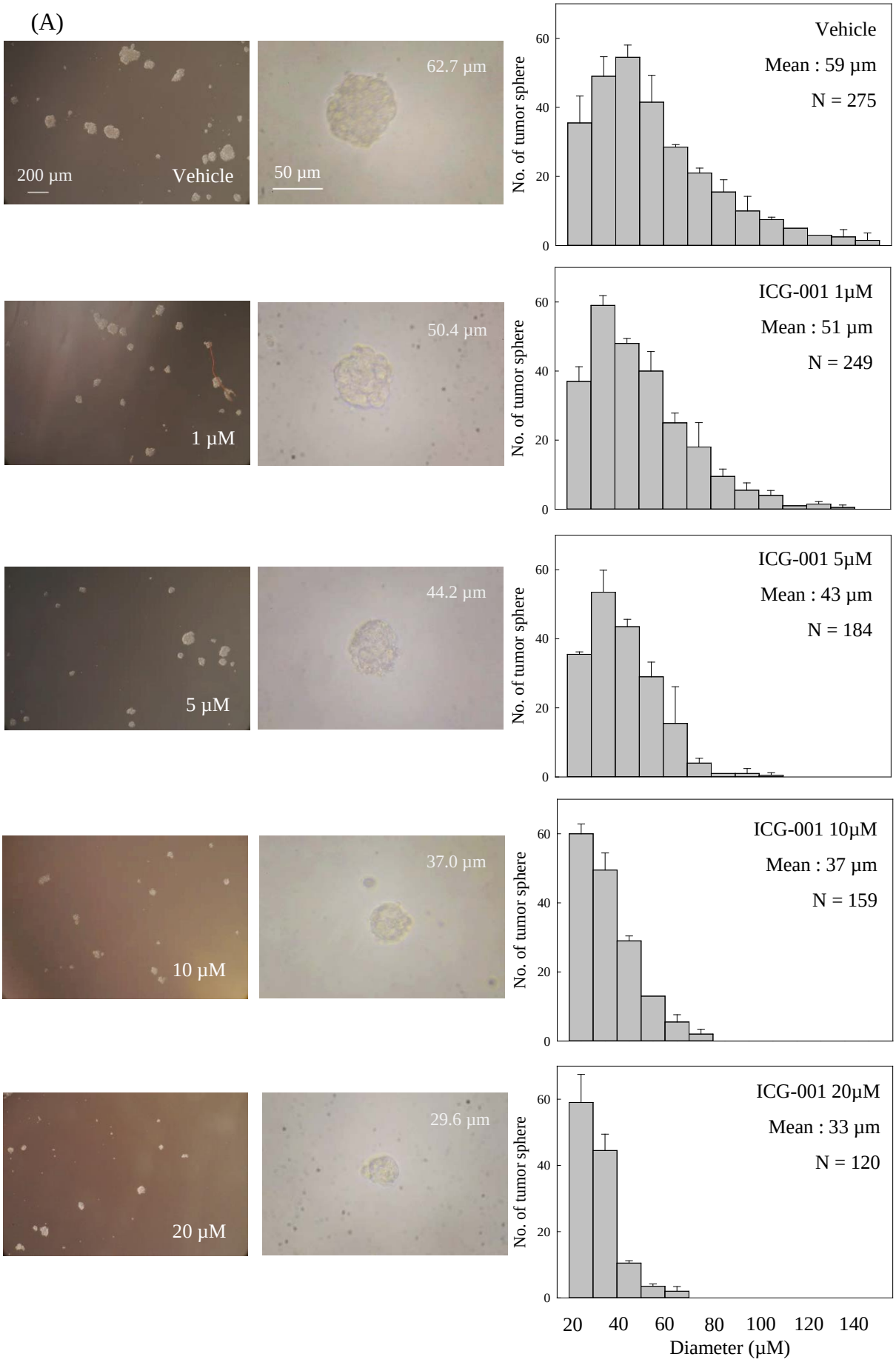
200 μm
Vehicle
62.7 μm
50 μm
Vehicle
Mean : 59 μm
N = 275
1 μM
50.4 μm
ICG-001 1μM
Mean : 51 μm
N = 249
5 μM
44.2 μm
ICG-001 5μM
Mean : 43 μm
N = 184
10 μM
37.0 μm
ICG-001 10μM
Mean : 37 μm
N = 159
20 μM
29.6 μm
ICG-001 20μM
Mean : 33 μm
N = 120
No. of tumor sphere
0
20
40
60
20
40
60
80
100
120
140
Diameter (μM)

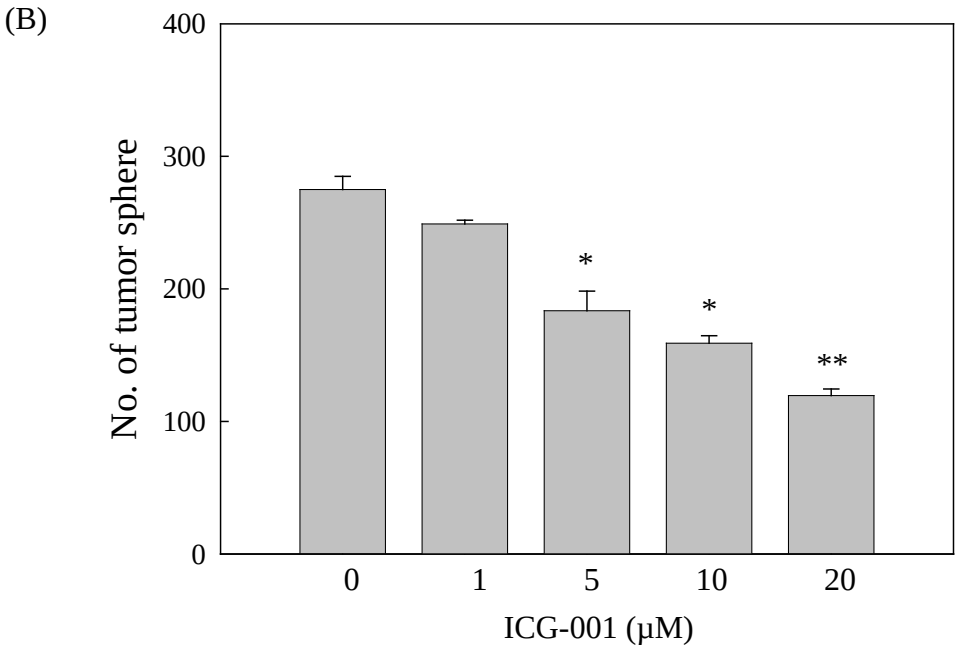

Figure 4.2 | Effect of ICG-001 on growth of established tumor spheres of C666-1 cells. Tumor spheres of C666-1 cells were formed and cultured in DMEM/F12 (1:1) medium supplemented with EGF, FGF and IGF in 24-well ultra-low attachment culture plates for 7 days. Then, the tumor spheres were treated with ICG-001 at 1, 5, 10 or 20 μM for another 7 days. Tumor spheres in vehicle control group were treated with 0.05% DMSO. Images of tumor spheres from the whole culture were captured under microscope. (A) Representative bright field images with low magnification (left panel), high magnification (middle panel) and the size profiles of the tumor spheres. (B) The total number of tumor spheres. Three individual experiments were carried out, and each experiment was performed in triplicate. *$p < 0.05$; **$p < 0.01$.

(A)

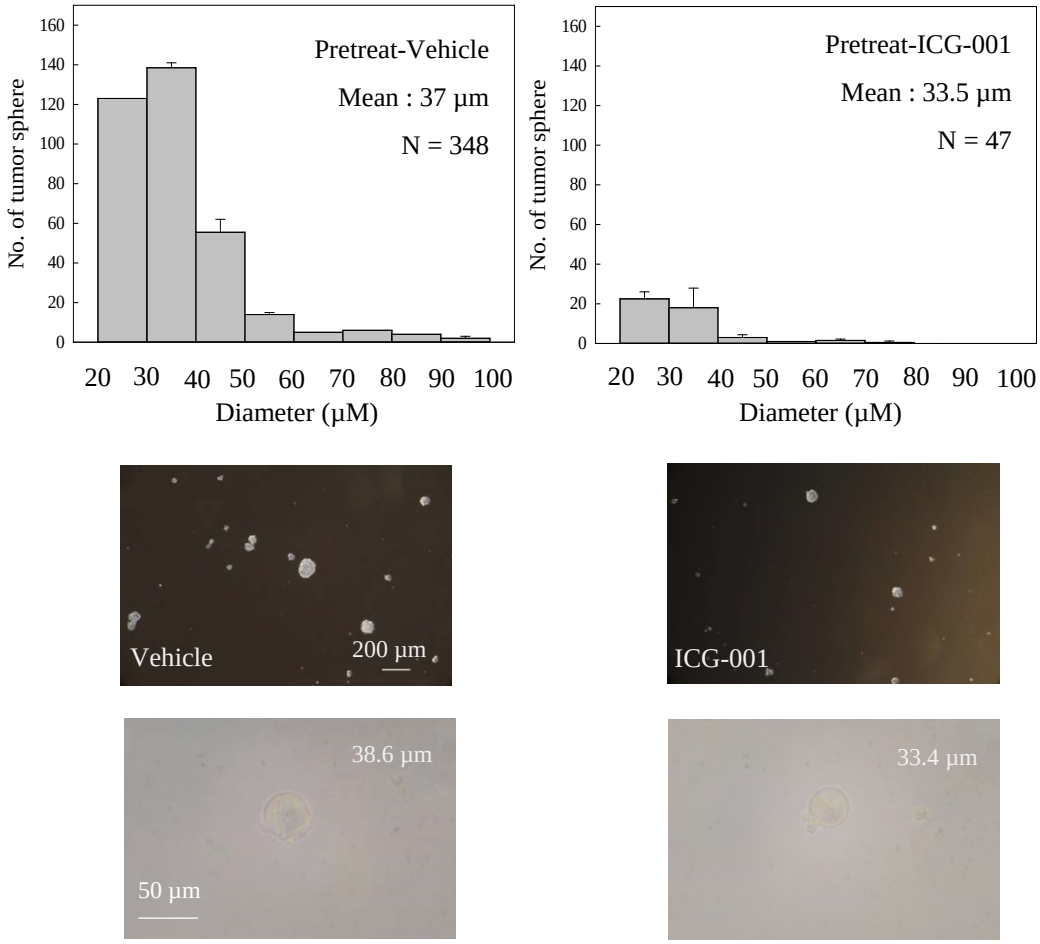
Pretreat-Vehicle
Mean : 37 μm
N = 348
No. of tumor sphere
Diameter (μM)
Pretreat-ICG-001
Mean : 33.5 μm
N = 47
No. of tumor sphere
Diameter (μM)
Vehicle
200 μm
ICG-001
38.6 μm
50 μm
33.4 μm

(B)

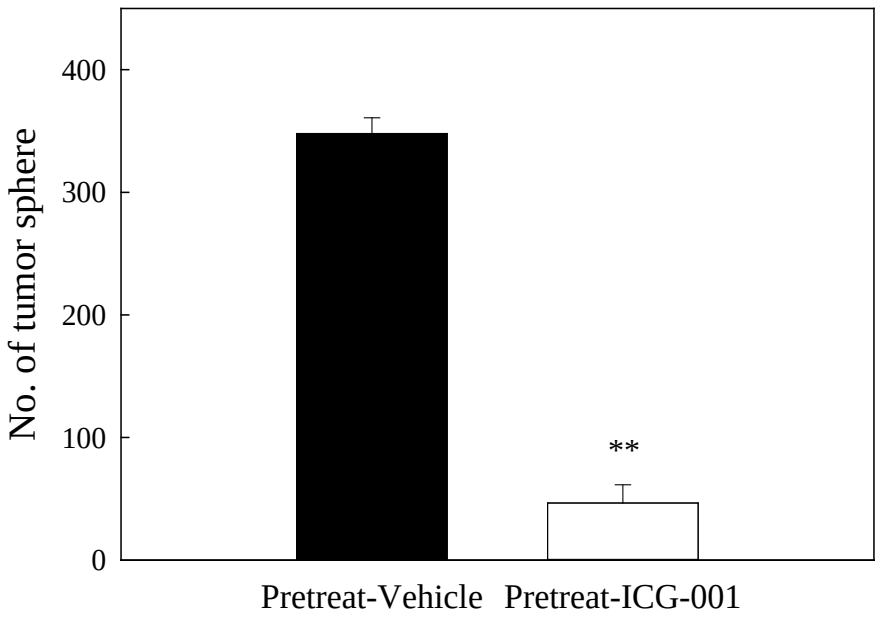
No. of tumor sphere
**
Pretreat-Vehicle
Pretreat-ICG-001

Figure 4.3 | Effect of ICG-001 pre-treatment on the growth of C666-1 tumor spheres. C666-1 cells in monolayer culture were treated with ICG-001 (10 μM) or DMSO (vehicle control) for 7 days. Then the treated cells were harvested and subjected to tumor spheroid formation assay for 7 days without any drug treatment. Tumor spheres from the whole culture were captured under microscope. (A) The size profiles (upper panel), representative bright field images with low magnification (middle panel) and high magnification (lower panel). (B) The total number of tumor spheres. Three individual experiments were carried out, and each experiment was performed in triplicate. $^{**}p < 0.01$.

(A)

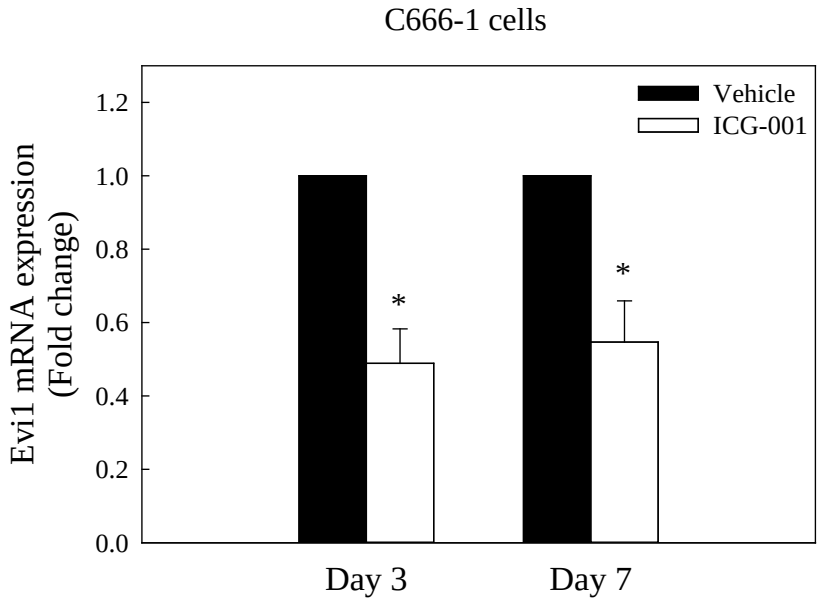
C666-1 cells
Vehicle
ICG-001
Evi1 mRNA expression
(Fold change)
1.2
1.0
0.8
0.6
0.4
0.2
0.0
*
*
Day 3
Day 7

(B)

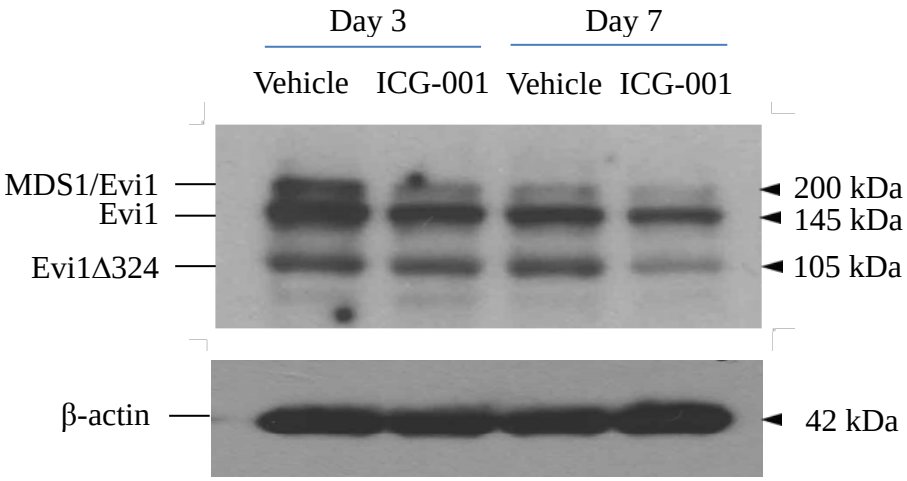
Day 3
Day 7
Vehicle
ICG-001
Vehicle
ICG-001
MDS1/Evi1
Evi1
Evi1Δ324
200 kDa
145 kDa
105 kDa
β-actin
42 kDa

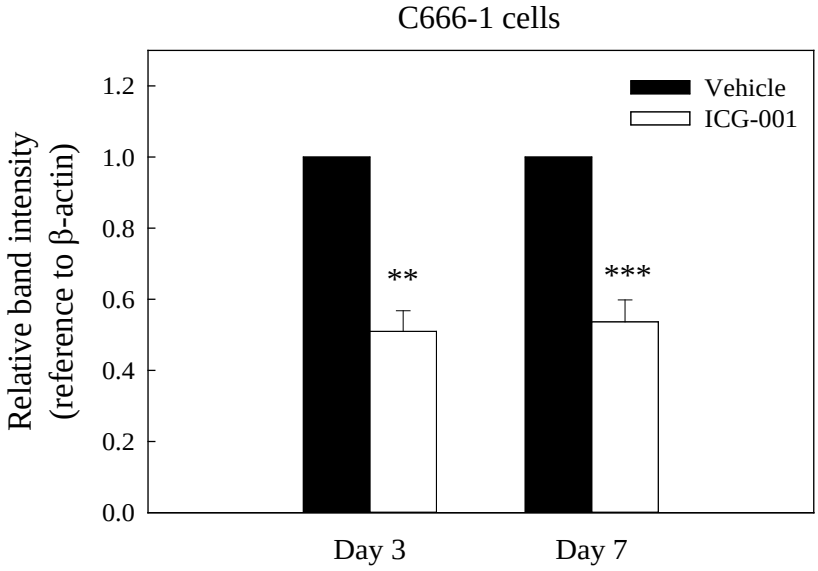
C666-1 cells
Vehicle
ICG-001
Relative band intensity
(reference to β-actin)
1.2
1.0
0.8
0.6
0.4
0.2
0.0
**
***
Day 3
Day 7

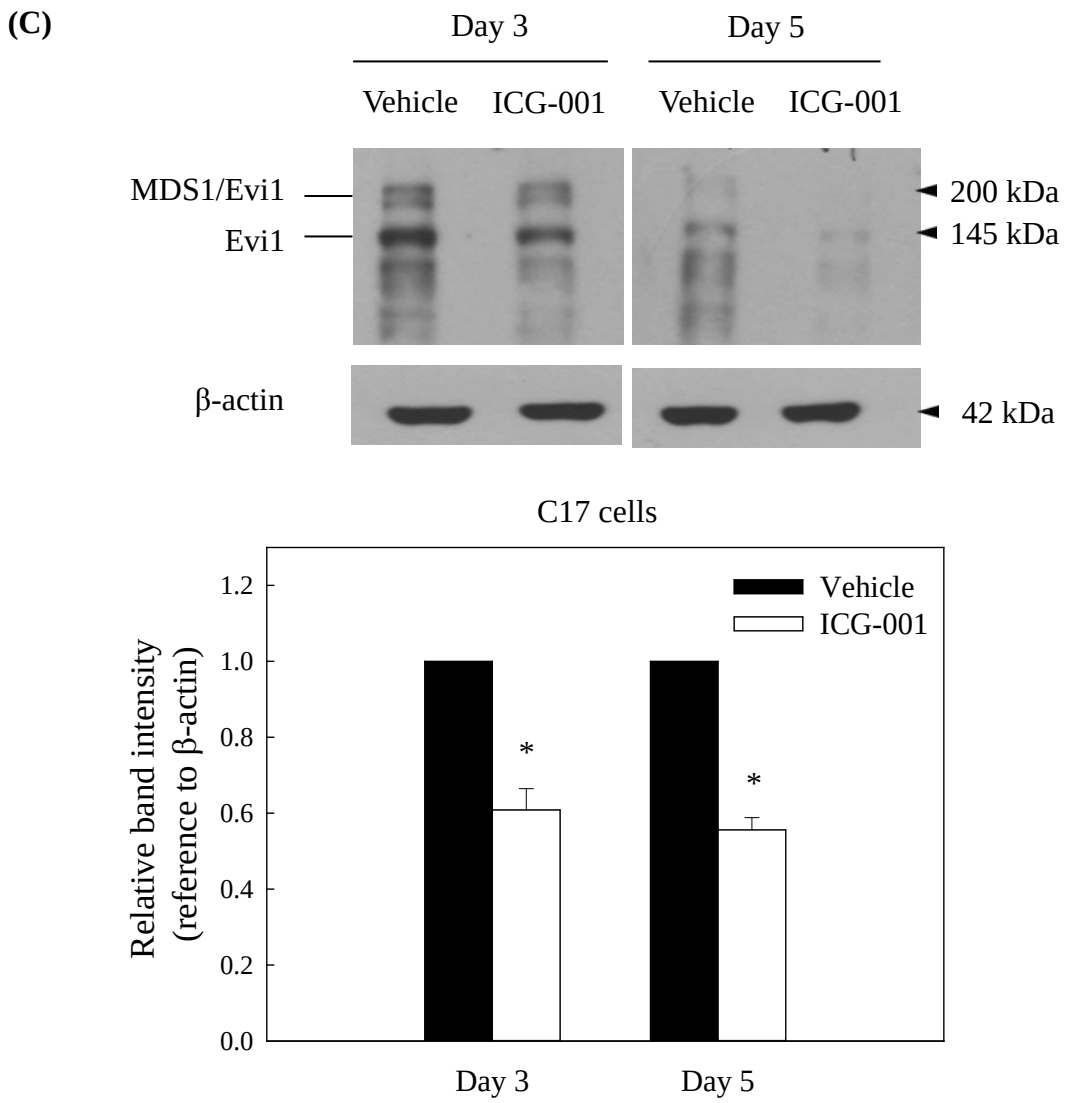

Figure 4.4 | ICG-001 down-regulates Evi1 expression. NPC cells were treated with ICG-001 (10 μM) or DMSO (vehicle control) for days indicated. (A) The expression level Evi1 mRNA in treated C666-1 cells was determined using qRT-PCR. The expression levels of Evi1 protein in (B) C666-1 cells and (C) C17 cells) were determined by Western-blotting analysis. Representative images were presented, and signal intensities were determined by quantitative densitometry and expressed as fold change of Evi1 normalized to β-actin. Values are presented as means ± SD of at least four independent experiments. *$p < 0.05$, **$p < 0.01$, *** $p < 0.001$compared with vehicle control

(A)

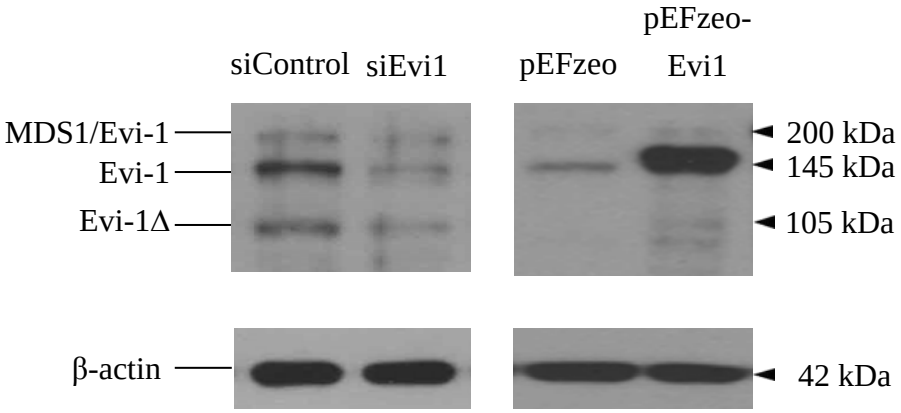
siControl
siEvi1
pEFzeo
pEFzeo-Evi1
MDS1/Evi-1
Evi-1
Evi-1Δ
β-actin
200 kDa
145 kDa
105 kDa
42 kDa

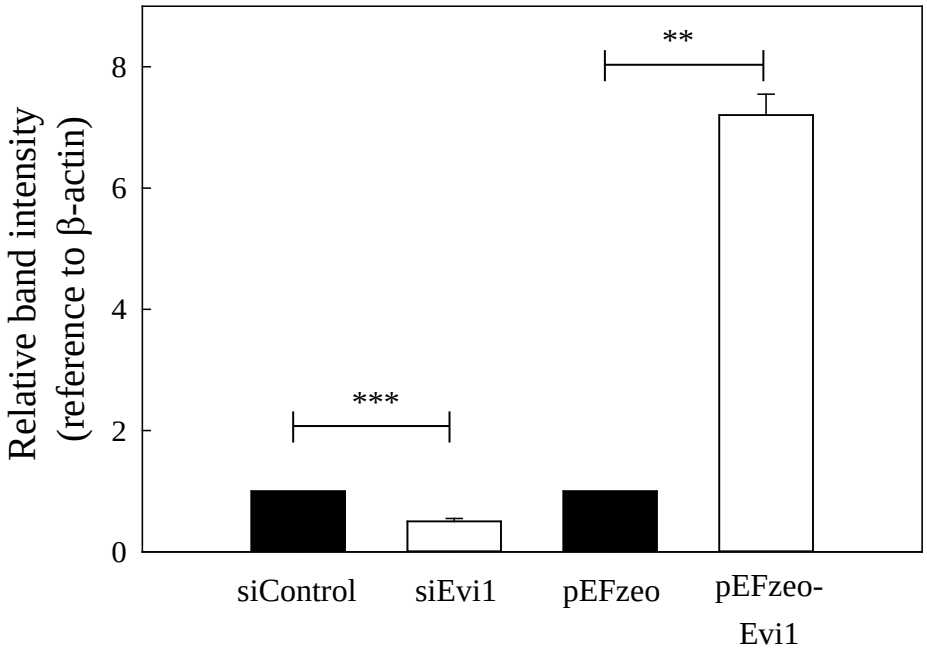
Relative band intensity
(reference to β-actin)
0
2
4
6
8
***
**
siControl
siEvi1
pEFzeo
pEFzeo-Evi1

(B)

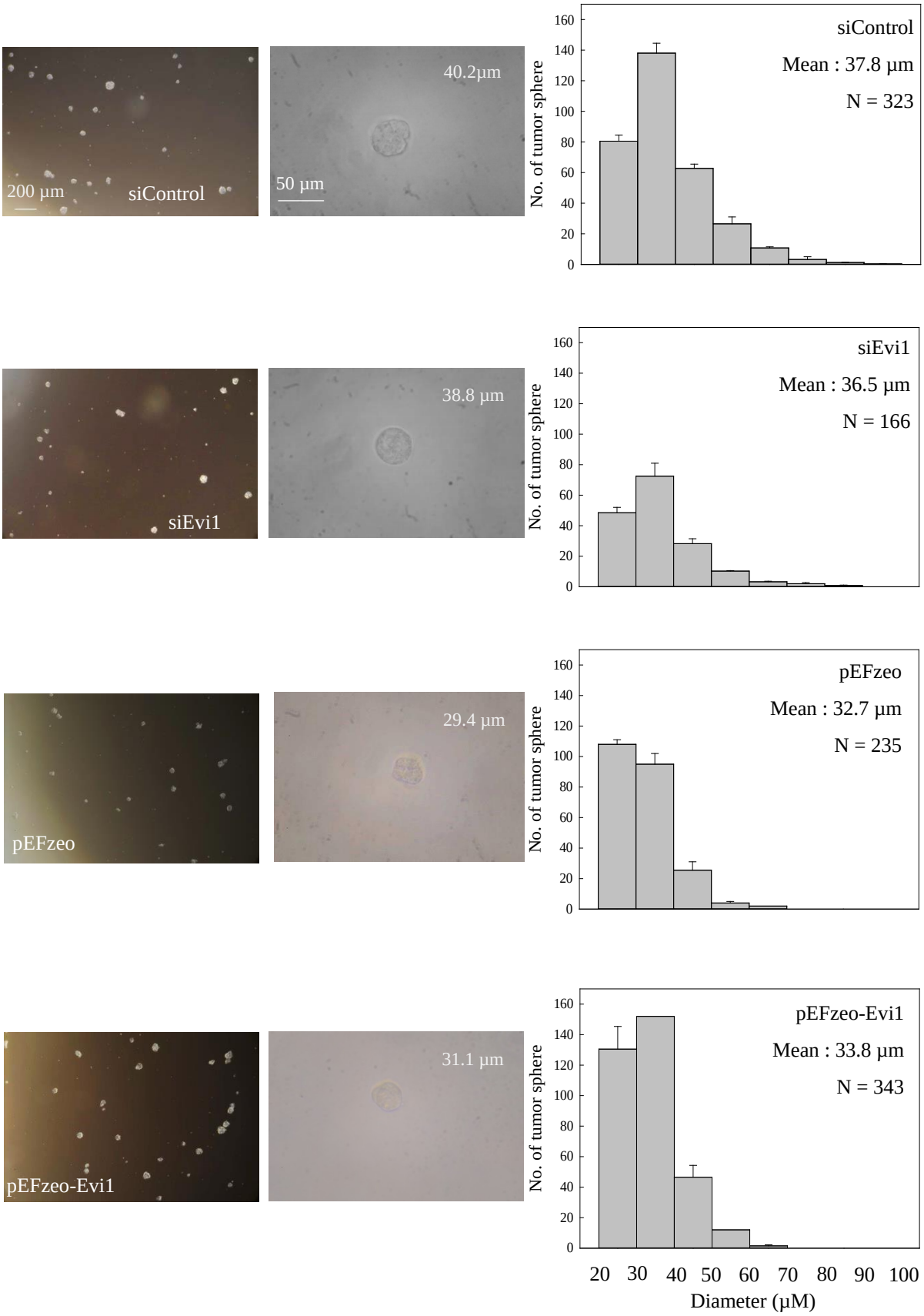
200 μm
siControl
40.2μm
50 μm
No. of tumor sphere
siControl
Mean : 37.8 μm
N = 323
siEvi1
38.8 μm
siEvi1
Mean : 36.5 μm
N = 166
pEFzeo
29.4 μm
pEFzeo
Mean : 32.7 μm
N = 235
pEFzeo-Evi1
31.1 μm
pEFzeo-Evi1
Mean : 33.8 μm
N = 343
0 20 40 60 80 100 120 140 160
20 30 40 50 60 70 80 90 100
Diameter (μM)

(C)

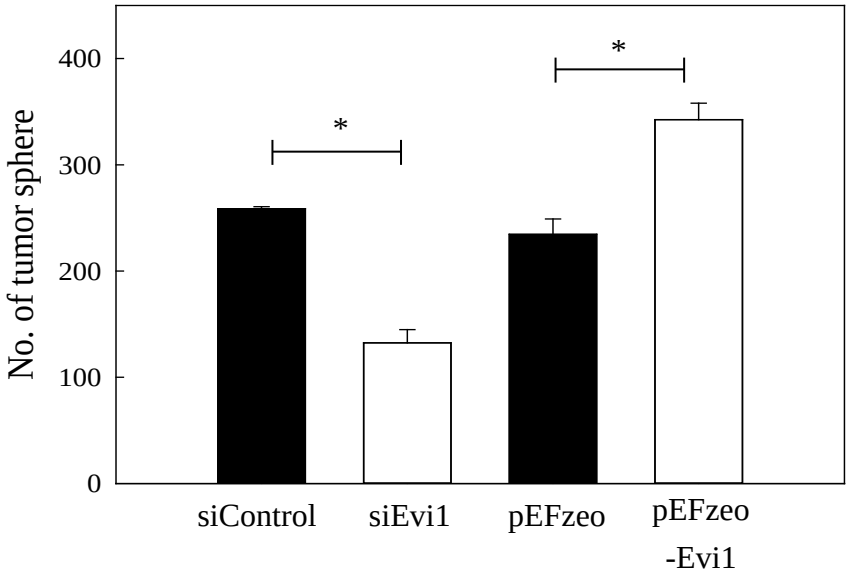
No. of tumor sphere
400
300
200
100
0
*
*
siControl
siEvi1
pEFzeo
pEFzeo
-Evi1

(D)

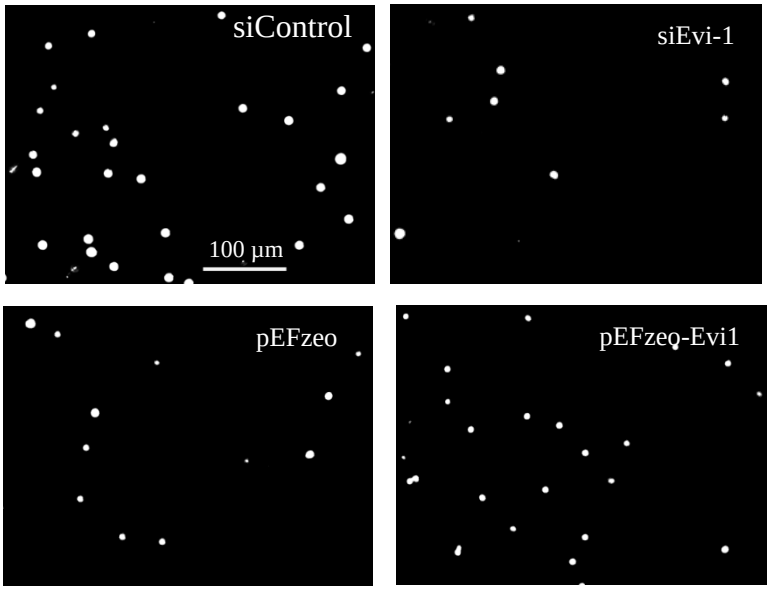
siControl
100 μm
siEvi-1
pEFzeo
pEFzeo-Evi1

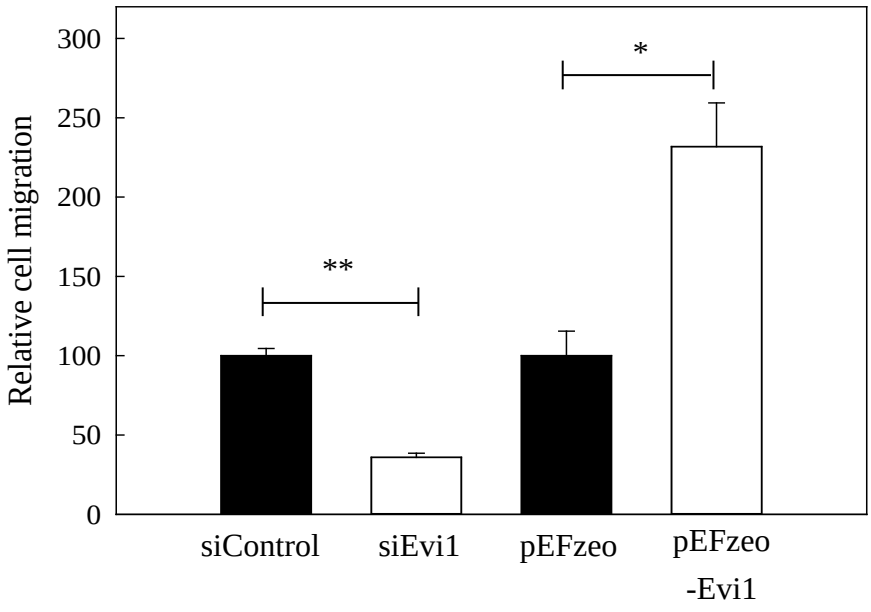
Relative cell migration
300
250
200
150
100
50
0
**
*
siControl
siEvi1
pEFzeo
pEFzeo
-Evi1

Figure 4.5 | Effect of Evi1 on the formation of tumor spheres and the migration of C666-1 cells. Cells were transfected with either Evi1 siRNA pool (siEvi1, 100 nM) or expression plasmid (pEFzeo-Evi1, 400 ng). Negative control siRNA (siControl) or pEFzeo vector without target insert were used as control experiments. (A) The transfection efficiency was assessed by Western blotting analysis. Representative image was presented in upper panel and signal intensities were determined by quantitative densitometry and expressed as fold change of Evi-1 normalized to β-actin in lower panel. (B, C) The transfected cells were harvested and subjected to tumor spheroid formation assay. The representative bright field images with low and high magnification, the size profile and the total number of tumor spheres were presented. (D) The migratory abilities of the transfected cells were assessed by transwell migration assay. The Representative images were presented in the upper panel and the migrated cells were counted and presented in percentage in lower panel. At least three independent experiments were carried out. *$p < 0.05$; **$p < 0.01$ compared corresponding control.

(A)

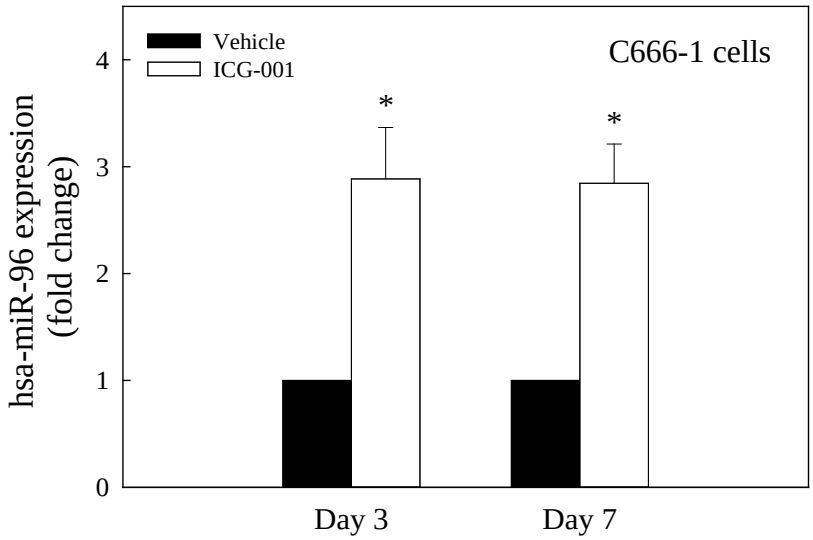
Vehicle
ICG-001
C666-1 cells
hsa-miR-96 expression
(fold change)
0
1
2
3
4
*
*
Day 3
Day 7

(B)

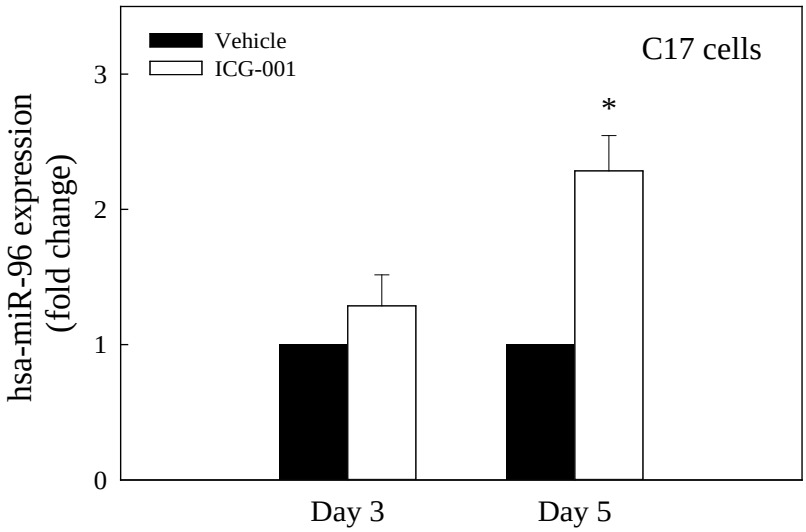
Vehicle
ICG-001
C17 cells
hsa-miR-96 expression
(fold change)
0
1
2
3
*
Day 3
Day 5

(C)

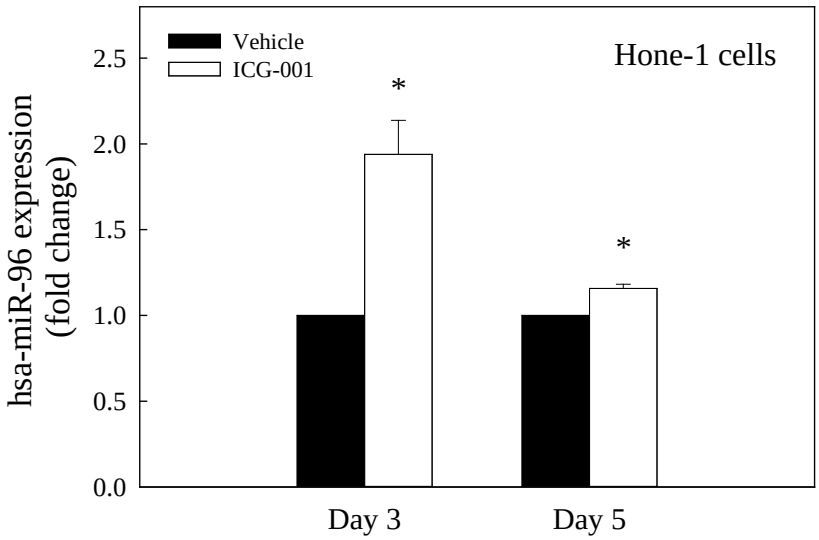
Vehicle
ICG-001
Hone-1 cells
hsa-miR-96 expression
(fold change)
0.0
0.5
1.0
1.5
2.0
2.5
*
*
Day 3
Day 5

Figure 4.6 | ICG-001 enhances the expression of miR-96 in NPC cells. (A) C666-1 cells (monolayer culture) were treated with ICG-001 (10 μM) or DMSO (Vehicle) for 3 or 7 days. (B) Another EBV-positive C17 cells were treated with ICG-001 (10 μM) or DMSO (Vehicle) for 3 or 5 days. (C) An EBV-negative HONE-1 cells were treated with ICG-001 (10 μM) or DMSO (Vehicle) for 3 or 5 days. The expression level of miR-96 in various samples was subsequently measured using qRT-PCR. At least three individual experiments were performed, and each experiment was in duplicate. $*p < 0.05$ compared to vehicle.

(A)

```
                    857                                 879
Evi1 3' UTR  ...CACUAAUAAAUUGUUUGCCAAAU...  3'
                                 ||||||
hsa-miR-96   UCGUUUUUACACGAUCACGGUUU       5'

                  1077                                1099
Evi1 3' UTR  ...GACCUGUGUAUGAGAGUGCCAAA...  3'
                       |||         |||||||
hsa-miR-96   UCGUUUUUACACGAU--CACGGUUU      5'
```

(B)

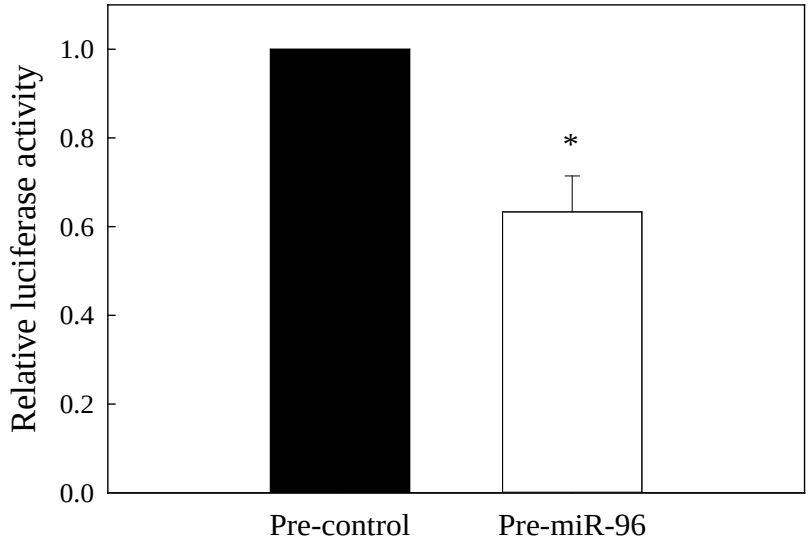

(C)

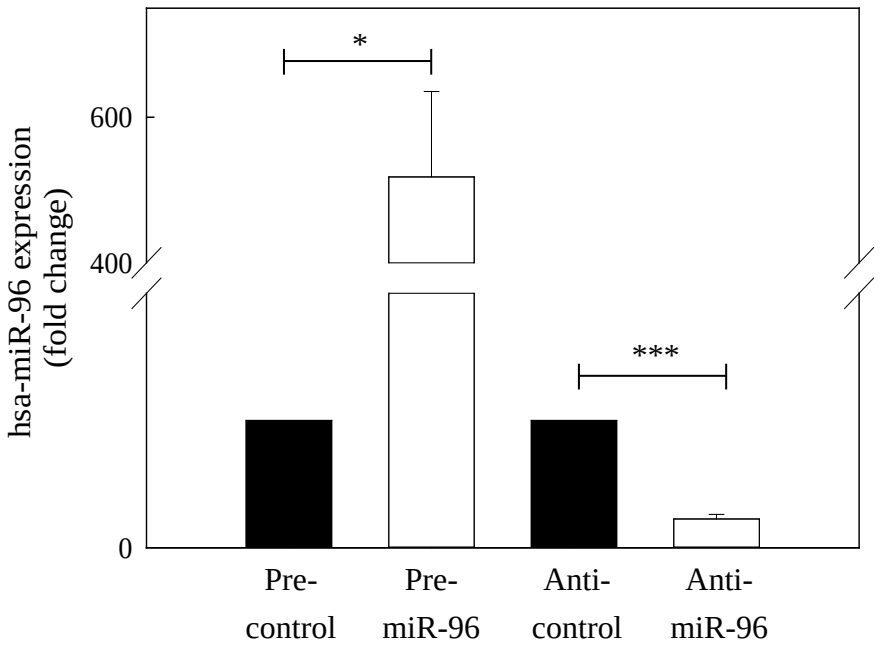

(D)

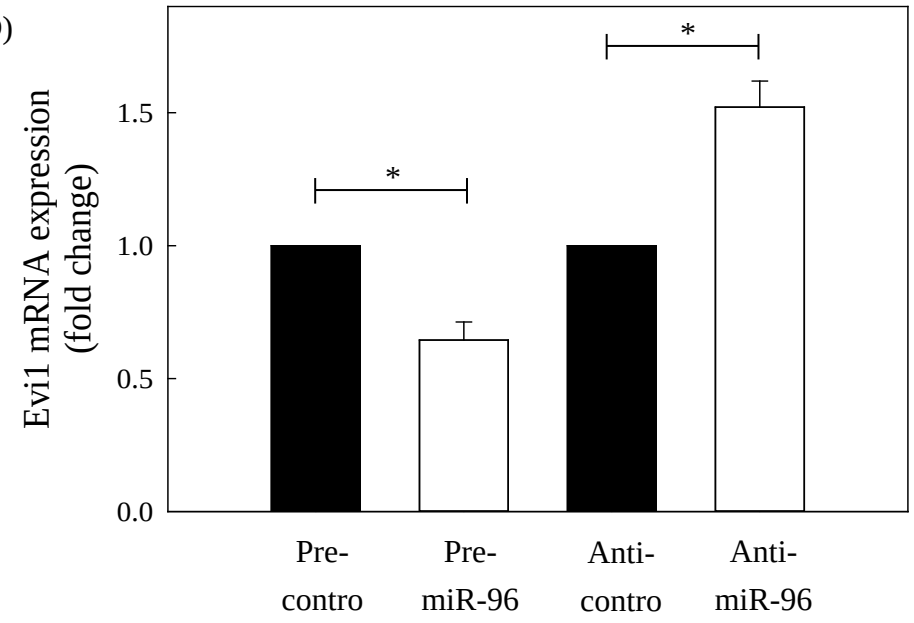
Evi1 mRNA expression
(fold change)
0.0
0.5
1.0
1.5
*
*
Pre-
contro
Pre-
miR-96
Anti-
contro
Anti-
miR-96

(E)

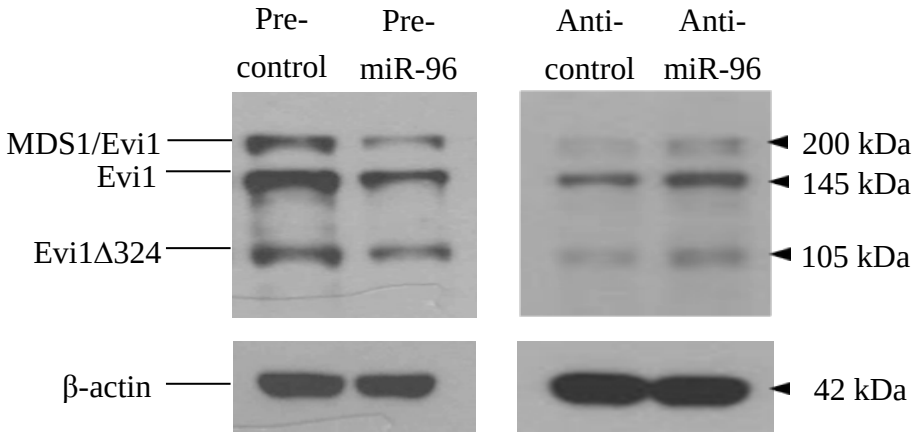
Pre-
control
Pre-
miR-96
Anti-
control
Anti-
miR-96
MDS1/Evi1
Evi1
Evi1Δ324
β-actin
200 kDa
145 kDa
105 kDa
42 kDa

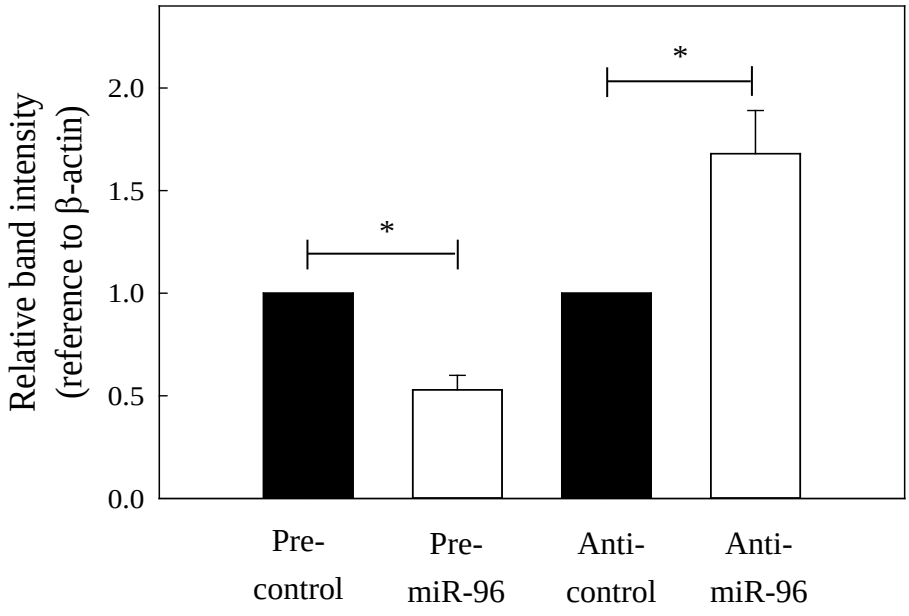
Relative band intensity
(reference to β-actin)
0.0
0.5
1.0
1.5
2.0
*
*
Pre-
control
Pre-
miR-96
Anti-
control
Anti-
miR-96

Figure 4.7 | miR-96 directly targets Evi1 transcript. (A) Putative binding site of miR-96 on Evi1 mRNA 3'-UTR was predicted using TargetScan. (B) C666-1 cells were co-transfected with miR-96 precursor (or miRNA precursor control) (100 nM) and Evi1 3'-UTR reporter vector (10 ng). Luciferase activity was normalized by the RFP signal. (C) The transfection efficiency of miR-96 precursor (pre-miR-96) or inhibitor (Anti-miR-96) (50 nM) in C666-1 cells was confirmed by real-time PCR. Cells transfected with miRNA precursor or inhibitor negative control (Pre-control or Anti-control) were used as control experiments. (D) miR-96 negatively regulates the expression of Evi1 transcript. (E) miR-96 negatively regulates the protein expression of Evi1. Values were presented as the means ± SD of at least three independent experiments. *$p < 0.05$; ***$p < 0.001$.

(A)

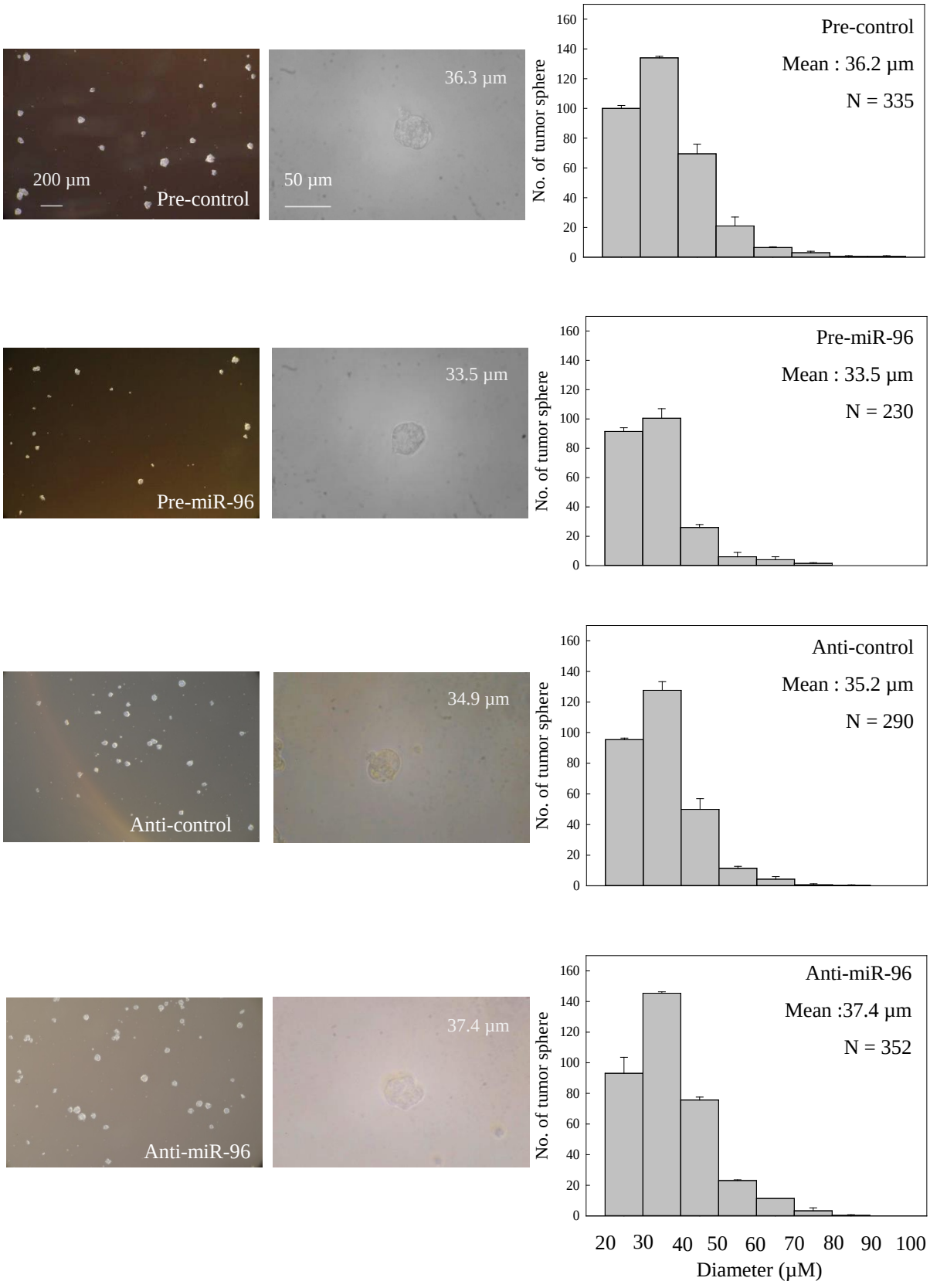
200 μm
Pre-control
36.3 μm
50 μm
Pre-control
Mean : 36.2 μm
N = 335
No. of tumor sphere
Pre-miR-96
33.5 μm
Pre-miR-96
Mean : 33.5 μm
N = 230
Anti-control
34.9 μm
Anti-control
Mean : 35.2 μm
N = 290
Anti-miR-96
37.4 μm
Anti-miR-96
Mean :37.4 μm
N = 352
0 20 40 60 80 100 120 140 160
20 30 40 50 60 70 80 90 100
Diameter (μM)

(B)

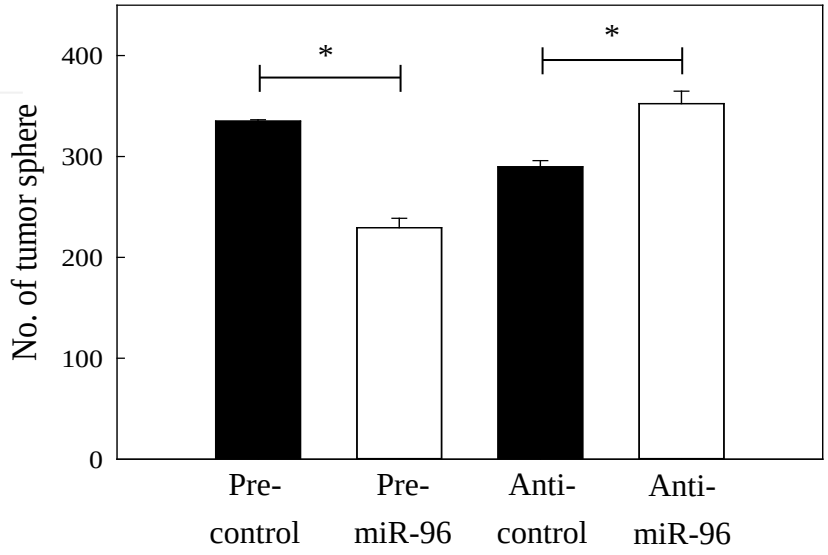
No. of tumor sphere
400
300
200
100
0
*
*
Pre-control
Pre-miR-96
Anti-control
Anti-miR-96

(C)

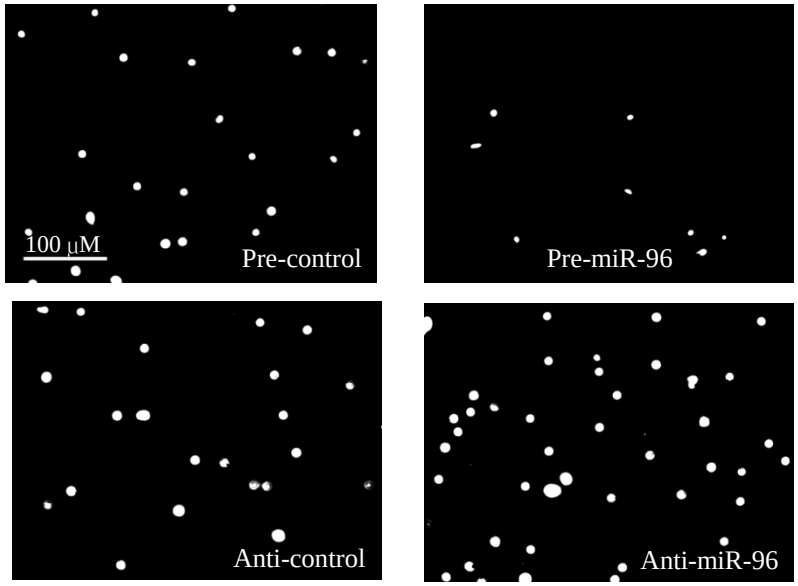
100 μM
Pre-control
Pre-miR-96
Anti-control
Anti-miR-96

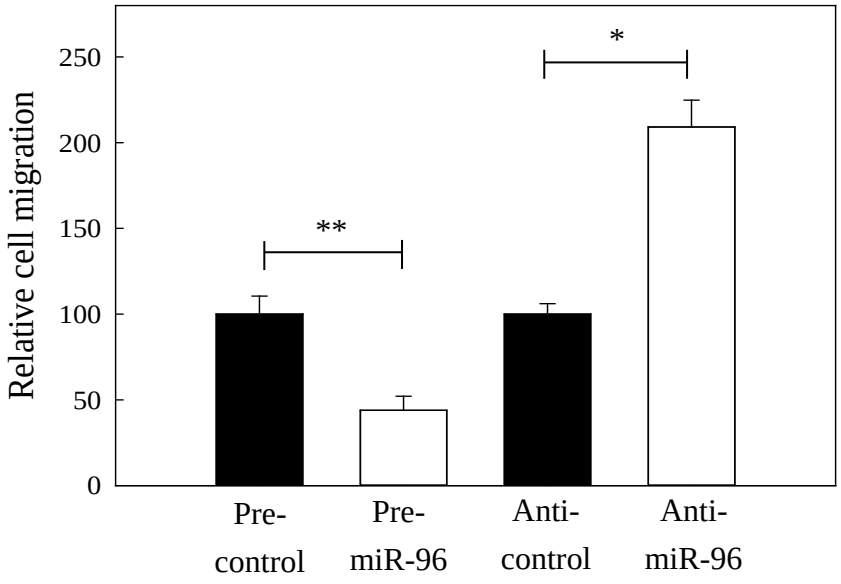
Relative cell migration
250
200
150
100
50
0
**
*
Pre-control
Pre-miR-96
Anti-control
Anti-miR-96

Figure 4.8 | Effect of miR-96 on the formation of tumor spheres and the migration of C666-1 cells. Cells were transfected with either miR-96 precursor or inhibitor at 50 nM, parallel with corresponding negative control experiments. (A, B) The transfected cells were harvested and subjected to tumor spheroid formation assay. The representative bright field images with low and high magnification, the size profile and the total number of tumor spheres were presented. (C) The migratory abilities of the transfected cells were assessed by transwell migration assay. The Representative images were presented in the upper panel and the migrated cells were counted and presented in percentage in lower panel. At least three independent experiments were carried out. *$p < 0.05$; **$p < 0.01$ compared corresponding control.

(A)

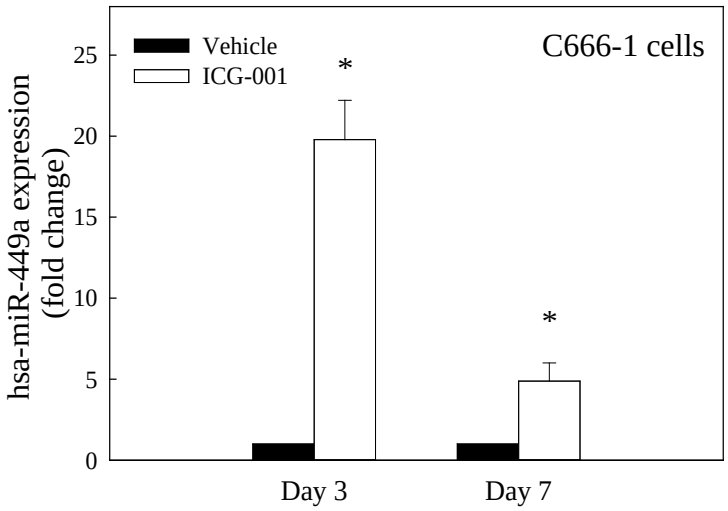
Vehicle
ICG-001
C666-1 cells
hsa-miR-449a expression
(fold change)
25
20
15
10
5
0
*
*
Day 3
Day 7

(B)

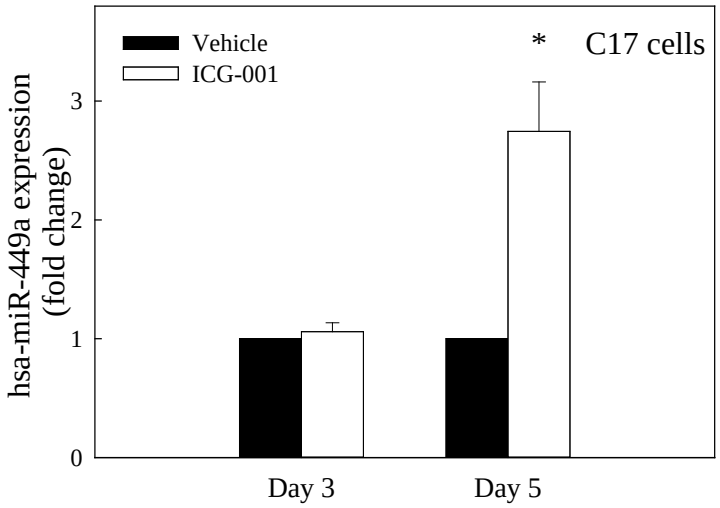
Vehicle
ICG-001
C17 cells
hsa-miR-449a expression
(fold change)
3
2
1
0
*
Day 3
Day 5

(C)

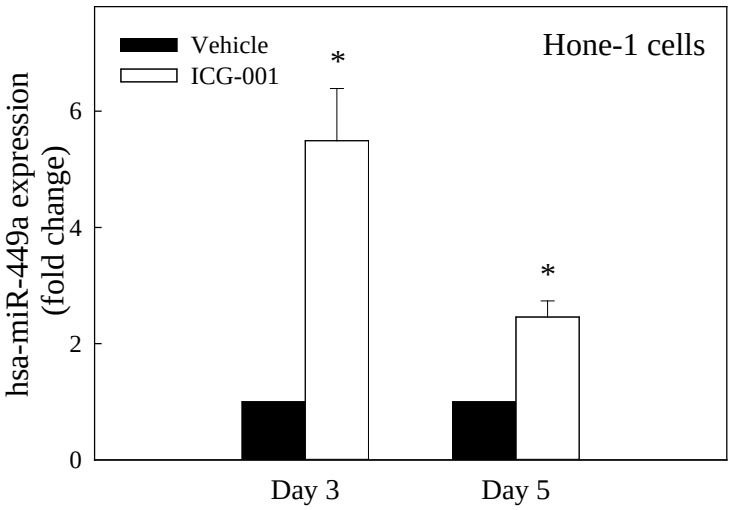
Vehicle
ICG-001
Hone-1 cells
hsa-miR-449a expression
(fold change)
6
4
2
0
*
*
Day 3
Day 5

Figure 4.9 | ICG-001 enhances the expression of miR-449a in NPC cells. (A) C666-1 cells (monolayer culture) were treated with ICG-001 (10 μM) or DMSO (Vehicle) for 3 or 7 days. (B) Another EBV-positive C17 cells were treated with ICG-001 (10 μM) or DMSO (Vehicle) for 3 or 5 days. (C) An EBV-negative HONE-1 cells were treated with ICG-001 (10 μM) or DMSO (Vehicle) for 3 or 5 days. The expression level of miR-449a in various samples was subsequently measured using qRT-PCR. At least three individual experiments were performed, and each experiment was in duplicate. $*p < 0.05$ compared to vehicle.

(A)

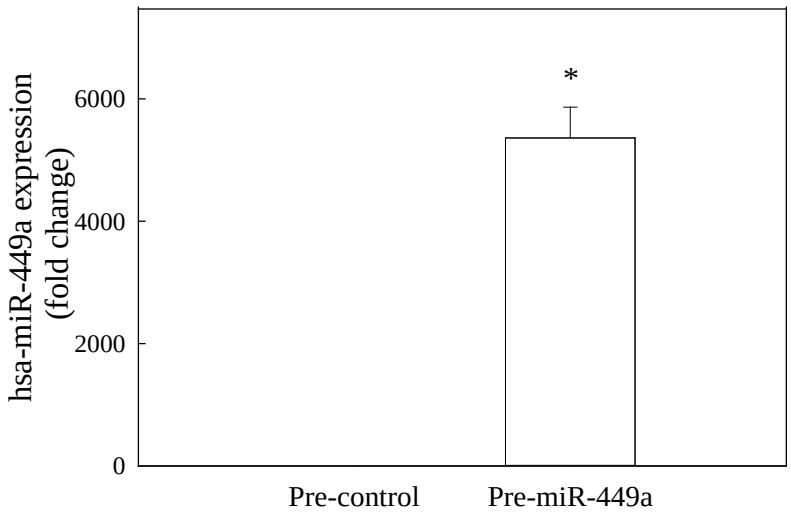
hsa-miR-449a expression
(fold change)
6000
4000
2000
0
*
Pre-control
Pre-miR-449a

(B)

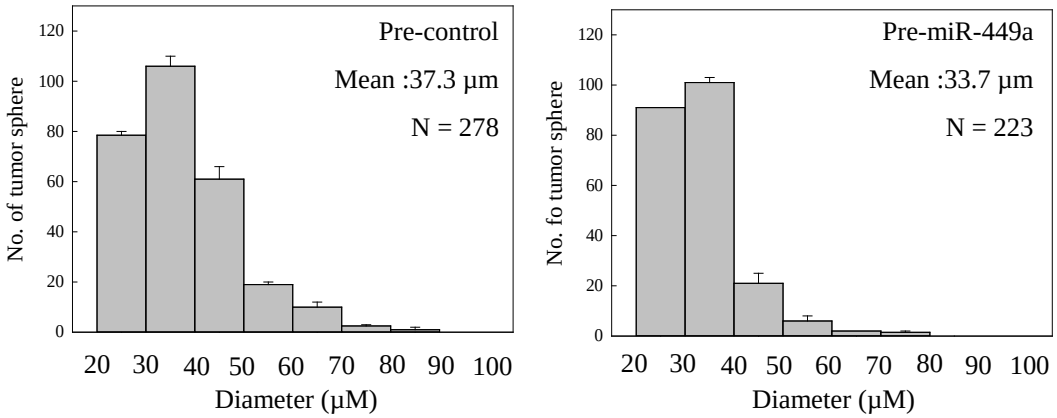
No. of tumor sphere
Pre-control
Mean :37.3 µm
N = 278
Diameter (µM)
No. fo tumor sphere
Pre-miR-449a
Mean :33.7 µm
N = 223
Diameter (µM)

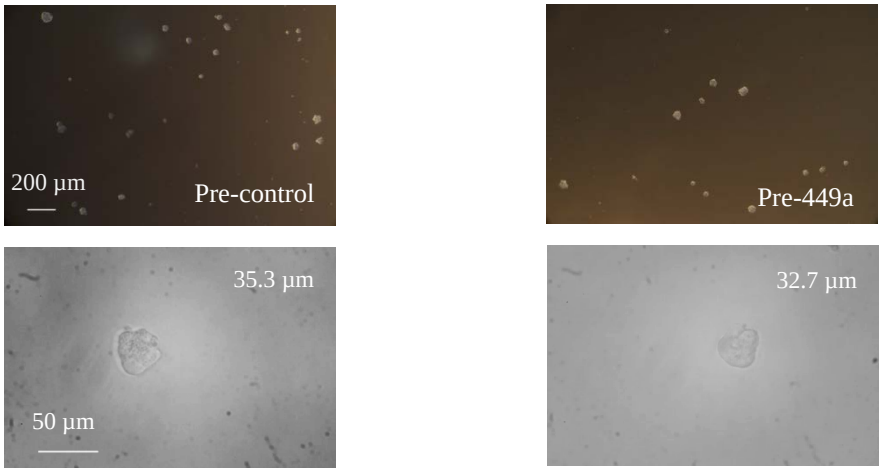
200 µm
Pre-control
Pre-449a
35.3 µm
50 µm
32.7 µm

(C)

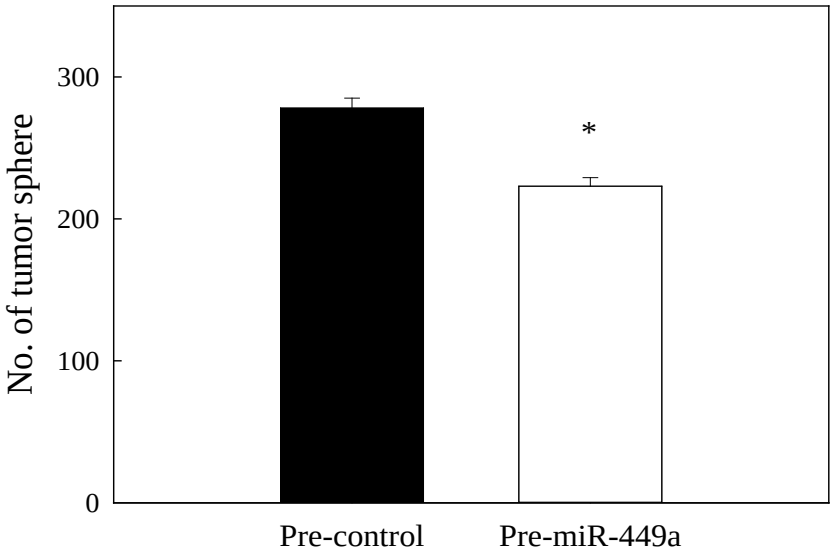
No. of tumor sphere
300
200
100
0
*
Pre-control
Pre-miR-449a

(D)

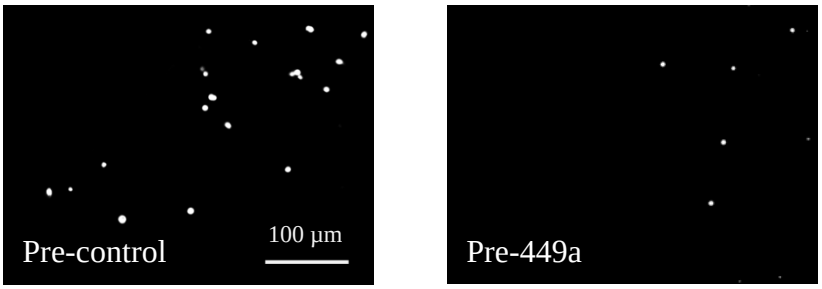
Pre-control
100 μm
Pre-449a

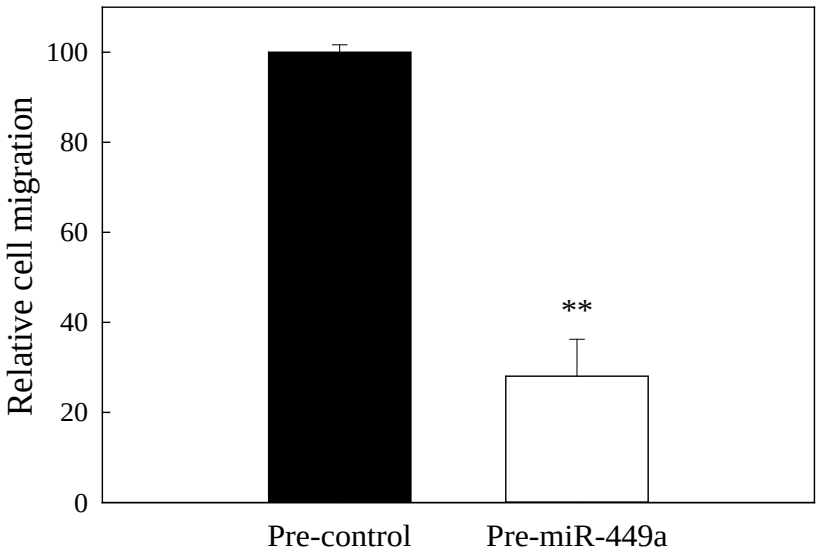
Relative cell migration
100
80
60
40
20
0
**
Pre-control
Pre-miR-449a

Figure 4.10 | Effect of miR-449a on the formation of tumor spheres and the migration of C666-1 cells. (A) The transfection efficiency of miR-449a precursor (pre-miR-449a) or inhibitor (Anti-miR-449a) (50 nM) compared with corresponding negative control in C666-1 cells was confirmed by real-time PCR. (B, C) The transfected cells were harvested and subjected to tumor spheroid formation assay. The size profile, representative bright field images with low and high magnification and the total number of tumor spheres were presented. (D) The migratory abilities of the transfected cells were assessed by transwell migration assay. The Representative images were presented in the upper panel and the migrated cells were counted and presented in percentage in lower panel. At least three independent experiments were carried out. *$p < 0.05$; **$p < 0.01$ compared corresponding control.

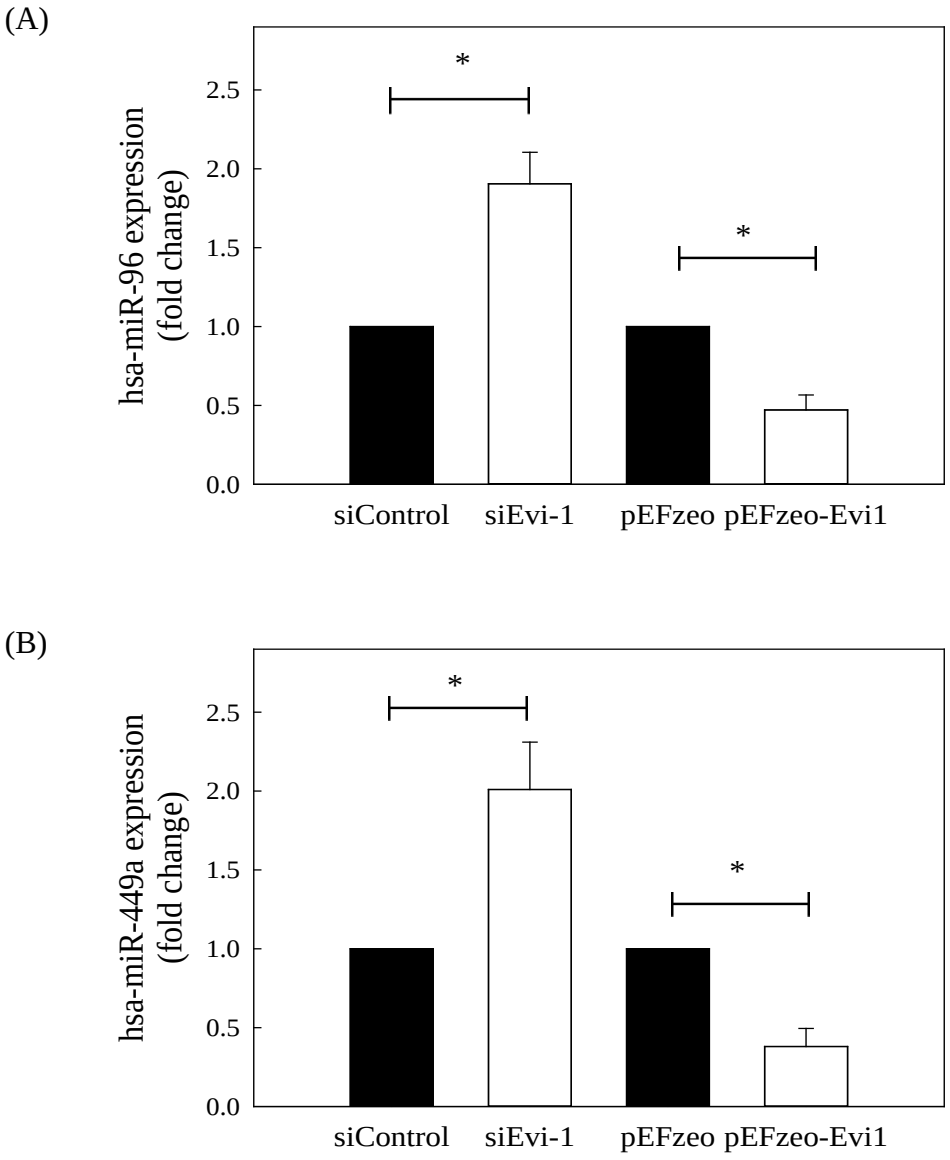

Figure 4.11 | Effect of Evi1 on the expression of miR-96 and miR-449a. Using qRT-PCR, the expression levels of (A) miR-96 and (B) miR-449a in the cells with either Evi1 knock-down or overexpression was measured. At least three individual experiments were performed, and each experiment was in duplicate. *$p < 0.05$ compared to corresponding control

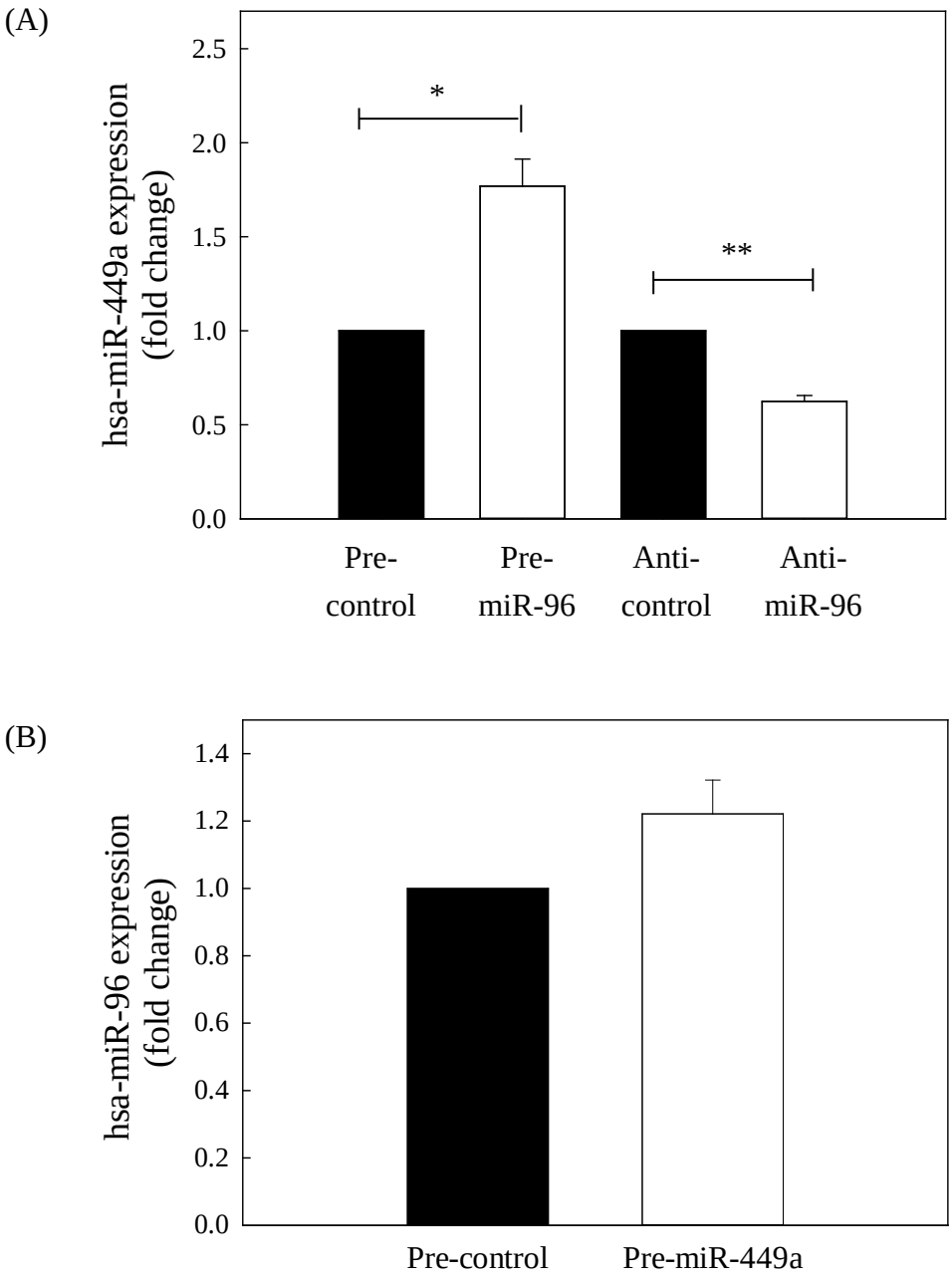

Figure 4.12 | miR-96 positively regulate the expressionof miR-449a. (A) Using qRT-PCR, the expression level of miR-449a was measured when the cells were transfected with either miR-96 precursor or inhibitor. (B) The other way round, the expression level of miR-96 was measured when the cells were transfected with either miR-449a precursor. At least three individual experiments were performed, and each experiment was in duplicate. *$p < 0.05$; **$p < 0.01$ compared to corresponding control

(A)

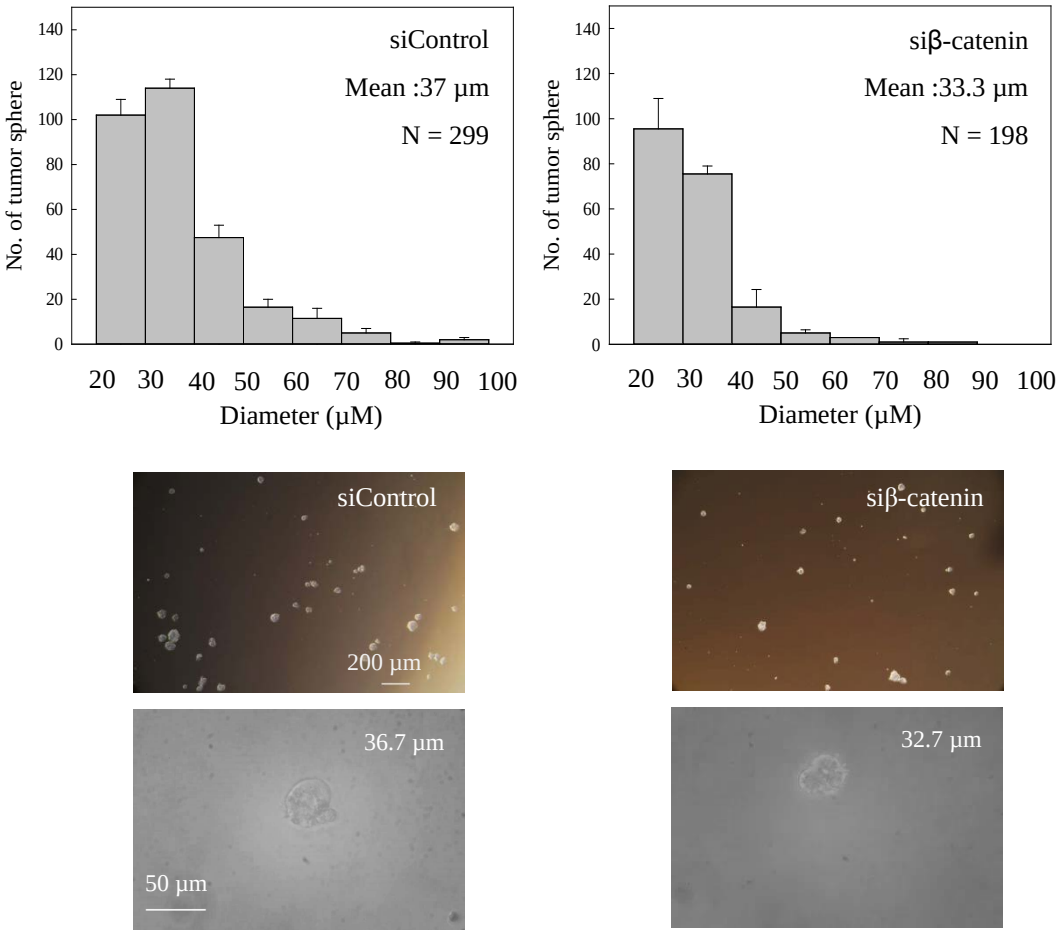
siControl
Mean :37 μm
N = 299
No. of tumor sphere
Diameter (μM)
siβ-catenin
Mean :33.3 μm
N = 198
No. of tumor sphere
Diameter (μM)
siControl
200 μm
siβ-catenin
36.7 μm
50 μm
32.7 μm

(B)

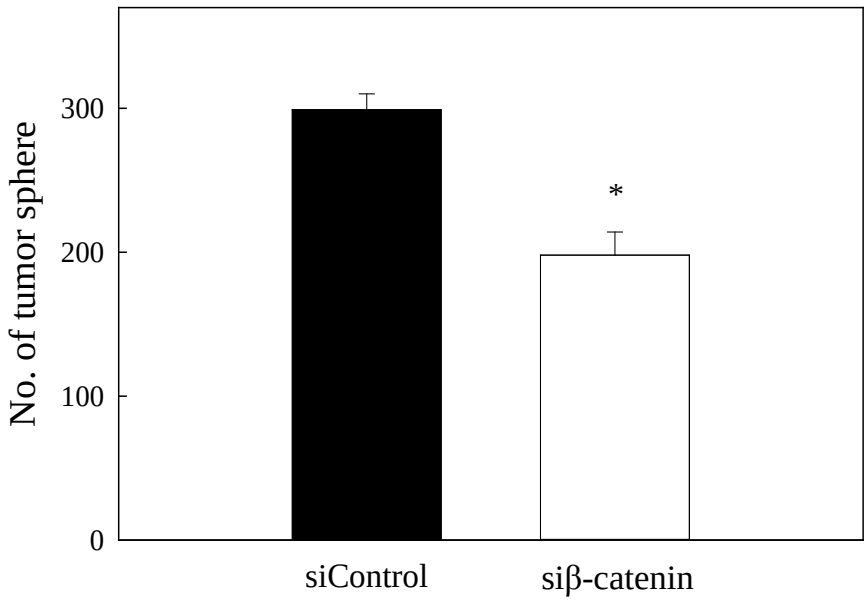
No. of tumor sphere
*
siControl
siβ-catenin

(C)

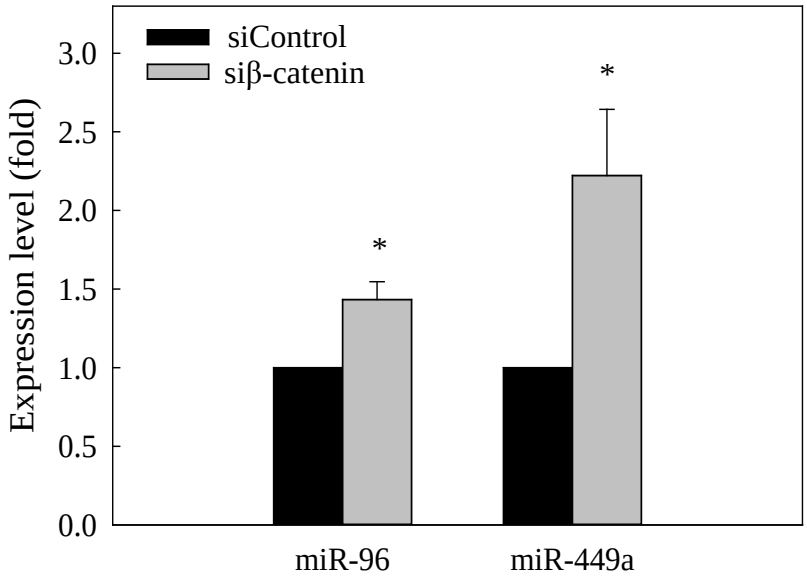

Figure 4.13 | Effect of β-catenin siRNA on the formation of tumor spheres and expression levels of miR-96 and miR-449a. C666-1 cells were transfected with β-catenin siRNA or negative control siRNA at 50 nM. (A, B) The transfected cells were harvested and subjected to tumor spheroid formation assay. The size profile, representative bright field images with low and high magnification and the total number of tumor spheres were presented. (C) The expression levels of miR-96 and miR-449a in the transfected cells were measued using qRT-PCR. Three independent experiments were carried out. *$p < 0.05$.

(A)

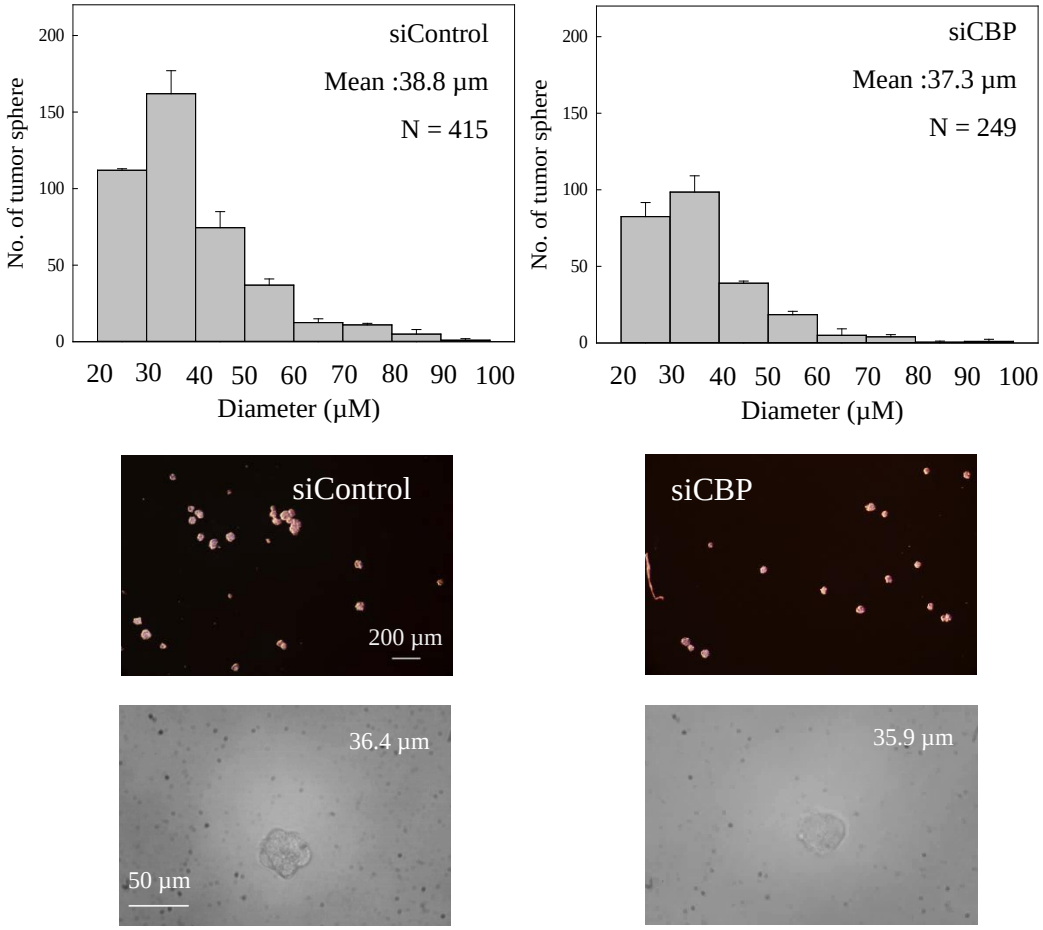
siControl
Mean :38.8 µm
N = 415
No. of tumor sphere
Diameter (µM)
siCBP
Mean :37.3 µm
N = 249
No. of tumor sphere
Diameter (µM)
siControl
200 µm
siCBP
36.4 µm
50 µm
35.9 µm

(B)

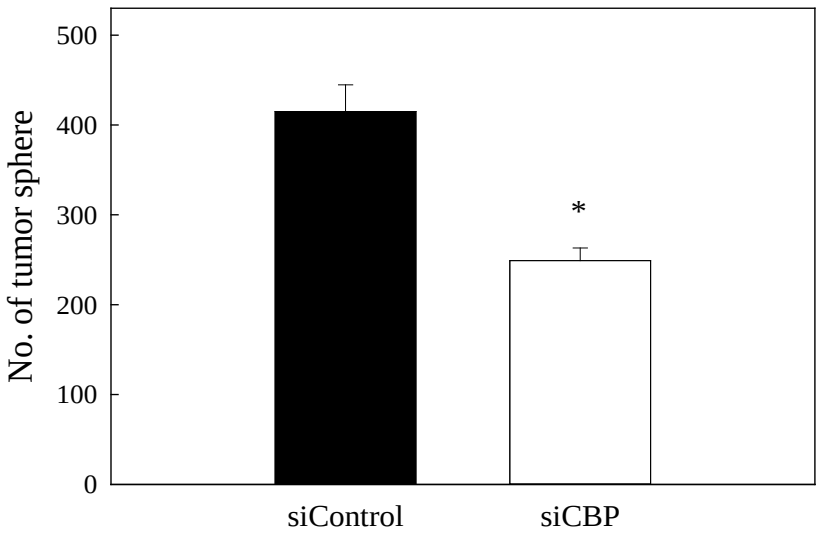
No. of tumor sphere
*
siControl
siCBP

(C)

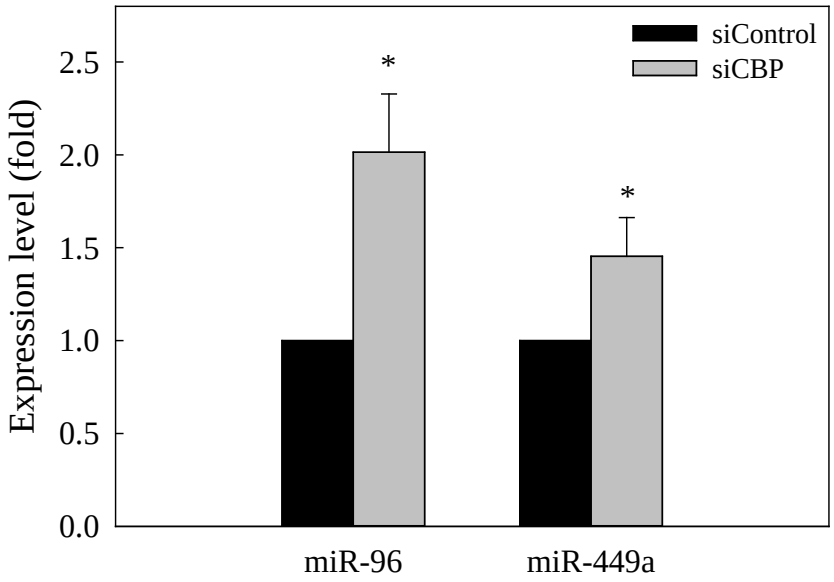

Figure 4.14 | Effect of CBP siRNA on the formation of tumor spheres and expression levels of miR-96 and miR-449a. C666-1 cells were transfected with CBP siRNA or negative control siRNA at 50 nM. (A, B) The transfected cells were harvested and subjected to tumor spheroid formation assay. The size profile, representative bright field images with low and high magnification and the total number of tumor spheres were presented. (C) The expression levels of miR-96 and miR-449a in the transfected cells were measued using qRT-PCR. Three independent experiments were carried out. *$p < 0.05$.

(A)

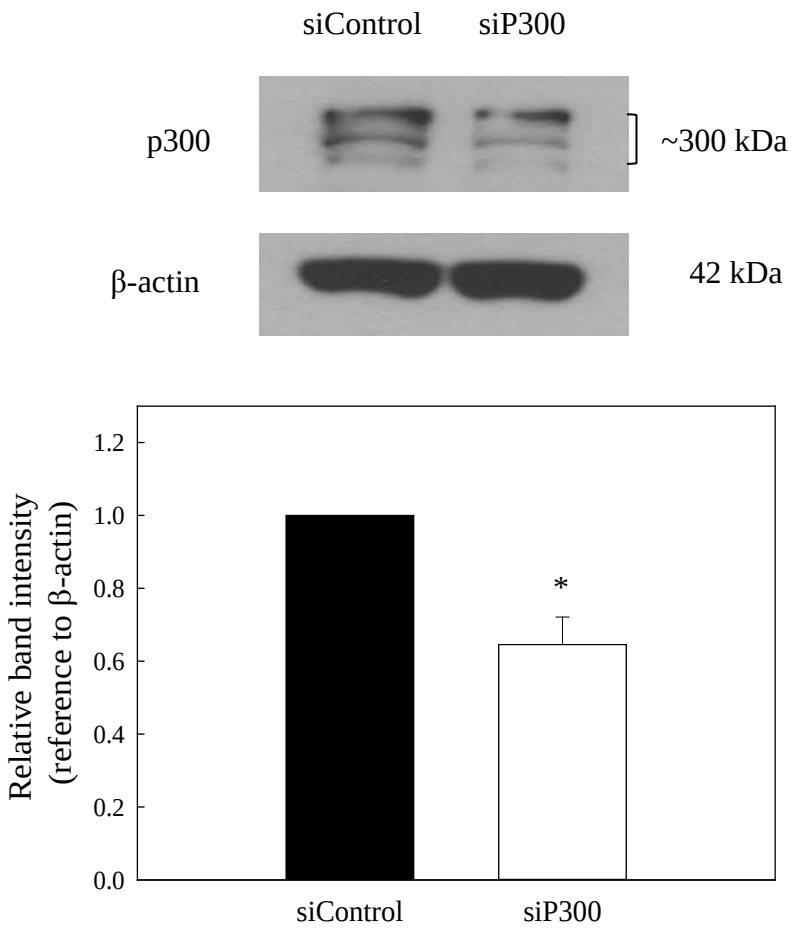
siControl
siP300
p300
~300 kDa
β-actin
42 kDa
Relative band intensity
(reference to β-actin)
1.2
1.0
0.8
0.6
0.4
0.2
0.0
*
siControl
siP300

(B)

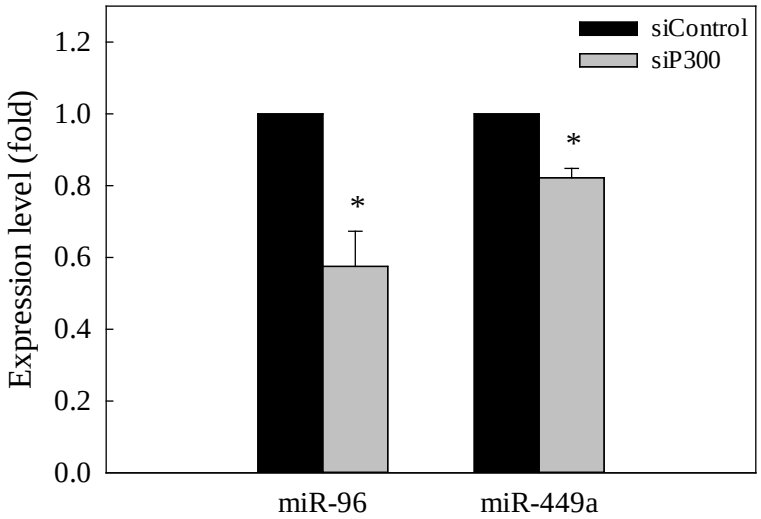
siControl
siP300
Expression level (fold)
1.2
1.0
0.8
0.6
0.4
0.2
0.0
*
*
miR-96
miR-449a

Figure 4.15 | Effect of p300 siRNA on the expression levels of miR-96 and miR-449a. C666-1 cells were transfected with p300 siRNA or negative control siRNA at 50 nM. (A) Transfection efficiency was confirmed. (B) The expression levels of miR-96 and miR-449a in the transfected cells were measued using qRT-PCR. Three independent experiments were carried out. *$p < 0.05$.

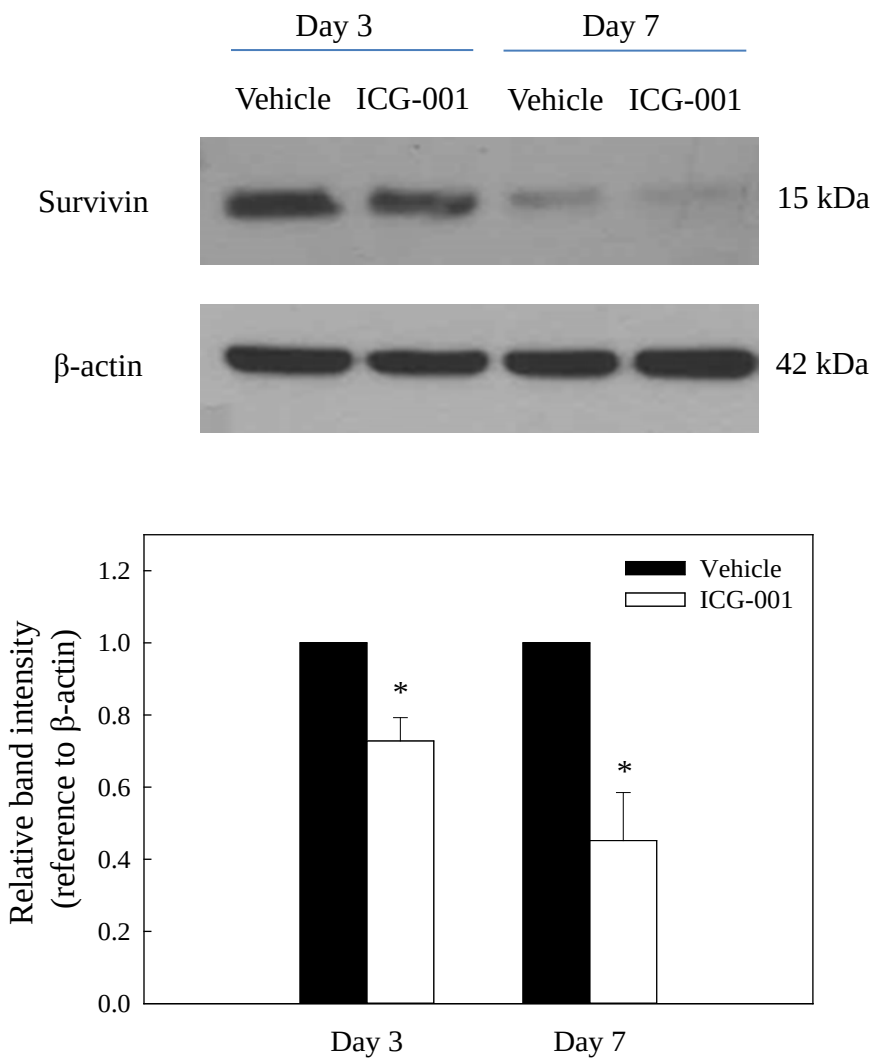

Figure 4.16 | ICG-001 down-regulates survivin expression. C666-1 cells were treated with ICG-001 (10 μM) or DMSO (vehicle control) for 3 or 7 days. The expression of survivin protein was determined by Western-blotting analysis (upper panel). Signal intensities were determined by quantitative densitometry and expressed as fold change of survivin normalized to β-actin (lower panel). Values are presented as means ± SD of three independent experiments. *$p < 0.05$, compared with vehicle control

(A)

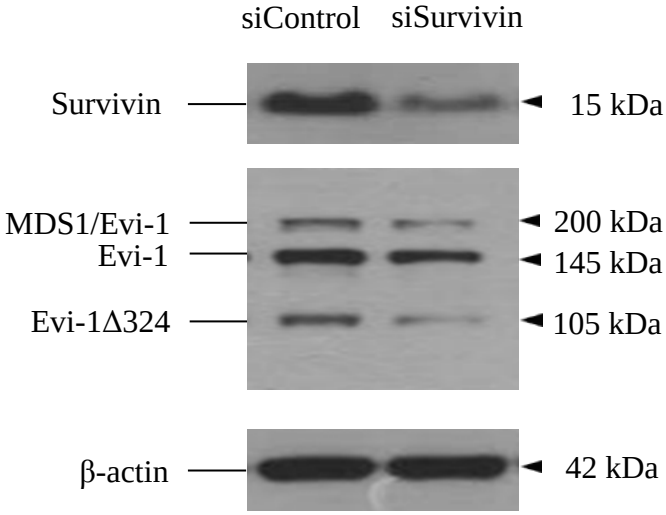
siControl
siSurvivin
Survivin
15 kDa
MDS1/Evi-1
Evi-1
200 kDa
145 kDa
Evi-1Δ324
105 kDa
β-actin
42 kDa

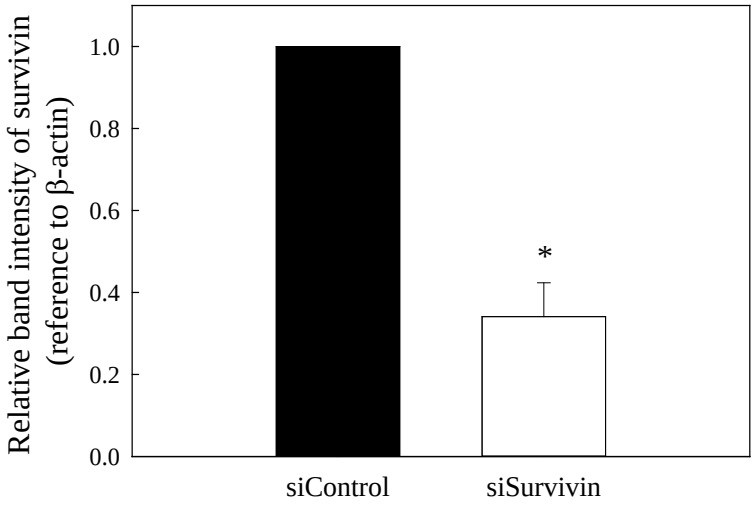
Relative band intensity of survivin
(reference to β-actin)
1.0
0.8
0.6
0.4
0.2
0.0
*
siControl
siSurvivin

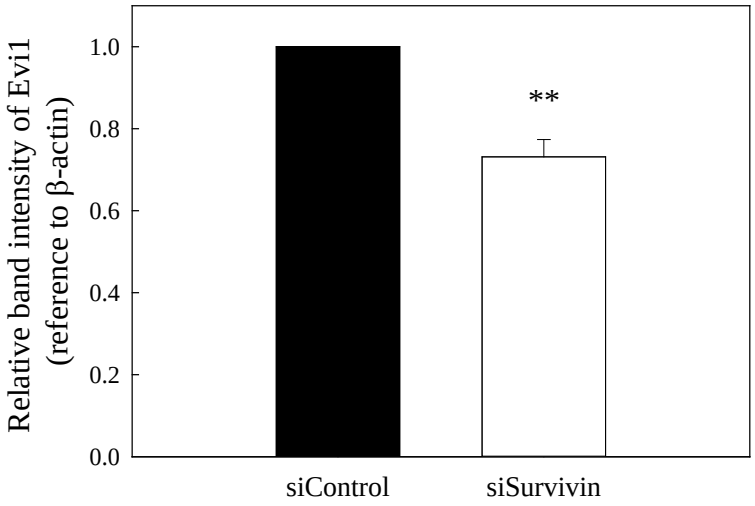
Relative band intensity of Evi1
(reference to β-actin)
1.0
0.8
0.6
0.4
0.2
0.0
**
siControl
siSurvivin

(B)

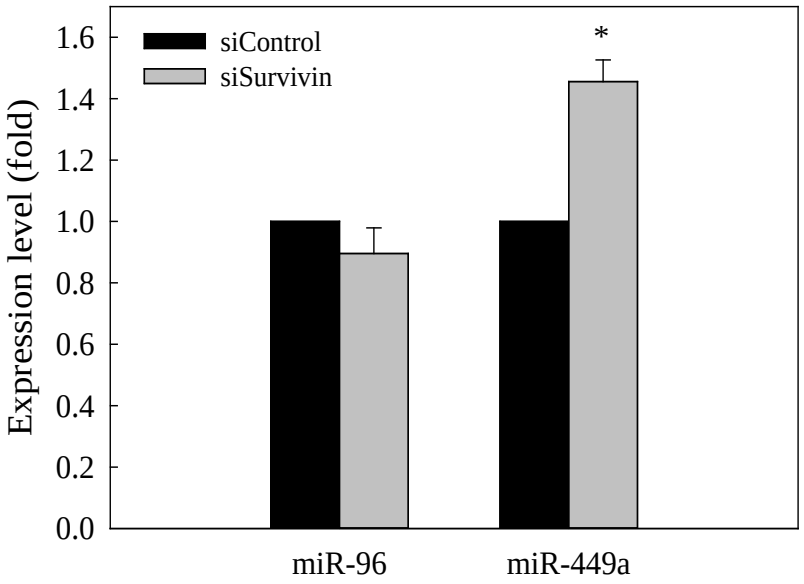

Figure 4.17 | Effect of survivin siRNA on the expression of Evi1 protein, miR-96 and miR-449a. C666-1 cells were transfected with survivin siRNA or negative control siRNA at 50 nM. (A) Using Western blotting analysis, the transfection efficiency was confirmed, and the protein expression of Evi1 in the transfected cells was reduced.. (B) The expression levels of miR-96 and miR-449a in the transfected cells were measued using qRT-PCR. At least three independent experiments were carried out. *$p < 0.05$; **$p < 0.01$.

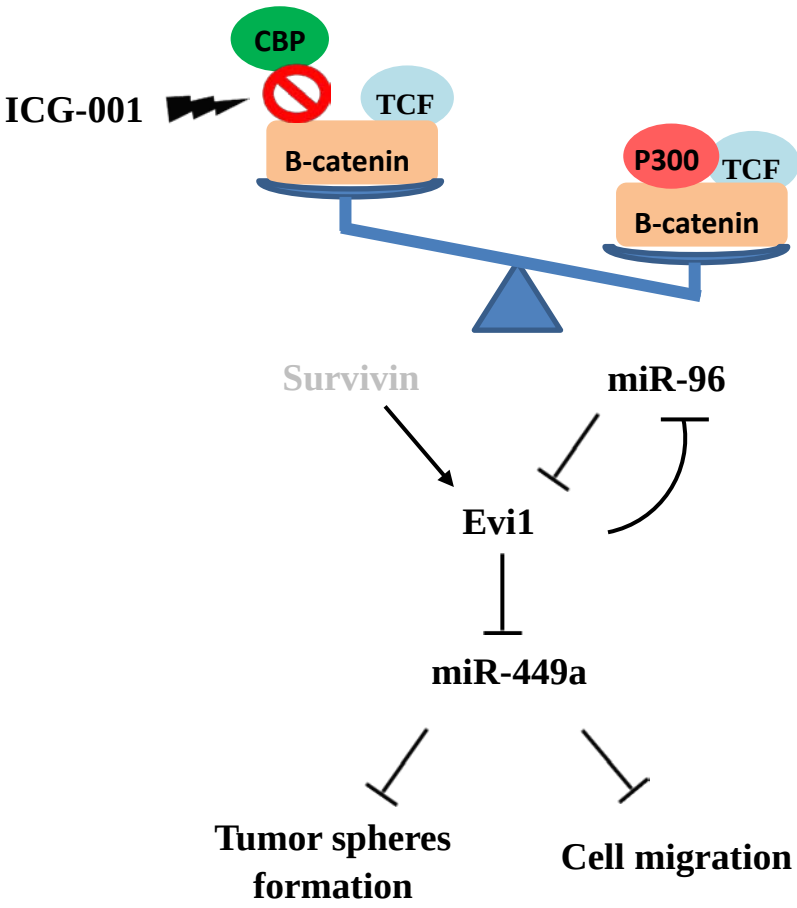

Figure 4.18 | A schematic diagram of Evi1/miR-449a axis regulated by survivin or miR-96 in ICG-001-treated cells. ICG-001 inhibits cell migration and tumor sphere growth of NPC cells via down-regulating survivin and up-regulating miR-96 that both funnel down to regulate Evi1 and miR-449a.

CHAPTER 5

ICG-001 enhances the treatment efficacy of cisplatin on NPC

5.1 Introduction

Cisplatin-based concurrent chemoradiotherapy is a contemporary approach for metastatic NPC (Xu *et al.*, 2016a). Cisplatin belongs to the class of platinum-containing drugs and is able to bind to the DNA. It works in part by blocking the DNA replication and so intentionally to kill the fastest proliferating cells. More importantly, it is believed to exhibit radiosensitization possibly by increasing DNA damage, inhibiting DNA repairing process and lowering the apoptosis threshold of the cells (Fong, 2016). Common side effects include renal and cardiac toxicities, gastrotoxicity, neurotoxicity, myelosuppression, nausea and vomiting (Dugbartey *et al.*, 2016). Although this conventional treatment regime is generally effective in early-stage NPC, it is far from satisfactory for late-stage diseases. In addition to the low survival rate reported for late stage primary NPC, 15%-58% of the patients were diagnosed with recurrent NPC, and the average 5-year overall survival rate after the re-treatment is only about 20% (Xu *et al.*, 2013). Alternative therapies to locally advanced, metastatic and recurrent NPC have been extensively under investigation.

The drug resistance and secondary malignancies encountered in NPC cases are believed to be resulted from the presence of CSCs, based on the CSC hypothesis. While the bulk tumor cells are more sensitive to cisplatin treatment, we tried to incorporate ICG-001 treatment to drive the CSCs to differentiate into more radio/chemo-sensitive cells. Here, we present the potential use of ICG-001 in concurrent with cisplatin in NPC treatment using *in vitro* and *in vivo* models.

5.2 Results

5.2.1 Effect of ICG-001/cisplatin concurrent therapy on the growth of NPC cells

Development of drug resistance is a major concern in cisplatin-based chemotherapy for metastatic NPC, possibly because the treatment is only effective in the eradication of the drug-sensitive bulk tumor cells. Therefore, this part of the study aims to incorporate ICG-001 treatment into a conventional cisplatin-based regimen to drive the CSCs to differentiate into cisplatin-sensitive cells, in order to increase the treatment efficacy.

Initially, the *in vitro* effect of ICG-001/cisplatin co-treatment was studied in C666-1 cells using cell growth assay. The cells were treated with 1 μM ICG-001 together with various concentrations of cisplatin for either 3 or 7 days. Total number of cells in various treatment groups (vehicle, cisplatin alone, ICG-001 alone and cisplatin/ICG-001 combined group) at day-3 and -7 were counted and the results were presented in Figure 5.1A and 5.2A.

The data in the cell growth assay was analyzed by CompuSyn software (Chou and Talalay, 1984; Chou, 2010). This program allows us to quantify the combination effect of cisplatin and ICG-001 by determining the CI values at IC_{50}, and provides us different simulation plots. Dose-effect curves of the treated NPC cells at day-3 and day-7 were plotted in Figure 5.1B and 5.2B, respectively. The curves showed that less viable cells could be seen in the co-treatment group than the groups treated with either ICG-001 or cisplatin alone. The synergistic effect between cisplatin and ICG-001 at day-3 and day-7 could be clearly shown in the

normalized isobolograms and the tables presented in Figure 5.1C and 5.2C, respectively. All the combination data points fall on the lower left of the hypotenuse in the isobolograms, and all the CI values in the tables were smaller than 1, meaning that co-treatment of cells with cisplatin and ICG-001 had a synergistic inhibitory effect on the growth of C666-1 cells. These observations are in accord with the results from the MTT assay conducted by Chan *et al.*, (2015).

5.2.2 Effect of ICG-001/cisplatin concurrent therapy on tumor spheroid formation

Next, we tried to demonstrate the combined effect of ICG-001 and cisplatin on the tumor spheroid forming capacity of C666-1 cells. Although treatment with either cisplatin alone or ICG-001 alone could significantly inhibited the growth of tumor spheres, the combined treatment could further suppress the growth of tumor spheres (Figure 5.3). Results from this part of study indicated that combination of ICG-001and cisplatin could further suppress the growth off CSC-enriched tumor spheres.

5.2.3 Effect of ICG-001/cisplatin concurrent therapy in nude mice tumorigenicity assay

Finally, the feasibility of using ICG-001/cisplatin combination therapy was demonstrated in two EBV-positive NPC xenografts, X2117 and C17 xenografts. Prior to the combination therapy, dose responses of X2117 (Figure 5.4) and C17 (Figure 5.6) to cisplatin were examined in order to acquire a sub-optimal dose of cisplatin for the following co-treatment experiments. Cisplatin at 3 mg/kg/week and at 1 mg/kg/4 days were found to be the sub-optimal doses for X2117 and C17, respectively. Also, mice were found to lose weight with increasing the dose of

cisplatin.

Subsequently, we tried to demonstrate the synergistic effect between ICG-001 and cisplatin in these two xenografts (Figure 5.5 for X2117, Figure 5.7 for C17). During the experiments, ICG-001 (~50 mg/kg/day) was steadily delivered from the implanted osmotic pumps and cisplatin (3 mg/kg/week for X2117, 1 mg/kg/4 days for C17) was regularly injected into corresponding mice. Compared to the control group, both cisplatin alone and ICG-001 alone groups showed a slight growth inhibition on the tumor. Excitingly, an obvious suppression on the growth of tumor was found in the co-treatment groups. In addition, all the mice gained weight at the end of the experiments, and the weight of the mice from all the treatment groups are comparable, meaning that the combination of ICG-001 with a lower dose of cisplatin is not toxic to the mice. Afterwards, the *in vivo* combination effect between ICG-001 and cisplatin was calculated using the Zheng-Jun Jin method (Jin, 1980; Li *et al.*, 2013; Liu *et al.*, 2015; Zheng *et al.*, 2015). The q values from both xenograft experiments are larger than 1.15, indicating ICG-001 and cisplatin could synergistically inhibited the growth of NPC tumors.

5.3 Discussion

A concurrent ICG-001/cisplatin treatment was demonstrated to exhibit a synergistic inhibition on NPC in this part of study. Given that C666-1 cells being cisplatin-resistant (Lun *et al.*, 2012), we demonstrated that ICG-001 could sensitize the cells to cisplatin treatment, resulting in a synergistic inhibition on cell growth and tumor sphere formation. The synergism could be also observed in the *in vivo* studies in terms of the sizes of tumors carried by the mice. Despite a lower dose of cisplatin used in the concurrent treatment, a significant efficacy was observed while the health conditions of all the mice were good with steady gain in weight.

Increased cisplatin sensitivity might be explained through CD44, Evi1 and the miRNAs modulated in the ICG-001 treatment. CD44 was able to protect P-glycoprotein (P-gp) from ubiquitination (Abhilash *et al.*, 2015), so suppression on CD44 may destabilize P-gp and result in less cytotoxic drug being pumped out of the cells. It is worthy to note that NPC cell with CD44 knock-down was found to exhibit greater cisplatin sensitivity in the cell viability assay (Shen *et al.*, 2016). We speculate that accumulation of cisplatin in ICG-001-treated cells by suppressing CD44 may drive the cells become more radio- or chemo- sensitive. Evi1 may be another poor prognosis factor contributing drug resistance. It appears to inhibit TGFβ responses to achieve chemo-resistance in colon cancer (Liu *et al.*, 2006). Suppression on Evi1 was revealed to restore the chemo-sensitivity in leukemia cells through reducing the cell adhesion ability (Yamakawa *et al.*, 2012). MiR-96 and miR-449a were identified to be under-expressed in cisplatin-resistant ovarian cancer cells (Zhou *et al.*, 2014; Liu *et al.*, 2016). Zhou *et al.* (2014)

demonstrated that ectopic expression of miR-449a enhanced the cisplatin sensitivity by suppressing Notch 1 pathway in ovarian cancer, and Hu *et al.*, 2014 pointed out that miR-449a could manage the cisplatin sensitivity through cyclin D1 and Bcl2 which are two important regulators in NPC as well. However, the relationship between miR-96 and the drug sensitivity has not yet been systematically studied. Therefore, we speculate that ICG-001 may drive the CSCs undergo differentiation and trigger the cells become more cisplatin-sensitive via suppression on CD44 and Evi1, and restoration on miR-96 and miR-449a in this study.

All in all, the present study suggests that ICG-001 may be used to inhibit the proliferation of NPC cells with CSC-like characteristics and lower the therapeutic doses of cisplatin while maintaining or improving the cancer treatment efficacy. Taken into account that the 20-fold more potent derivative of ICG-001, termed PRI-724, has entered into multiple clinical studies and conferred little cytotoxicity (Weinberg, 2013), clinical investigations of PRI-724 combined with cisplatin may provide a better treatment outcome to NPC patients.

(A)

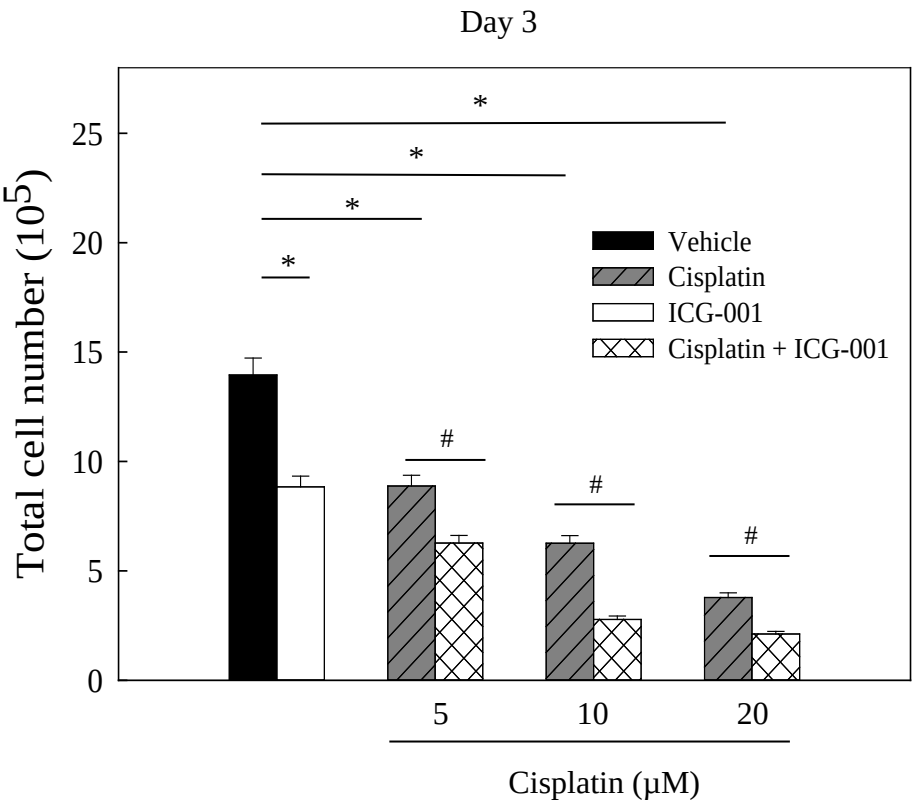
Day 3
Total cell number (10^5)
25
20
15
10
5
0
*
*
*
*
#
#
#
Vehicle
Cisplatin
ICG-001
Cisplatin + ICG-001
5
10
20
Cisplatin (μM)

(B)

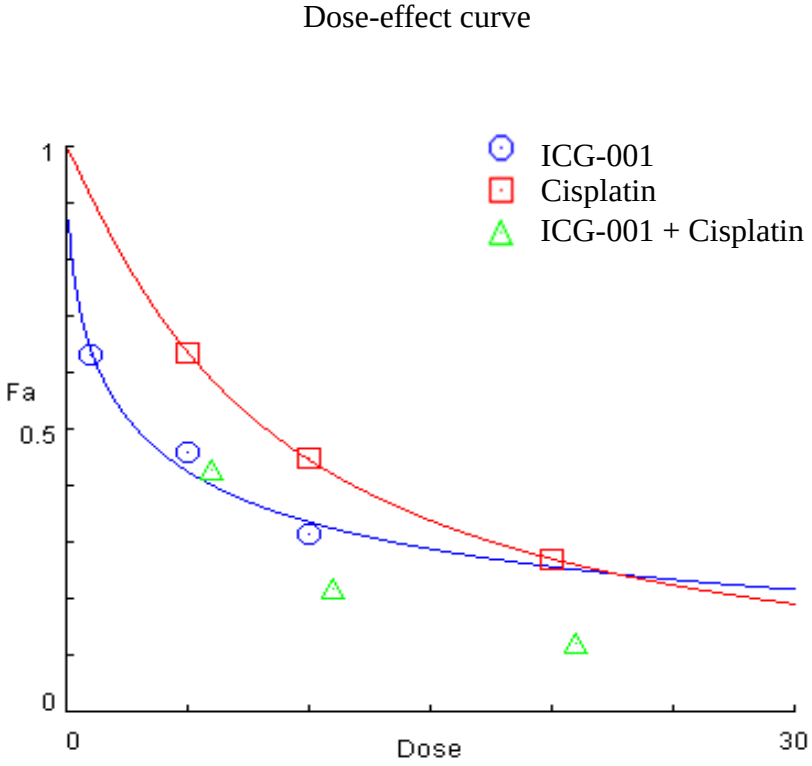
Dose-effect curve
ICG-001
Cisplatin
ICG-001 + Cisplatin
Fa
1
0.5
0
0
Dose
30

(C) Normalized isobologram

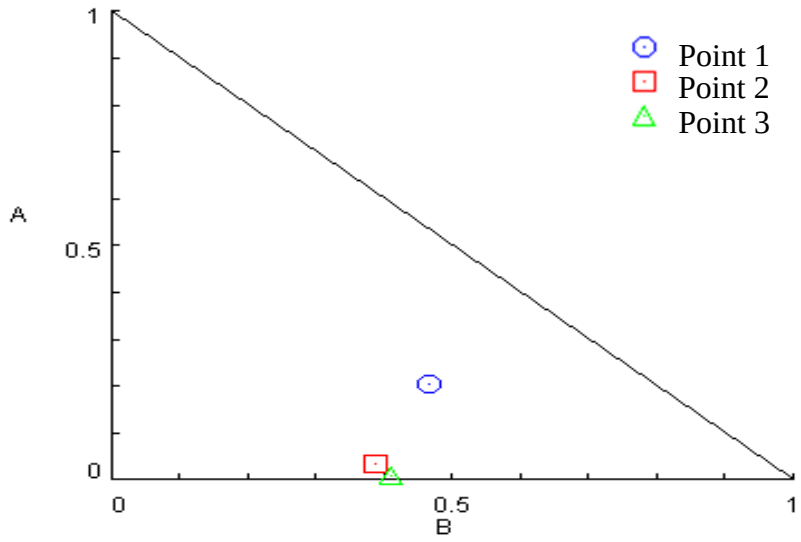

Point	Dose ICG-001 (μM)	Dose Cisplatin (μM)	Effect	CI
1	1.0	5.0	0.4293	0.67257
2	1.0	10.0	0.2193	0.42161
3	1.0	20.0	0.1217	0.42108

Figure 5.1 | Synergistic inhibitory effect of ICG-001 and cisplatin on the growth of C666-1 cells. (A) The growth of C666-1 cells treated with either ICG-001 (1 μM), cisplatin (5, 10, 20 μM) or the combination of ICG-001 and cisplatin for 3 days. Total number of viable cells were counted using trypan blue exclusion assay. The data were analyzed by CompuSyn software with the results showing (B) dose-effect curve and (C, upper panel) normalized isobologram. The table in (C, lower panel) lists the concentrations of the drugs, inhibitory effects (ranged from 0 to 1) and the CI values. Representative result was presented from at least three separate experiments. *Fa*, the fraction of cell death, with 0 meaning no cell killing and 1 meaning 100% of cell killing. *$p < 0.05$ compared to DMSO vehicle control; #$p < 0.05$ compared to corresponding cisplatin treatment groups.

(A)

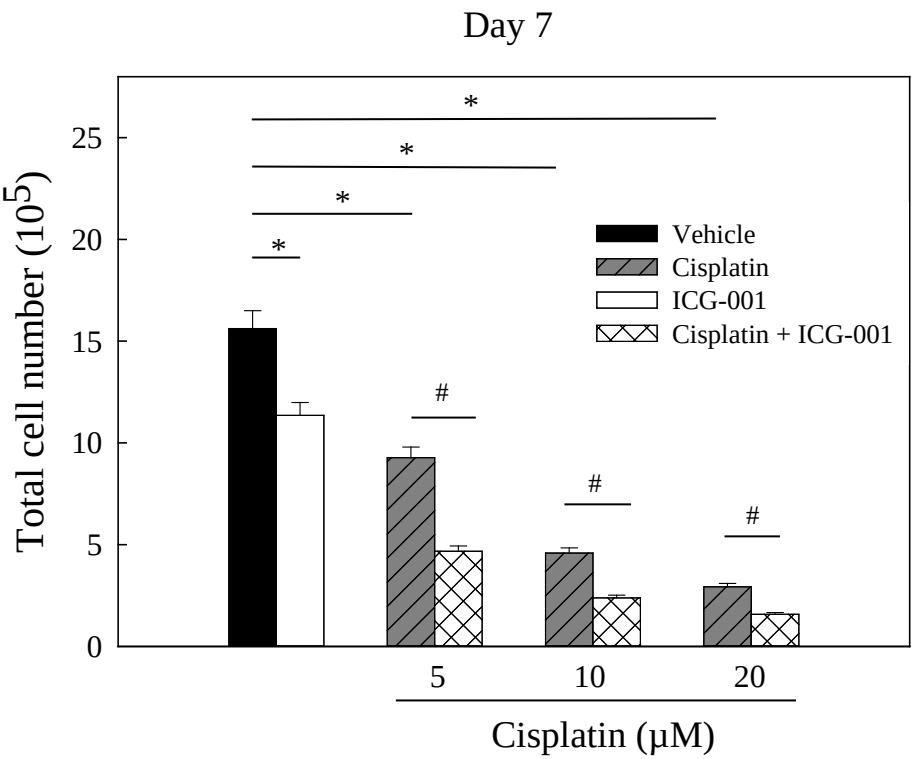
Day 7
Total cell number (10^5)
25
20
15
10
5
0
*
*
*
*
#
#
#
Vehicle
Cisplatin
ICG-001
Cisplatin + ICG-001
5
10
20
Cisplatin (μM)

(B)

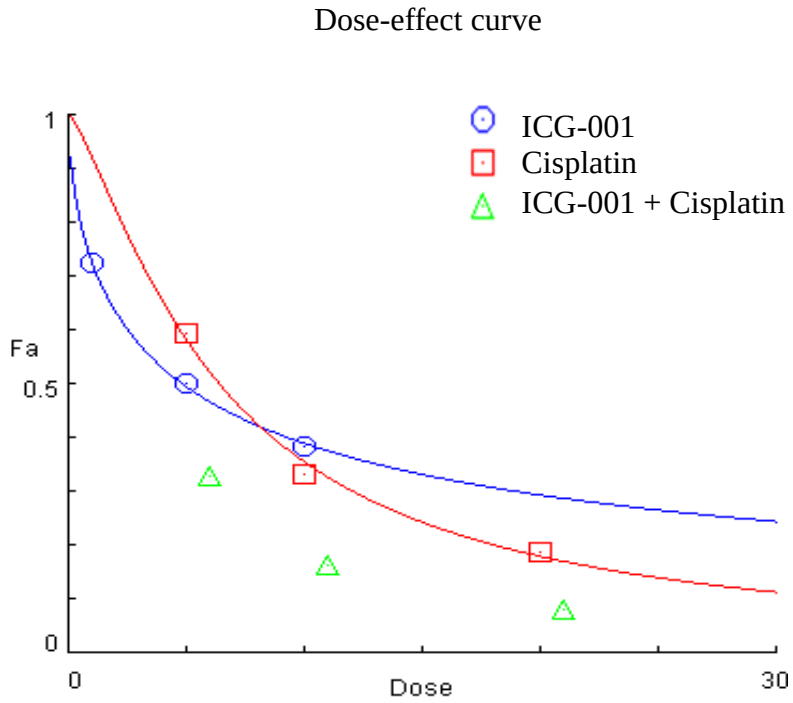
Dose-effect curve
ICG-001
Cisplatin
ICG-001 + Cisplatin
Fa
1
0.5
0
0
Dose
30

(C)

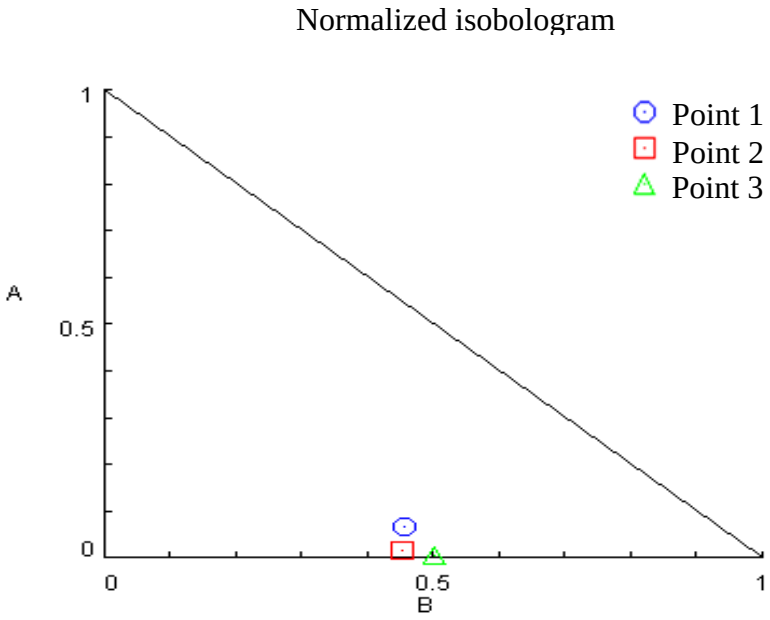

Point	Dose ICG-001 (μM)	Dose Cisplatin (μM)	Effect	CI
1	1.0	5.0	0.3294	0.52281
2	1.0	10.0	0.1625	0.47015
3	1.0	20.0	0.0809	0.50735

Figure 5.2 | Synergistic inhibitory effect on the growth of C666-1 cells. (A) The growth histogram of C666-1 cells treated with either ICG-001 (1 μM), cisplatin (5, 10, 20 μM) or the combination for 7 days. Total number of viable cells were counted using trypan blue cell growth assay. The data were analyzed by CompuSyn software with the results showing (B) dose-effect curve and (C, upper panel) normalized isobologram. The table in (C, lower panel) lists the concentrations of the drugs, inhibitory effects (ranged from 0 to 1) and the CI values. Representative result was presented from at least three separate experiments. *Fa*, the fraction of cell death, with 0 meaning no cell killing and 1 meaning 100% of cell killing. **p* < 0.05 compared to DMSO vehicle control; #*p* < 0.05 compared to corresponding cisplatin treatment groups.

(A)

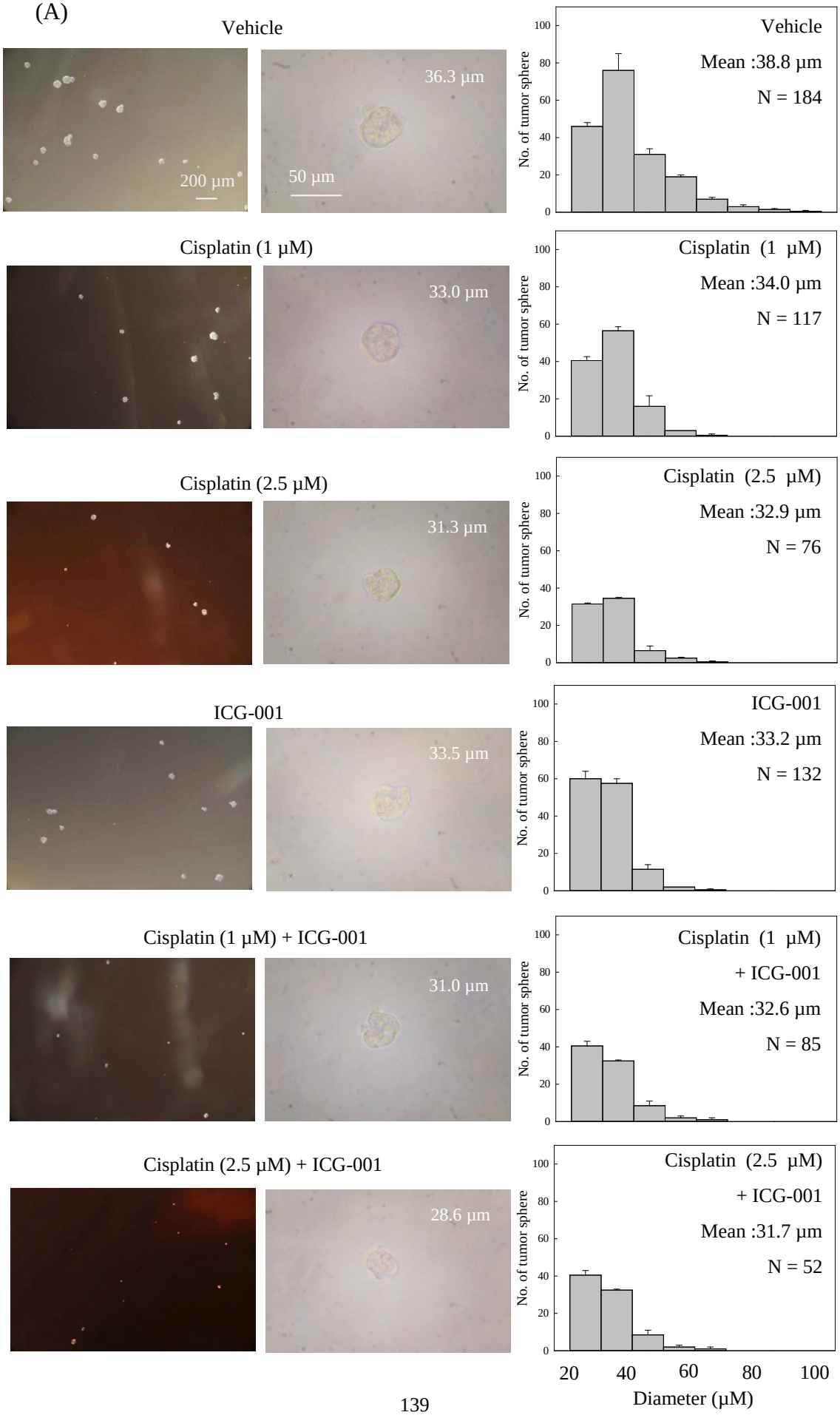
Vehicle
200 μm
36.3 μm
50 μm
Vehicle
Mean :38.8 μm
N = 184
Cisplatin (1 μM)
33.0 μm
Cisplatin (1 μM)
Mean :34.0 μm
N = 117
Cisplatin (2.5 μM)
31.3 μm
Cisplatin (2.5 μM)
Mean :32.9 μm
N = 76
ICG-001
33.5 μm
ICG-001
Mean :33.2 μm
N = 132
Cisplatin (1 μM) + ICG-001
31.0 μm
Cisplatin (1 μM)
+ ICG-001
Mean :32.6 μm
N = 85
Cisplatin (2.5 μM) + ICG-001
28.6 μm
Cisplatin (2.5 μM)
+ ICG-001
Mean :31.7 μm
N = 52
No. of tumor sphere
0
20
40
60
80
100
20
40
60
80
100
Diameter (μM)

(B)

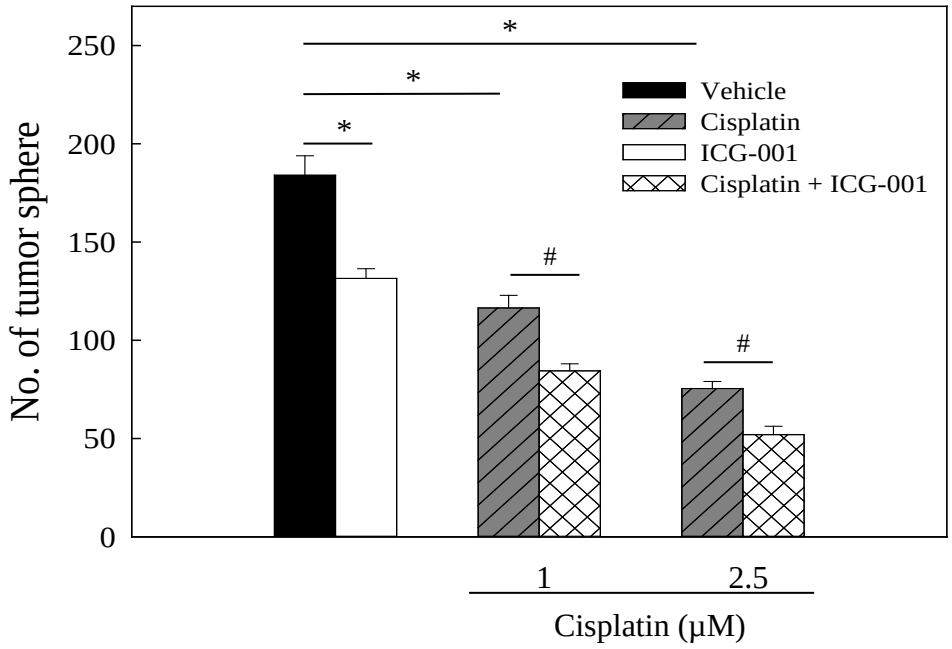

Figure 5.3 | The combined effect of ICG-001 and cisplatin on C666-1 tumor spheroid formation. C666-1 cells were treated with various concentrations of cisplatin (0, 1 or 2.5 μM) in the presence or absence of ICG-001 (1 μM). Images of the tumor spheres were captured under microscope and measured by ImageJ software. (A) Representative bright field images with low and high magnification, the size profile, and (B) the total number of tumor spheres were presented. Three individual experiments were carried out, and each experiment was performed in duplicate. *$p < 0.05$ compared to DMSO vehicle control; #$p < 0.05$ compared to corresponding cisplatin treatment groups.

(A)

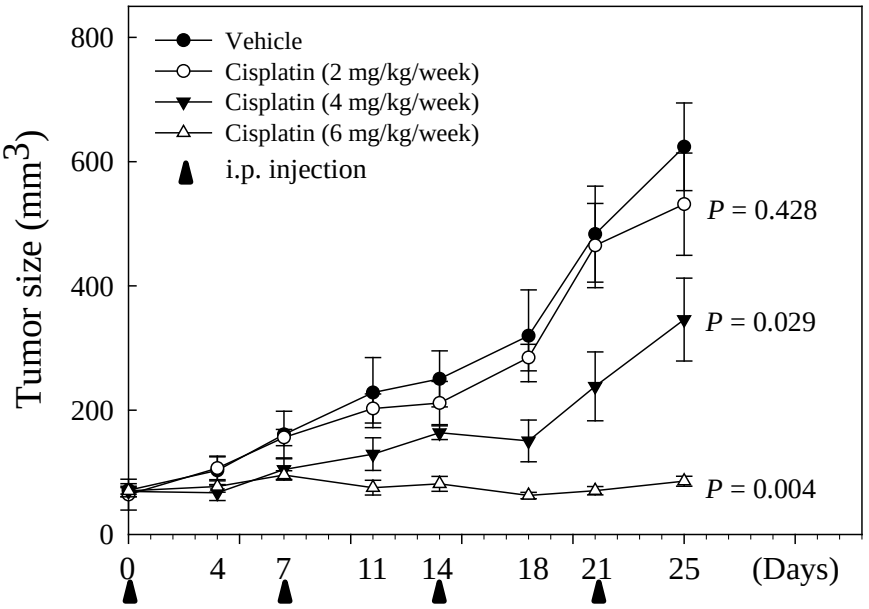
Vehicle
Cisplatin (2 mg/kg/week)
Cisplatin (4 mg/kg/week)
Cisplatin (6 mg/kg/week)
i.p. injection
Tumor size (mm3)
800
600
400
200
0
0
4
7
11
14
18
21
25
(Days)
P = 0.428
P = 0.029
P = 0.004

(B)

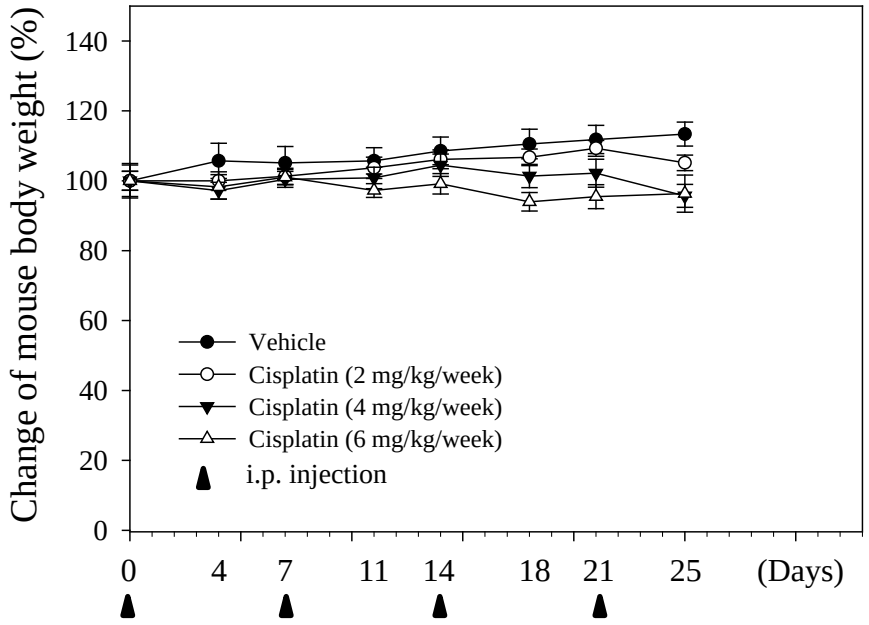
Change of mouse body weight (%)
140
120
100
80
60
40
20
0
Vehicle
Cisplatin (2 mg/kg/week)
Cisplatin (4 mg/kg/week)
Cisplatin (6 mg/kg/week)
i.p. injection
0
4
7
11
14
18
21
25
(Days)

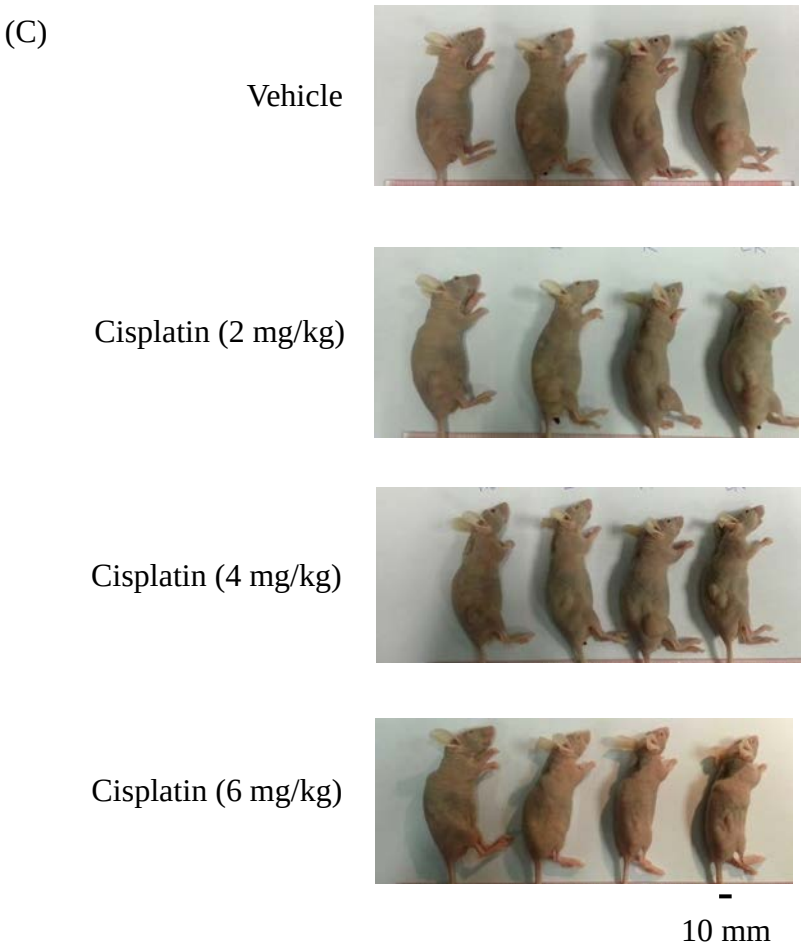

Figure 5.4 | Dose response study of cisplatin on X2117 NPC xenografts. (A) Cisplatin was i.p. injected at 2, 4 or 6 mg/kg into the nude mice transplanted with X2117 NPC xenografts weekly. The mice administrated with DMF were used as vehicle control group. (A) Tumor volumes and (B) body weight of the mice were measured twice weekly. Values are means ± SEM. (C) Images of the sacrificed mice (N = 4).

(A)

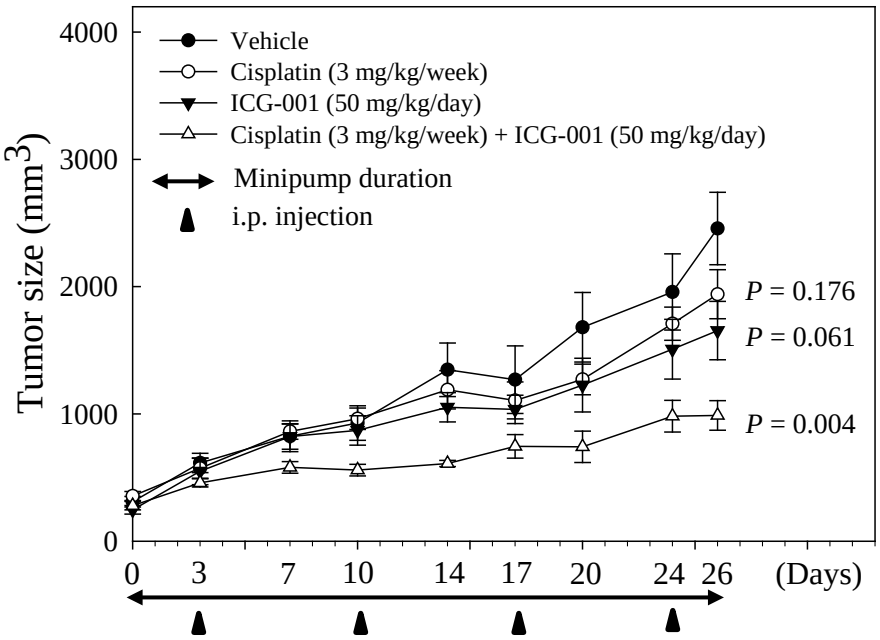
Tumor size (mm3)
4000
3000
2000
1000
0
Vehicle
Cisplatin (3 mg/kg/week)
ICG-001 (50 mg/kg/day)
Cisplatin (3 mg/kg/week) + ICG-001 (50 mg/kg/day)
Minipump duration
i.p. injection
P = 0.176
P = 0.061
P = 0.004
0 3 7 10 14 17 20 24 26 (Days)

(B)

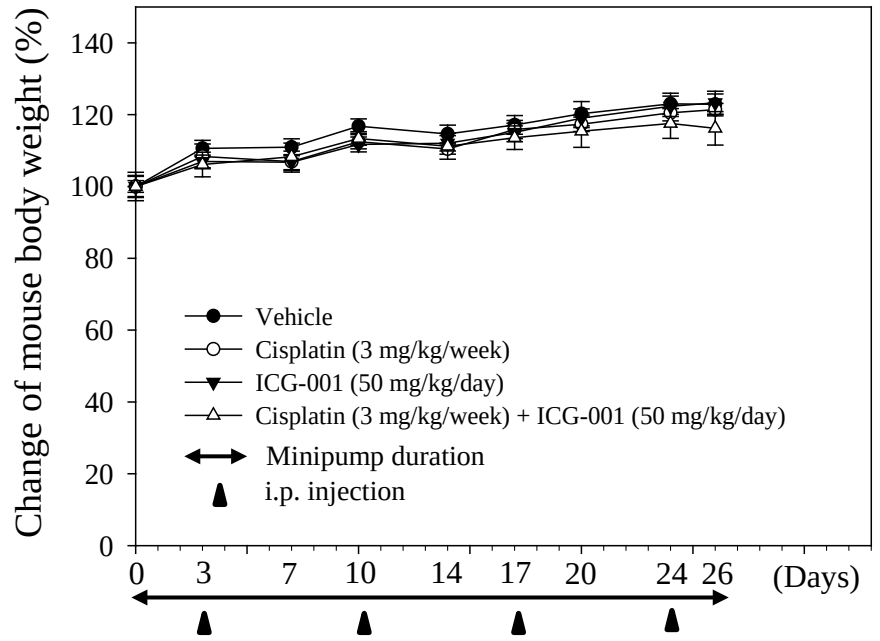
Change of mouse body weight (%)
140
120
100
80
60
40
20
0
Vehicle
Cisplatin (3 mg/kg/week)
ICG-001 (50 mg/kg/day)
Cisplatin (3 mg/kg/week) + ICG-001 (50 mg/kg/day)
Minipump duration
i.p. injection
0 3 7 10 14 17 20 24 26 (Days)

(C)

Vehicle

Cisplatin(3 mg/kg/week)

ICG-001 (50 mg/kg/day)

Cisplatin (3 mg/kg/week) +
ICG-001 (50 mg/kg/day)

10 mm

(D)

Group	Inhibition rate (%)
Cisplatin	21.03
ICG-001	32.65
Cisplatin + ICG-001	59.80

q value = 1.28

Figure 5.5 | Synergistic anti-tumor effect of ICG-001 and cisplatin on X2117 NPC xenografts. Micro-osmotic pumps with ICG-001 (50 mg/kg/day) or PBS were implanted into the nude mice bearing X2117 NPC xenografts (Day 0). Cisplatin at 3 mg/kg or DMF was administrated by i.p. injection weekly. (A) Tumor volumes and (B) body weight of the mice were measured twice weekly. Values are means ± SEM. (C) Images of the sacrificed mice (left panel) and the dissected tumors (right panel). n=5. (D) The inhibition rate of the drug treatments. According to Jin's formula, q > 1.15 indicating that cisplatin and ICG-001 synergistically inhibited the growth of X2117 xenografts.

(A)

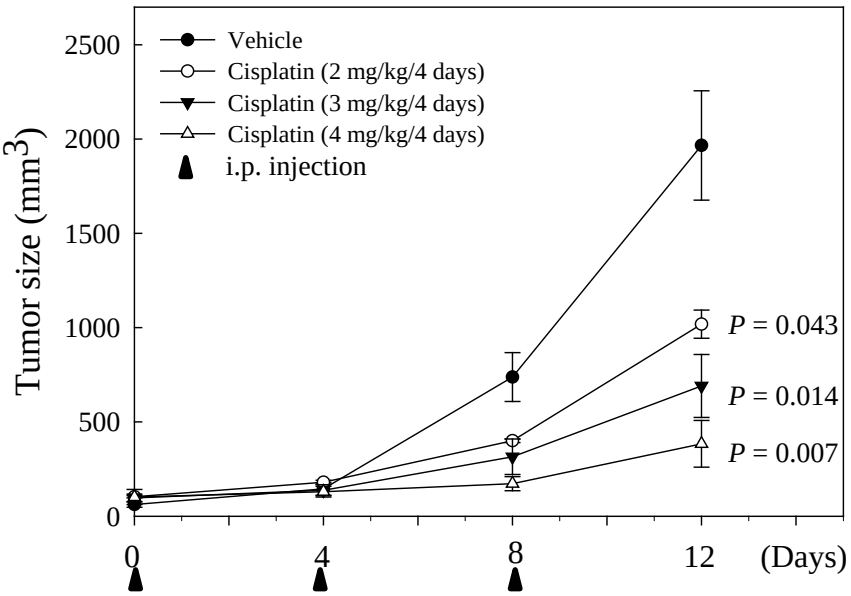
Vehicle
Cisplatin (2 mg/kg/4 days)
Cisplatin (3 mg/kg/4 days)
Cisplatin (4 mg/kg/4 days)
i.p. injection
Tumor size (mm3)
2500
2000
1500
1000
500
0
P = 0.043
P = 0.014
P = 0.007
0
4
8
12
(Days)

(B)

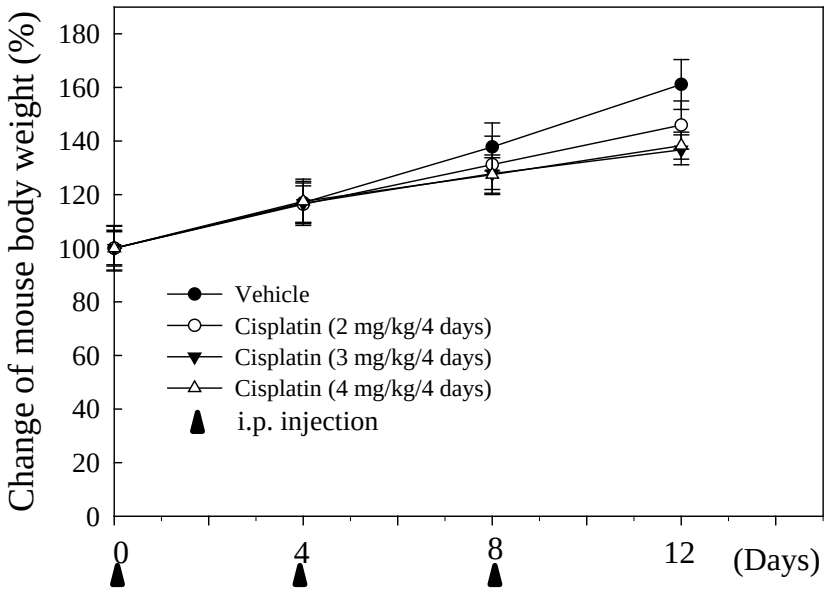
Change of mouse body weight (%)
180
160
140
120
100
80
60
40
20
0
Vehicle
Cisplatin (2 mg/kg/4 days)
Cisplatin (3 mg/kg/4 days)
Cisplatin (4 mg/kg/4 days)
i.p. injection
0
4
8
12
(Days)

(C)

Vehicle

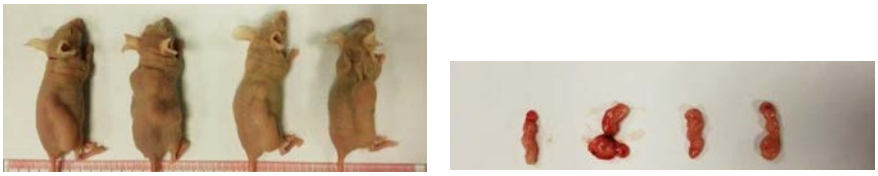

Cisplatin (2 mg/kg)

Cisplatin (3 mg/kg)

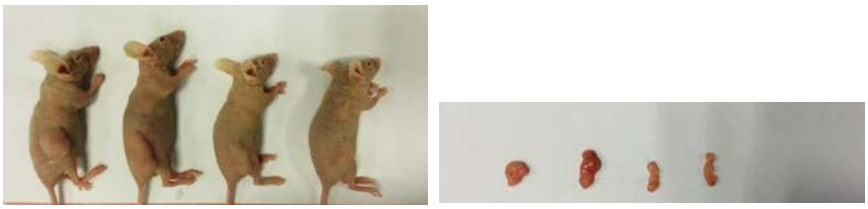

Cisplatin (4 mg/kg)

10 mm

Figure 5.6 | Dose response study of cisplatin on C17 NPC xenograft. Cisplatin was i.p. injected at 2, 3 or 4 mg/kg into the nude mice transplanted with C17 NPC xenograft on day 0, 4 and 8 (as the arrows pointed). The mice administrated with DMF were used as vehicle control group. (A) Tumor volumes. (B) Body weight of the mice. Values are means ± SEM. (C) Photos of the sacrificed mice (left panel) and the dissected tumors (right panel). n=4.

(A)

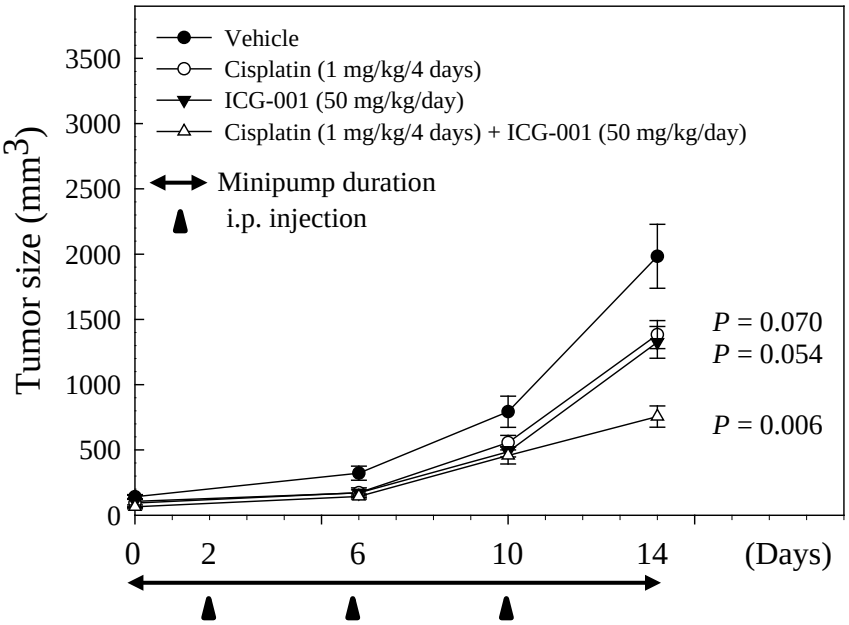
Vehicle
Cisplatin (1 mg/kg/4 days)
ICG-001 (50 mg/kg/day)
Cisplatin (1 mg/kg/4 days) + ICG-001 (50 mg/kg/day)
Minipump duration
i.p. injection
Tumor size (mm3)
3500
3000
2500
2000
1500
1000
500
0
P = 0.070
P = 0.054
P = 0.006
0
2
6
10
14
(Days)

(B)

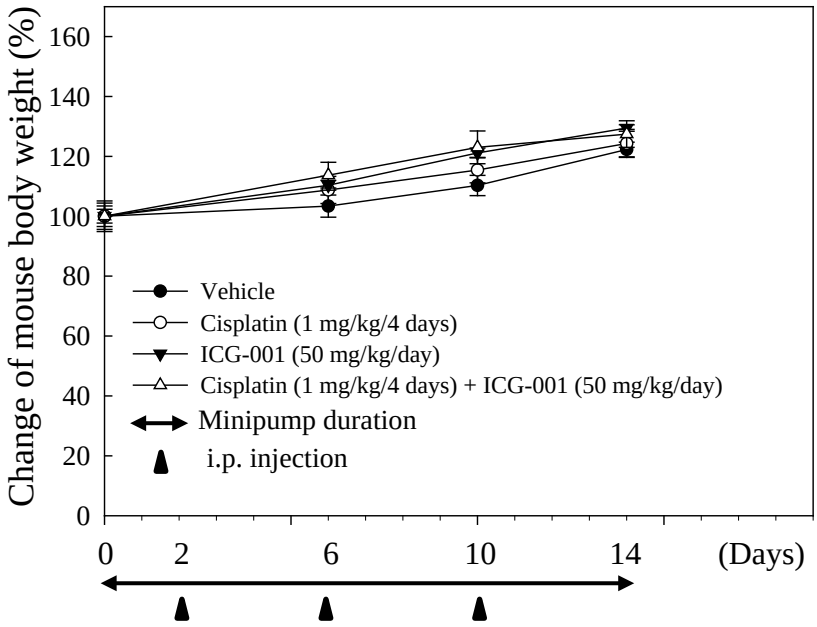
Change of mouse body weight (%)
160
140
120
100
80
60
40
20
0
Vehicle
Cisplatin (1 mg/kg/4 days)
ICG-001 (50 mg/kg/day)
Cisplatin (1 mg/kg/4 days) + ICG-001 (50 mg/kg/day)
Minipump duration
i.p. injection
0
2
6
10
14
(Days)

(C)

Vehicle

Cisplatin (1 mg/kg)

ICG-001 (50 mg/kg/day)

Cisplatin (1 mg/kg) + ICG-001 (50 mg/kg/day)

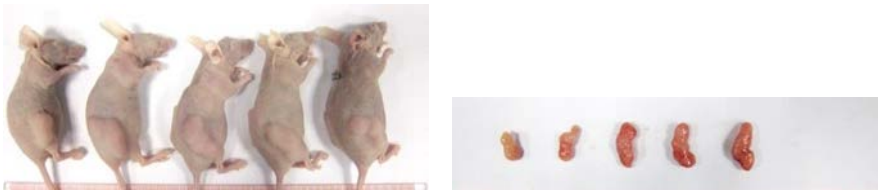

10 mm

(D)

Group	Inhibition rate (%)
Cisplatin	30.26
ICG-001	33.21
Cisplatin + ICG-001	61.88

q value = 1.16

Figure 5.7 | Synergistic anti-tumor effect of cisplatin and ICG-001 on C17 NPC xenografts. Micro-osmotic pumps with ICG-001 (50 mg/kg/day) or PBS were implanted into the nude mice bearing C17 NPC xenografts (Day 0). On Day 2, 6 and 10 after pump implantation (as the arrows pointed), cisplatin at 1 mg/kg was i.p. injected into the nude mice. (A) Tumor volumes. (B) Body weight of the mice. Values are means ± SEM. (C) Photos of the sacrificed mice (left panel) and the dissected tumors (right panel). n=5. (D) The inhibition rate of the drug treatments. According to Jin's formula, q > 1.15 indicating that cisplatin and ICG-001 synergistically inhibited the growth of C17 xenografts.

CHAPTER 6

Conclusions and future perspectives

6. Conclusions and future perspectives

Wnt dysregulation is commonly seen in NPC and it is also regarded as a driver to maintain the CSCs potency within the tumor mass. In our studies, we tried to explore the potential use of ICG-001 in NPC treatment. We hypothesized that ICG-001 could block the β-catenin/CBP interaction and initiate a cascade to biological changes to make the tumor less aggressive and more sensitive to the contemporary chemotherapy and radiotherapy. Figure 6.1 summarizes the main findings in our studies.

In the first part of the study, ICG-001 was found to inhibit NPC cell migration via the restoration of miR-150 and the reduction of CD44 expression. MiR-150 was also validated as a novel miRNA to regulate CD44 directly. ICG-001 could also reduce the expression of Dnmt1 and subsequently increase the endogenous level of miR-150. Therefore, we speculate that Dnma1 may play a role in the expression of miR-150. The effect of ICG-001 on the level of promoter methylation of *miR-150* gene using bisulfite sequencing should be studied in the future studies.

In the second part of the study, we found that ICG-001 could reduce the expression of Evi1 which could regulate the cell migration and tumor sphere formation of NPC cells. MiR-96 was found to target the expression of Evi1 directly and miR-449a was demonstrated as a downstream effector of Evi1. Restored expression of miR-96 and miR-449a was detected in ICG-001-treated NPC cells. On the other hand, survivin downregulated by ICG-001 was shown to affect the expression of Evi1 and miR-449a. Therefore, ICG-001 appears to

inhibit Evi1/miR-449a via two different upstream regulators, namely miR-96 and survivin. Further characterization of these two regulatory axes in CSCs-enriched subsets can be performed in next step of experiments. Results in these two parts of the study further provided the underlying mechanisms of anti-tumor effects of ICG-001 on NPC cells.

In the third part of the study, ICG-001 was found to sensitize NPC cells to cisplatin, and the combined use of ICG-001 and cisplatin in the present studies demonstrated a synergistic inhibition on the tumor growth without significant adverse effect. All the results presented in this thesis supported the further development of this CBP antagonist for the therapeutic use in NPC.

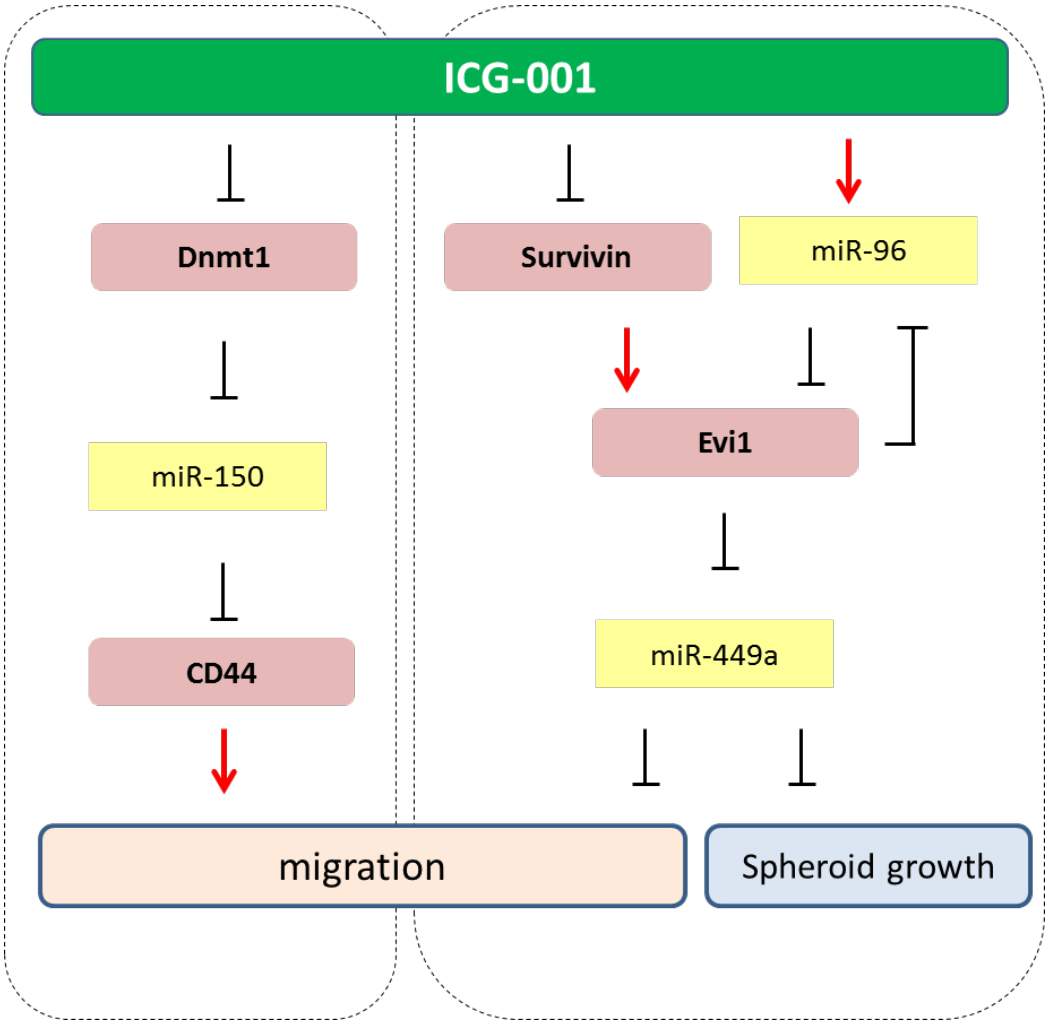

Figure 6.1 | A schematic diagram of the biological pathways studied in the thesis.

*In this thesis, Figure 5.5, the names of some culture medium, NPC cells/xenografts, drugs/reagents and organizations were appeared/mentioned in one of my co-authored publications (Chan KC, **Chan LS**, Ip JC, Lo C, Yip TT, Ngan RK, Wong RN, Lo KW, Ng WT, Lee AW, Tsao GS, Kahn M, Lung ML, Mak NK. Therapeutic targeting of CBP/β-catenin signaling reduces cancer stem-like population and synergistically suppresses growth of EBV-positive nasopharyngeal carcinoma cells with cisplatin. Sci Rep. 2015 Apr 21;5:9979).*

REFERENCES

Al-Hajj M, Wicha MS, Benito-Hernandez A, Morrison SJ, Clarke MF. Prospective identification of tumorigenic breast cancer cells. *Proc Natl Acad Sci U S A.* 2003; 100(7):3983-8.

Assumpcao MB, Moreira FC, Hamoy IG, Magalhaes L, Vidal A, Pereira A, Burbano R, Khayat A, Silva A, Santos S, Demachki S, Ribeiro-Dos-Santos A, Assumpcao P. High-Throughput miRNA Sequencing Reveals a Field Effect in Gastric Cancer and Suggests an Epigenetic Network Mechanism. *Bioinform Biol Insights.* 2015; 9:111-7.

Atena, M., Reza, A. and Mehran, G. A Review on the Biology of Cancer Stem Cells. *Stem Cell Discovery.* 2014; 4, 83-89.

Bao Y, Guo Y, Li Z, Fang W, Yang Y, Li X, Li Z, Xiong B, Chen Z, Wang J, Kang K, Gou D, Yang W. MicroRNA profiling in Muc2 knockout mice of colitis-associated cancer model reveals epigenetic alterations during chronic colitis malignant transformation. *PLoS.One*. 2014; 9:e99132.

Bard-Chapeau EA, Gunaratne J, Kumar P, Chua BQ, Muller J, Bard FA, Blackstock W, Copeland NG, Jenkins NA. EVI1 oncoprotein interacts with a large and complex network of proteins and integrates signals through protein phosphorylation. *Proc Natl Acad Sci U S A.* 2013; 110(31):E2885-94.

Bei JX, Li Y, Jia WH, Feng BJ, Zhou G, Chen LZ, Feng QS, Low HQ, Zhang H, He F, Tai ES, Kang T, Liu ET, Liu J, Zeng YX. A genome-wide association study of nasopharyngeal carcinoma identifies three new susceptibility loci. *Nat Genet*. 2010; 42(7):599-603.

Bei JX, Su WH, Ng CC, Yu K, Chin YM, Lou PJ, Hsu WL, McKay JD, Chen CJ, Chang YS, Chen LZ, Chen MY, Cui Q, Feng FT, Feng QS, Guo YM, Jia WH, Khoo AS, Liu WS, Mo HY, Pua KC, Teo SH, Tse KP, Xia YF, Zhang H, Zhou GQ, Liu JJ, Zeng YX, Hildesheim A; International Nasopharyngeal Carcinoma (NPC) Genetics Working Group. A GWAS Meta-analysis and Replication Study Identifies a Novel Locus within CLPTM1L/TERT Associated with

Nasopharyngeal Carcinoma in Individuals of Chinese Ancestry. *Cancer Epidemiol Biomarkers Prev*. 2016; 25(1):188-92.

Birdwell CE, Queen KJ, Kilgore PC, Rollyson P, Trutschl M, Cvek U, Scott RS. Genome-wide DNA methylation as an epigenetic consequence of Epstein-Barr virus infection of immortalized keratinocytes. *J Virol*. 2014; 88(19):11442-58.

Bordonaro M, Lazarova DL. Determination of the Role of CBP- and p300-Mediated Wnt Signaling on Colonic Cells. *JMIR Res Protoc*. 2016; 5(2):e66.

Bretscher A., Reczek D., Berryman M. Ezrin: a protein requiring conformational activation to link microfilaments to the plasma membrane in the assembly of cell surface structures. *J.Cell Sci.* 1997; 110(Pt 24):3011-3018.

Cabrera MC, Hollingsworth RE, Hurt EM. Cancer stem cell plasticity and tumor hierarchy. *World J Stem Cells*. 2015; 7(1):27-36.

Campbell PM, Szyf M. Human DNA methyltransferase gene DNMT1 is regulated by the APC pathway. *Carcinogenesis.* 2003; 24:17-24.

Chan AT, Grégoire V, Lefebvre JL, Licitra L, Hui EP, Leung SF, Felip E; EHNS–ESMO–ESTRO Guidelines Working Group.. Nasopharyngeal cancer: EHNS-ESMO-ESTRO Clinical Practice Guidelines for diagnosis, treatment and follow-up. *Ann Oncol*. 2012; 23(Suppl 7):vii83-5.

Chan KC, Chan LS, Ip JC, Lo C, Yip TT, Ngan RK, Wong RN, Lo KW, Ng WT, Lee AW, Tsao GS, Kahn M, Lung ML, Mak NK. Therapeutic targeting of CBP/beta-catenin signaling reduces cancer stem-like population and synergistically suppresses growth of EBV-positive nasopharyngeal carcinoma cells with cisplatin. *Sci.Rep.* 2015; 5:9979.

Chen HC, Chen GH, Chen YH, Liao WL, Liu CY, Chang KP, Chang YS, Chen SJ. MicroRNA deregulation and pathway alterations in nasopharyngeal carcinoma. *Br J Cancer*. 2009; 100(6):1002-11.

Chen S, Wang Z, Dai X, Pan J, Ge J, Han X, Wu Z, Zhou X, Zhao T. Re-expression of microRNA-150 induces EBV-positive Burkitt lymphoma differentiation by modulating c-Myb in vitro. *Cancer Sci.* 2013; 04:826-834.

Chen W, Dong J, Haiech J, Kilhoffer MC, Zeniou M. Cancer Stem Cell Quiescence and Plasticity as Major Challenges in Cancer Therapy. *Stem Cells Int*. 2016; 2016:1740936

Cheung CC, Lun SW, Chung GT, Chow C, Lo C, Choy KW, Lo KW. MicroRNA-183 suppresses cancer stem-like cell properties in EBV-associated nasopharyngeal carcinoma. *BMC Cancer*. 2016; 16:495.

Chou J, Lin YC, Kim J, You L, Xu Z, He B, Jablons DM. Nasopharyngeal carcinoma--review of the molecular mechanisms of tumorigenesis. *Head Neck*. 2008; 30(7):946-63.

Chou TC, Talalay P. Quantitative analysis of dose-effect relationships: the combined effects of multiple drugs or enzyme inhibitors. *Adv Enzyme Regul. 1984; 22:27–55.*

Chou TC. Drug combination studies and their synergy quantification using the Chou-Talalay method. *Cancer Res*. 2010; 70(2):440-6.

Chua ML, Wee JT, Hui EP, Chan AT. Nasopharyngeal carcinoma. *Lancet*. 2016; 387(10022):1012-24.

Clarke MF, Dick JE, Dirks PB, Eaves CJ, Jamieson CH, Jones DL, Visvader J, Weissman IL, Wahl GM. Cancer stem cells--perspectives on current status and future directions: AACR Workshop on cancer stem cells. *Cancer Res*. 2006; 66(19):9339-44.

Cohen JI, Fauci AS, Varmus H, Nabel GJ. Epstein-Barr virus: an important vaccine target for cancer prevention. *Sci Transl Med*. 2011; 3(107):107fs7.

Cohnheim J (1880) Vorlesungen über allgemeine Pathologie. *Ein Handbuch für Aerzte und Studirende. Hirschwald, Berlin, Germany*, pp. 634-50.

Dai W, Zheng H, Cheung AK, Lung ML. Genetic and epigenetic landscape of nasopharyngeal carcinoma. *Chin Clin Oncol*. 2016; 5(2):16.

De Weer A, Van der Meulen J, Rondou P, Taghon T, Konrad TA, De Preter K, Mestdagh P, Van Maerken T, Van Roy N, Jeison M, Yaniv I, Cauwelier B, Noens L, Poirel HA, Vandenberghe P, Lambert F, De Paepe A, Sánchez MG, Odero M, Verhasselt B, Philippé J, Vandesompele J, Wieser R, Dastugue N, Van Vlierberghe P, Poppe B, Speleman F. EVI1-mediated down regulation of MIR449A is essential for the survival of EVI1 positive leukaemic cells. *Br J Haematol*. 2011; 154(3):337-48.

Deng X, Cao Y, Liu Y, Li F, Sambandam K, Rajaraman S, Perkins AS, Fields AP, Hellmich MR, Townsend CM Jr, Thompson EA, Ko TC. Overexpression of Evi-1 oncoprotein represses TGF-β signaling in colorectal cancer. *Mol Carcinog*. 2013; 52(4):255-64.

Dick JE. Looking ahead in cancer stem cell research. *Nat Biotechnol*. 2009; 27(1):44-6.

Donatello S, Babina IS, Hazelwood LD, Hill AD, Nabi IR, Hopkins AM. Lipid raft association restricts CD44-ezrin interaction and promotion of breast cancer cell migration. *Am.J.Pathol.* 2012; 181:2172-2187.

Dugbartey GJ, Peppone LJ, de Graaf IA. An integrative view of cisplatin-induced renal and cardiac toxicities: Molecular mechanisms, current treatment challenges and potential protective measures. *Toxicology*. 2016; 371:58-66.

El-Khoueiry AB, Ning Y, Yang D, Cole S, Kahn M, Zoghbi M, Berg J, Fujimori M, Inada T, Kouji H, Lenz HJ. A phase I first-in-human study of PRI-724 in patients (pts) with advanced solid tumors. *J Clin Oncol*. 2013; 31(Suppl):2501.

Emami KH, Nguyen C, Ma H, Kim DH, Jeong KW, Eguchi M, Moon RT, Teo JL, Kim HY, Moon SH, Ha JR, Kahn M. A small molecule inhibitor of beta-catenin/CREB-binding protein transcription [corrected]. *Proc Natl Acad Sci U S A*. 2004; 101(34):12682-7. Erratum in: *Proc Natl Acad Sci U S A*. 2004; 101(47):16707.

Endo K, Kondo S, Shackleford J, Horikawa T, Kitagawa N, Yoshizaki T, Furukawa M, Zen Y, Pagano JS. Phosphorylated ezrin is associated with EBV latent membrane protein 1 in nasopharyngeal carcinoma and induces cell migration. *Oncogene*. 2009; 28:1725-1735.

Feng J, Yu J, Pan X, Li Z, Chen Z, Zhang W, Wang B, Yang L, Xu H, Zhang G, Xu Z. HERG1 functions as an oncogene in pancreatic cancer and is downregulated by miR-96. *Oncotarget*. 2014; 5(14):5832-44.

Ferlay J, Soerjomataram I, Ervik M, Dikshit R, Eser S, Mathers C, Rebelo M, Parkin DM, Forman D, Bray, F. GLOBOCAN 2012 v1.0, Cancer Incidence and Mortality Worldwide: IARC CancerBase No. 11 [Internet]. *Lyon, France: International Agency for Research on Cancer*. 2013. Available from: http://globocan.iarc.fr, accessed on 6th Mar, 2017.

Fong CW. Platinum based radiochemotherapies: Free radical mechanisms and radiotherapy sensitizers. *Free Radic Biol Med*. 2016; 99:99-109.

Fukuda S, Hoggatt J, Singh P, Abe M, Speth JM, Hu P, Conway EM, Nucifora G, Yamaguchi S, Pelus LM. Survivin modulates genes with divergent molecular functions and regulates proliferation of hematopoietic stem cells through Evi-1. *Leukemia*. 2015; 29(2):433-40.

Grotenhuis BA, Wijnhoven BP, van Lanschot JJ. Cancer stem cells and their potential implications for the treatment of solid tumors. *J Surg Oncol*. 2012; 106(2):209-15.

Guo X, Johnson RC, Deng H, Liao J, Guan L, Nelson GW, Tang M, Zheng Y, de The G, O'Brien SJ, Winkler CA, Zeng Y. Evaluation of nonviral risk factors for nasopharyngeal carcinoma in a high-risk population of Southern China. *Int J Cancer*. 2009; 124(12):2942-7.

Guo X, Lui WO, Qian CN, Chen JD, Gray SG, Rhodes D, Haab B, Stanbridge E, Wang H, Hong MH, Min HQ, Larsson C, Teh BT. Identifying cancer-related genes in nasopharyngeal carcinoma cell lines using DNA and mRNA expression profiling analyses. *Int J Oncol*. 2002; 21(6):1197-204.

Hao SP, Tsang NM. Surgical management of recurrent nasopharyngeal carcinoma. *Chang Gung Med J*. 2010; 33(4):361-9.

Hatton OL, Harris-Arnold A, Schaffert S, Krams SM, Martinez OM. The interplay between Epstein-Barr virus and B lymphocytes: implications for infection, immunity, and disease. *Immunol Res*. 2014; 58(2-3):268-76.

Hitt E. Wnt Signaling Inhibition: Will Decades of Effort Be Fruitful at Last? [Internet] *OncLive*. 2013. Available from: http://www.onclive.com/publications/oncology-live/2012/december-2012/wnt-signaling-inhibition-will-decades-of-effort-be-fruitful-at-last?p=2, assessed on 9th Mar, 2017.

Hoareau-Aveilla C, Valentin T, Daugrois C, Quelen C, Mitou G, Quentin S, Jia J, Spicuglia S, Ferrier P, Ceccon M, Giuriato S, Gambacorti-Passerini C, Brousset P, Lamant L, Meggetto F. Reversal of microRNA-150 silencing disadvantages crizotinib-resistant NPM-ALK(+) cell growth. *J Clin Invest.* 2015; 125:3505-3518.

Hong Kong Cancer Registry. Nasopharyngeal Cancer in 2014. [Internet]. *Hong Kong Cancer Registry, Hospital Authority, HKSAR.* 2016. Available from: http://www3.ha.org.hk/cancereg/default.asp, assessed on 6th Mar, 2017.

Hong Y, Liang H, Uzair-Ur-Rehman, Wang Y, Zhang W, Zhou Y, Chen S, Yu M, Cui S, Liu M, Wang N, Ye C, Zhao C, Liu Y, Fan Q, Zhang CY, Sang J, Zen K, Chen X. miR-96 promotes cell proliferation, migration and invasion by targeting PTPN9 in breast cancer. *Sci Rep*. 2016; 6:37421.

Hu J, Fang Y, Cao Y, Qin R, Chen Q. miR-449a Regulates proliferation and chemosensitivity to cisplatin by targeting cyclin D1 and BCL2 in SGC7901 cells. *Dig Dis Sci*. 2014; 59(2):336-45.

Huang X, Lv W, Zhang JH, Lu DL. miR-96 functions as a tumor suppressor gene by targeting NUAK1 in pancreatic cancer. *Int J Mol Med*. 2014; 34(6):1599-605.

Hui AB, Or YY, Takano H, Tsang RK, To KF, Guan XY, Sham JS, Hung KW, Lam CN, van Hasselt CA, Kuo WL, Gray JW, Huang DP, Lo KW. Array-based comparative genomic hybridization analysis identified cyclin D1 as a target oncogene at 11q13.3 in nasopharyngeal carcinoma. *Cancer Res*. 2005; 65(18):8125-33.

Hui EP, Ma BB, King AD, Mo F, Chan SL, Kam MK, Loong HH, Ahuja AT, Zee BC, Chan AT. Hemorrhagic complications in a phase II study of sunitinib in patients of nasopharyngeal carcinoma who has previously received high-dose radiation. *Ann Oncol*. 2011; 22(6):1280-7.

Jain A, Chia WK, Toh HC. Immunotherapy for nasopharyngeal cancer-a review. *Chin Clin Oncol*. 2016; 5(2):22.

Jiani Liu, Jiangxue Wu, Ling Zhou, Changchuan Pan, Yi Zhou, Wuying Du, Jie-min Chen, Xiaofeng Zhu, Jingnan Shen, Shuai Chen, Ran-yi Liu, and Wenlin Huang. ZD6474, a new treatment strategy for human osteosarcoma, and its potential synergistic effect with celecoxib. *Oncotarget*. 2015; 6(25):21341–21352.

Jin ZJ. Addition in drug combination (author's transl). *Zhongguo Yao Li Xue Bao*. 1980; 1:70–76.

Jonas S, Izaurralde E. Towards a molecular understanding of microRNA-mediated gene silencing. *Nat Rev Genet*. 2015; 16(7):421-33.

Kahn M. Targeting the CBP/Catenin Interaction to Eliminate Cancer Stem Cells. *American Society of Clinical Oncology, 2011 Educational Book.* 2011.

Kim YM, Kahn M. The role of the Wnt signaling pathway in cancer stem cells: prospects for drug development. *Res Rep Biochem*. 2014; 4:1-12.

Ko AH, Chiorean EG, Kwak EL, Lenz HJ, Nadler PI, Wood DL, Fujimori M, Inada T, Kouji H, McWilliams RR. Final results of a phase Ib dose-escalation study of PRI-724, a CBP/beta-catenin modulator, plus gemcitabine (GEM) in patients with advanced pancreatic adenocarcinoma (APC) as second-line therapy after FOLFIRINOX or FOLFOX. *J Clin Oncol*. 2016; 34(suppl; abstr e15721).

Kohichiroh Yasui, Chika Konishi, Yasuyuki Gen, Mio Endo, Osamu Dohi, Akira Tomie, Tomoko Kitaichi, Nobuhisa Yamada, Naoto Iwai, Taichiro Nishikawa, Kanji Yamaguchi, Michihisa Moriguchi, Yoshio Sumida, Hironori Mitsuyoshi, Shinji Tanaka, Shigeki Arii, Yoshito Itoh *EVI1*, a target gene for amplification at 3q26, antagonizes transforming growth factor-β-mediated growth inhibition in hepatocellular carcinoma. *Cancer Sci*. 2015; 106(7):929–937.

Küppers R. B cells under influence: transformation of B cells by Epstein-Barr virus. *Nat Rev Immunol*. 2003; 3(10):801-12.

Lapidot T, Sirard C, Vormoor J, Murdoch B, Hoang T, Caceres-Cortes J, Minden M, Paterson B, Caligiuri MA, Dick JE. A cell initiating human acute myeloid leukaemia after transplantation into SCID mice. *Nature*. 1994; 367(6464):645-8.

Lee AW, Ma BB, Ng WT, Chan AT. Management of Nasopharyngeal Carcinoma: Current Practice and Future Perspective. *J Clin Oncol*. 2015; 33(29):3356-64.

Li LL, Shu XS, Wang ZH, Cao Y, Tao Q. Epigenetic disruption of cell signaling in nasopharyngeal carcinoma. *Chin J Cancer*. 2011a; 30(4):231-9.

Li LX, Zhang YL, Zhou L, Ke ML, Chen JM, Fu X, Ye CL, Wu JX, Liu RY, Huang W. Antitumor efficacy of a recombinant adenovirus encoding endostatin combined with an E1B55KD-deficient adenovirus in gastric cancer cells. *J Transl Med*. 2013; 11:257.

Li T, Chen JX, Fu XP, Yang S, Zhang Z, Chen K, Li Y. MicroRNA expression profiling of nasopharyngeal carcinoma. *Oncol.Rep.* 2011b; 25:1353-1363.

Lin DC, Meng X, Hazawa M, Nagata Y, Varela AM, Xu L, Sato Y, Liu LZ, Ding LW, Sharma A, Goh BC, Lee SC, Petersson BF, Yu FG, Macary P, Oo MZ, Ha C S, Yang H, Ogawa S, Loh KS, Koeffler HP. The genomic landscape of nasopharyngeal carcinoma. *Nat.Genet.* 2014; 46:866-871.

Lin HH, Feng WC, Lu LC, Shao YY, Hsu CH, Cheng AL. Inhibition of the Wnt/β-catenin signaling pathway improves the anti-tumor effects of sorafenib against hepatocellular carcinoma. *Cancer Lett*. 2016; 381(1):58-66.

Lin S, Gregory RI. MicroRNA biogenesis pathways in cancer. *Nat Rev Cancer*. 2015; 15(6):321-33.

Liu J, Wu X, Liu H, Liang Y, Gao X, Cai Z, Wang W, Zhang H. Expression of microRNA-30a-5p in drug-resistant and drug-sensitive ovarian cancer cell lines. *Oncol Lett*. 2016; 12(3):2065-2070.

Liu Q, Yu FY, Tang W, Su SC, Song EW. Cancer Stem Cell. *Recent Advances in Cancer Research and Therapy.* 2012; pp. 173-196.

Liu Y, Chen L, Ko TC, Fields AP, Thompson EA. Evi1 is a survival factor which conveys resistance to both TGFbeta- and taxol-mediated cell death via PI3K/AKT. *Oncogene*. 2006; 25(25):3565-75.

Lo KW, Chung GT, To KF. Deciphering the molecular genetic basis of NPC through molecular, cytogenetic, and epigenetic approaches. *Semin Cancer Biol*. 2012; 22:79–86.

Lukaszewicz AI, McMillan MK, Kahn M. Small molecules and stem cells. Potency and lineage commitment: the new quest for the fountain of youth. *J Med Chem*. 2010; 53(9):3439-53.

Lun SW, Cheung ST, Cheung PF, To KF, Woo JK, Choy KW, Chow C, Cheung CC, Chung GT, Cheng AS, Ko CW, Tsao SW, Busson P, Ng MH, Lo KW. CD44+ cancer stem-like cells in EBV-associated nasopharyngeal carcinoma. *PLoS One*. 2012; 7(12):e52426.

Luo W, Li S, Peng B, Ye Y, Deng X, Yao K. Embryonic stem cells markers SOX2, OCT4 and Nanog expression and their correlations with epithelial-mesenchymal transition in nasopharyngeal carcinoma. *PLoS One*. 2013; 8(2):e56324.

Luo WR, Gao F, Li SY, Yao KT. Tumour budding and the expression of cancer stem cell marker aldehyde dehydrogenase 1 in nasopharyngeal carcinoma. *Histopathology*. 2012a; 61(6):1072-81.

Luo Z, Zhang L, Li Z, Li X, Li G, Yu H, Jiang C, Dai Y, Guo X, Xiang J, Li G. An in silico analysis of dynamic changes in microRNA expression profiles in stepwise development of nasopharyngeal carcinoma. *BMC Med Genomics*. 2012b; 5:3.

Ma Y, Liang AJ, Fan YP, Huang YR, Zhao XM, Sun Y, Chen XF. Dysregulation and functional roles of miR-183-96-182 cluster in cancer cell proliferation, invasion and metastasis. *Oncotarget*. 2016; 7(27):42805-42825.

Machova, P. K., Lopotova, T., Klamova, H., Burda, P., Trneny, M., Stopka, T., Moravcova, J. Expression patterns of microRNAs associated with CML phases and their disease related targets. *Mol.Cancer.* 2011; 10:41.

Manachai N, Saito Y, Nakahata S, Bahirvani AG, Osato M, Morishita K. Activation of EVI1 transcription by the LEF1/β-catenin complex with p53-alteration in myeloid blast crisis of chronic myeloid leukemia. *Biochem Biophys Res Commun*. 2017; 482(4):994-1000.

Manegold PC, Teo JL, Kahn M. Wnt signaling in stem cells. *Targeting the Wnt Pathway in Cancer, New York: Springer*. 2011; pp. 35–50.

Morris VA, Zhang A, Yang T, Stirewalt DL, Ramamurthy R, Meshinchi S, Oehler VG. MicroRNA-150 expression induces myeloid differentiation of human acute leukemia cells and normal hematopoietic progenitors. *PLoS.One.* 2013; 8:e75815.

Nagaraj AB, Joseph P, Kovalenko O, Singh S, Armstrong A, Redline R, Resnick K, Zanotti K, Waggoner S, DiFeo A. Critical role of Wnt/β-catenin signaling in driving epithelial ovarian cancer platinum resistance. *Oncotarget*. 2015; 6(27):23720-34.

Nanjundan M, Nakayama Y, Cheng KW, Lahad J, Liu J, Lu K, Kuo WL, Smith-McCune K, Fishman D, Gray JW, Mills GB. Amplification of MDS1/EVI1 and EVI1, located in the 3q26.2 amplicon, is associated with favorable patient prognosis in ovarian cancer. *Cancer Res*. 2007; 67(7):3074-84.

Niller HH, Szenthe K, Minarovits J. Epstein-Barr virus-host cell interactions: an epigenetic dialog? *Front Genet*. 2014; 5:367.

Nowell PC. The clonal evolution of tumor cell populations. *Science*. 1976; 194(4260):23-8.

Perri, F., Della Vittoria, S. G., Giuliano, M., D'Aniello, C., Gnoni, A., Cavaliere, Perri F, Della Vittoria Scarpati G, Giuliano M, D'Aniello C, Gnoni A, Cavaliere C, Licchetta A, Pisconti S. Epstein-Barr virus infection and nasopharyngeal carcinoma: the other side of the coin. *Anticancer Drugs.* 2015; 26:1017-1025.

Queisser A, Hagedorn S, Wang H, Schaefer T, Konantz M, Alavi S, Deng M, Vogel W, von Mässenhausen A, Kristiansen G, Duensing S, Kirfel J, Lengerke C, Perner S. Ecotropic viral integration site 1, a novel oncogene in prostate cancer. *Oncogene*. 2016.

Rapti SM, Kontos CK, Papadopoulos IN, Scorilas A. High miR-96 levels in colorectal adenocarcinoma predict poor prognosis, particularly in patients without distant metastasis at the time of initial diagnosis. *Tumour Biol*. 2016; 37(9):11815-11824.

Ring A, Kim YM, Kahn M. Wnt/catenin signaling in adult stem cell physiology and disease. *Stem Cell Rev*. 2014; 10(4):512-25.

Schmitt M, Metzger M, Gradl D, Davidson G, Orian-Rousseau V. CD44 functions in Wnt signaling by regulating LRP6 localization and activation. *Cell Death Differ*. 2015; 22(4):677-89.

Shen YA, Wang CY, Chuang HY, Hwang JJ, Chi WH, Shu CH, Ho CY, Li WY, Chen YJ. CD44 and CD24 coordinate the reprogramming of nasopharyngeal carcinoma cells towards a cancer stem cell phenotype through STAT3 activation. *Oncotarget*. 2016; 7(36):58351-58366.

Sheu JJ, Lee CH, Ko JY, Tsao GS, Wu CC, Fang CY, Tsai FJ, Hua CH, Chen CL, Chen JY. Chromosome 3p12.3-p14.2 and 3q26.2-q26.32 are genomic markers for prognosis of advanced nasopharyngeal carcinoma. *Cancer Epidemiol Biomarkers Prev*. 2009; 18(10):2709-16.

Shi W, Bastianutto C, Li A, Perez-Ordonez B, Ng R, Chow KY, Zhang W, Jurisica I, Lo KW, Bayley A, Kim J, O'Sullivan B, Siu L, Chen E, Liu FF. Multiple dysregulated pathways in nasopharyngeal carcinoma revealed by gene expression profiling. *Int J Cancer*. 2006; 119(10):2467-75.

Soria JC, Deutsch E. Hemorrhage caused by antiangiogenic therapy within previously irradiated areas: expected consequence of tumor shrinkage or a warning for antiangiogenic agents combined to radiotherapy? *Ann Oncol*. 2011; 22(6):1247-9.

Szwed M, Kania KD, Jozwiak Z. Toxicity of doxorubicin-transferrin conjugate is connected to the modulation of Wnt/β-catenin pathway in human leukemia cells. *Leuk Res*. 2015; 39(10):1096-102.

Takahashi-Yanaga F, Kahn M. Targeting Wnt signaling: can we safely eradicate cancer stem cells? *Clin.Cancer Res.* 2010; 16:3153-3162.

Takebe N, Harris PJ, Warren RQ, Ivy SP. Targeting cancer stem cells by inhibiting Wnt, Notch, and Hedgehog pathways. *Nat Rev Clin Oncol*. 2011; 8(2):97-106.

Takebe N, Miele L, Harris PJ, Jeong W, Bando H, Kahn M, Yang SX, Ivy SP. Targeting Notch, Hedgehog, and Wnt pathways in cancer stem cells: clinical update. *Nat Rev Clin Oncol*. 2015; 12(8):445-64.

Tan WL, Tan EH, Lim DW, Ng QS, Tan DS, Jain A, Ang MK. Advances in systemic treatment for nasopharyngeal carcinoma. *Chin Clin Oncol*. 2016; 5(2):21.

Tanaka M, Suzuki HI, Shibahara J, Kunita A, Isagawa T, Yoshimi A, Kurokawa M, Miyazono K, Aburatani H, Ishikawa S, Fukayama M. EVI1 oncogene promotes KRAS pathway through suppression of microRNA-96 in pancreatic carcinogenesis. *Oncogene*. 2014; 33(19):2454-63.

Tang M, Lautenberger JA, Gao X, Sezgin E, Hendrickson SL, Troyer JL, David VA, Guan L, McIntosh CE, Guo X, Zheng Y, Liao J, Deng H, Malasky M, Kessing B, Winkler CA, Carrington M, Dé The G, Zeng Y, O'Brien SJ. The principal genetic determinants for nasopharyngeal carcinoma in China involve the HLA class I antigen recognition groove. *PLoS Genet*. 2012; 8(11):e1003103.

Teo JL, Kahn M. The Wnt signaling pathway in cellular proliferation and differentiation: A tale of two coactivators. *Adv Drug Deliv Rev*. 2010; 62(12):1149-55.

Tobo T, Hirahashi M, Yao T, Aishima S, Oda Y. Ezrin expression and its phosphorylation in gastric carcinoma with lymphoid stroma and Epstein-Barr virus infection. *Mol.Clin.Oncol.* 2013; 1:220-224.

Tsang CM, Yip YL, Lo KW, Deng W, To KF, Hau PM, Lau VM, Takada K, Lui VW, Lung ML, Chen H, Zeng M, Middeldorp JM, Cheung AL, Tsao SW. Cyclin D1 overexpression supports stable EBV infection in nasopharyngeal epithelial cells. *Proc Natl Acad Sci U S A*. 2012; 109(50):E3473-82.

Tulalamba W, Janvilisri T. Nasopharyngeal carcinoma signaling pathway: an update on molecular biomarkers. *Int J Cell Biol*. 2012; 2012:594681.

Union for International Cancer Control. Nasopharyngeal Carcinoma. [Internet]. *Union for International Cancer Control, World Health Organization*. 2014. Available from: http://www.who.int/selection_medicines/committees/expert/20/applications/NasopharyngealCarcinoma.pdf?ua=1, assessed on 6th Mar2017.

Wang HY, Chang YL, To KF, Hwang JS, Mai HQ, Feng YF, Chang ET, Wang CP, Kam MK, Cheah SL, Lee M, Gao L, Zhang HZ, He JH, Jiang H, Ma PQ, Zhu XD, Zeng L, Chen CY, Chen G, Huang MY, Fu S, Shao Q, Han AJ, Li HG, Shao CK, Huang PY, Qian CN, Lu TX, Li JT, Ye W, Ernberg I, Ng HK, Wee JT, Zeng YX, Adami HO, Chan AT, Shao JY. A new prognostic histopathologic classification of nasopharyngeal carcinoma. *Chin J Cancer*. 2016; 35:41.

Wang L, Lin GN, Jiang XL, Lu Y. Expression of ezrin correlates with poor prognosis of nasopharyngeal carcinoma. *Tumour Biol.* 2011; 32:707-712.

Wang M, Yang W, Li M, Li Y. Low expression of miR-150 in pediatric intestinal Burkitt lymphoma. *Exp Mol Pathol.* 2014; 96:261-266.

Wang S, Mo Y, Midorikawa K, Zhang Z, Huang G, Ma N, Zhao W, Hiraku Y, Oikawa S, Murata M. The potent tumor suppressor miR-497 inhibits cancer phenotypes in nasopharyngeal carcinoma by targeting ANLN and HSPA4L. *Oncotarget.* 2015; 6:35893-35907.

Watanabe A, Tagawa H, Yamashita J, Teshima K, Nara M, Iwamoto K, Kume M, Kameoka Y, Takahashi N, Nakagawa T, Shimizu N, Sawada K. The role of microRNA-150 as a tumor suppressor in malignant lymphoma. *Leukemia.* 2011; 25:1324-1334.

Weinberg RA. The Rational treatment of cancer. *The Biology of Cancer, New York: Garland Science, Taylor & Francis Group.* 2013; pp.797-875.

Wielenga VJ, Smits R, Korinek V, Smit L, Kielman M, Fodde R, Clevers H, Pals ST. Expression of CD44 in Apc and Tcf mutant mice implies regulation by the WNT pathway. *Am J Pathol.* 1999; 154:515-523.

Won HS, Lee KM, Oh JE, Nam EM, Lee KE. Inhibition of β-Catenin to Overcome Endocrine Resistance in Tamoxifen-Resistant Breast Cancer Cell Line. *PLoS One*. 2016; 11(5):e0155983.

Wu L, Zeng X, Teng YD. A concise review on the definitions of cancer stem cells. *J Stem Cell Res Ther*. 2016; 1(2):00015-8.

Xie M, Steitz JA. Versatile microRNA biogenesis in animals and their viruses. *RNA Biol*. 2014; 11(6):673-81.

Xiong G, Zhang B, Huang MY, Zhou H, Chen LZ, Feng QS, Luo X, Lin HJ, Zeng YX. Epstein-Barr virus (EBV) infection in Chinese children: a retrospective study of age-specific prevalence. *PLoS One*. 2014; 9(6):e99857.

Xu C, Chen YP, Ma J. Clinical trials in nasopharyngeal carcinoma-past, present and future. *Chin Clin Oncol*. 2016a; 5(2):20.

Xu H, Tian Y, Yuan X, Wu H, Liu Q, Pestell RG, Wu K. The role of CD44 in epithelial-mesenchymal transition and cancer development. *Onco Targets Ther*. 2015; 8:3783-92.

Xu L, Zhong J, Guo B, Zhu Q, Liang H, Wen N, Yun W, Zhang L. MiR-96 promotes the growth of prostate carcinoma cells by suppressing MTSS1. *Tumour Biol*. 2016b; 37(9):12023-12032.

Xu T, Tang J, Gu M, Liu L, Wei W, Yang H. Recurrent nasopharyngeal carcinoma: a clinical dilemma and challenge. *Curr Oncol*. 2013; 20(5):e406-19.

Yamakawa N, Kaneda K, Saito Y, Ichihara E, Morishita K. The increased expression of integrin α6 (ITGA6) enhances drug resistance in EVI1(high) leukemia. *PLoS One*. 2012; 7(1):e30706.

Yau TO, Tang CM, Yu J. Epigenetic dysregulation in Epstein-Barr virus-associated gastric carcinoma: disease and treatments. *World J Gastroenterol*. 2014; 20:6448-6456.

Yee Ko JM, Dai W, Wun Wong EH, Kwong D, Tong Ng W, Lee A, Kai Cheong Ngan R, Chung Yau C, Tung S, Li Lung M. Multigene pathway-based analyses identify nasopharyngeal carcinoma risk associations for cumulative adverse effects of TERT-CLPTM1L and DNA double-strand breaks repair. *Int J Cancer*. 2014; 135(7):1634-45.

Yokobori T, Suzuki S, Tanaka N, Inose T, Sohda M, Sano A, Sakai M, Nakajima M, Miyazaki T, Kato H, Kuwano H. MiR-150 is associated with poor prognosis in esophageal squamous cell carcinoma via targeting the EMT inducer ZEB1. *Cancer Sci*. 2013; 104:48-54.

Yu F, Sim AC, Li C, Li Y, Zhao X, Wang DY, Loh KS. Identification of a subpopulation of nasopharyngeal carcinoma cells with cancer stem-like cell properties by high aldehyde dehydrogenase activity. *Laryngoscope*. 2013; 123(8):1903-11.

Yu N, Fu S, Liu Y, Xu Z, Liu Y, Hao J, Wang B, Zhang A. miR-96 suppresses renal cell carcinoma invasion via downregulation of Ezrin expression. *J Exp Clin Cancer Res*. 2015; 34:107.

Zeng ZY, Zhou YH, Zhang WL, Xiong W, Fan SQ, Li XL, Luo XM, Wu MH, Yang YX, Huang C, Cao L, Tang K, Qian J, Shen SR, Li GY. Gene expression profiling of nasopharyngeal carcinoma reveals the abnormally regulated Wnt signaling pathway. *Hum Pathol*. 2007; 38(1):120-33.

Zhao JJ, Lin J, Lwin T, Yang H, Guo J, Kong W, Dessureault S, Moscinski LC, Rezania D, Dalton WS, Sotomayor E, Tao J, Cheng JQ. MicroRNA expression profile and identification of miR-29 as a prognostic marker and pathogenetic factor by targeting CDK6 in mantle cell lymphoma. *Blood*. 2010; 115:2630-2639.

Zheng H, Dai W, Cheung AKL, Ko JMY, Kan R, Wong BWY, Leong MML, Deng M, Kwok TCT, Chan J, Kwong DLW, Lee AWM, Ng WT, Ngan RKC, Yau CC, Yung S, Lee VHF, Lam KO, Kwan CK, Li WS, Yau S, Chan KW, Lung ML. Whole-exome sequencing identifies multiple novel loss-of-function mutations of NF-kB pathway regulators in nasopharyngeal carcinoma. *Proc Natl Acad Sci U S A*. 2016; 113(40):11283-11288.

Zheng SY, Ge JF, Zhao J, Jiang D, Li F Adenovirus-mediated IL-24 confers radiosensitization to human lung adenocarcinoma in vitro and in vivo. *Mol Biol Rep*. 2015; 42(6):1069-80.

Zhou Y, Chen Q, Qin R, Zhang K, Li H. MicroRNA-449a reduces cell survival and enhances cisplatin-induced cytotoxicity via downregulation of NOTCH1 in ovarian cancer cells. *Tumour Biol*. 2014; 35(12):12369-78.

CURRICULUM VITAE

Academic qualifications of the thesis author, Mrs. CHAN Lai Sheung:

- Received the degree of Bachelor of Science (Honours) in Applied Biology from Hong Kong Baptist University, November 2006.

- Received the degree of Master of Philosophy (By Research) from Hong Kong Baptist University, November 2009.

July 2017

Publications

Research articles:

Keung MH, **Chan LS**, Kwok HH, Wong RN, Yue PY. Role of microRNA-520h in 20(R)-ginsenoside-Rg3-mediated angiosuppression. Ginseng Res. 2016 Apr;40(2):151-9.

Kwok HH, **Chan LS**, Poon PY, Yue PY, Wong RN. Ginsenoside-Rg1 induces angiogenesis by the inverse regulation of MET tyrosine kinase receptor expression through miR-23a. Toxicol Appl Pharmacol. 2015 Sep 15;287(3):276-83.

Chan KC, **Chan LS**, Ip JC, Lo C, Yip TT, Ngan RK, Wong RN, Lo KW, Ng WT, Lee AW, Tsao GS, Kahn M, Lung ML, Mak NK. Therapeutic targeting of CBP/β-catenin signaling reduces cancer stem-like population and synergistically suppresses growth of EBV-positive nasopharyngeal carcinoma cells with cisplatin. Sci Rep. 2015 Apr 21;5:9979.

Chan LS, Yue PY, Wong YY, Wong RN. MicroRNA-15b contributes to ginsenoside-Rg1-induced angiogenesis through increased expression of VEGFR-2. Biochem Pharmacol. 2013 Aug 1;86(3):392-400.

Chan LS, Yue PY, Kok TW, Keung MH, Mak NK, Wong RN. Ginsenoside-Rb1 promotes adipogenesis through regulation of PPARγ and microRNA-27b. Horm Metab Res. 2012 Oct;44(11):819-24.

Chan YK, Kwok HH, **Chan LS**, Leung KS, Shi J, Mak NK, Wong RN, Yue PY. An indirubin derivative, E804, exhibits potent angiosuppressive activity. Biochem Pharmacol. 2012 Mar 1;83(5):598-607.

Chan HM, **Chan LS**, Wong RN, Li HW. Direct quantification of single-molecules of microRNA by total internal reflection fluorescence microscopy. Anal Chem. 2010 Aug 15;82(16):6911-8.

Chan LS, Yue PY, Mak NK, Wong RN. Role of microRNA-214 in ginsenoside-Rg1-induced angiogenesis. Eur J Pharm Sci. 2009 Nov 5;38(4): 370-7.

Conference posters:

Chan LS, Yue PY, Kok TW, Lam YK, Wong RN. Effects of ginsenosides on adipogenesis. Presented at The 10th International Symposium on Ginseng, 2010, Seoul, Korea, September 13-16, 2010.

Chan LS, Yue PY, Mak NK, Wong RN. Role of microRNA-214 in ginsenoside-Rg1-induced angiogenesis. Presented at 9th Meeting of the Consortium for Globalization of Chinese Medicine, Hong Kong, August 23-25, 2010.

Chan LS, Yue PY, Mak NK, Wong RN. Role of microRNAs in ginsenoside-Rg1-induced angiogenesis. Presented at 2008 International Conference on Ginseng, Jilin, China, September 1-3, 2008.

Chan LS, Yue PY, Mak NK, Wong RN. Role of microRNAs in ginsenoside-Rg1-induced angiogenesis. Presented at the 4th Annual RNAi Europe, Barcelona, Spain, September 19-21, 2007.